DEFINING NEW MECHANISMS FOR DNA DAMAGE TOLERANCE IN CANCER

Elizabeth Mutter-Rottmayer

A dissertation submitted to the faculty at the University of North Carolina at Chapel Hill in partial fulfillment of the requirements for the degree of Doctor of Philosophy in the Curriculum in Toxicology in the School of Medicine.

Chapel Hill
2018

Approved by:

Cyrus Vaziri

Dale Ramsden

Kenneth Pearce

Gaorav Gupta

Jeff Sekelsky

Ilona Jaspers

ABSTRACT

Elizabeth Mutter-Rottmayer: Defining New Mechanisms for DNA Damage Tolerance in
Cancer
(Under the direction of Cyrus Vaziri)

Cancer cells rely on DNA damage tolerance pathways to cope with intrinsic

oncogenic stresses and evade DNA-damaging environmental and therapeutic agents.

However, the mechanisms by which neoplastic cells hijack tightly controlled DNA

damage tolerance-signaling cascades to promote mutagenesis and chemoresistance

are not understood. Thus, limitations in our knowledge of DNA damage tolerance and

mutagenesis impede effective prevention and treatment of cancer. We have discovered

two unique regulators of RAD18 and replication-associated DNA damage tolerance that

are overexpressed in cancer: RNF168 (an apical mediator of double strand break

signaling) and MAGEA4 (a cancer cell-specific protein with no known function). RNF168

is mutated in human RIDDLE syndrome, a disease characterized by severe

immunodeficiency, developmental defects, radiosensitivity and a predisposition to

cancer. We show here that RNF168 is a novel component of the RAD18 complex,

facilitating its recruitment to stalled replication forks and promoting damage tolerance

following replication stress. We have also identified the cancer/testis antigen (CTA)

MAGEA4 as a stabilizing binding partner of RAD18 that promotes trans-lesion DNA

synthesis. Thus, the findings in this thesis offer neomorphic cancer cell-specific roles for

regulators of DNA damage tolerance.

Identification of mechanisms of DNA damage tolerance that drive carcinogenesis and confer chemoresistance will allow for the development of more effective cancer treatment regimens. CTAs are absent from normal somatic cells but aberrantly overexpressed in many cancers. Interestingly, CTAs have been correlated with chemotherapeutic resistance and poor prognostic outcomes, though their contributions to carcinogenesis are not understood. We have found that depletion of several CTAs (MAGEA4, MAGEA10, or HORMAD1) sensitizes non-small cell lung cancer (NSCLC) cells to DNA-damaging therapies. These studies identify novel mechanisms by which NSCLC cells aberrantly overexpress germ cell proteins to alter genome maintenance, offering a cancer cell-specific mechanism by which neoplastic cells acquire chemoresistance and evade therapy. Accordingly, these CTAs are promising therapeutic targets whose inhibition should be innocuous to normal somatic cells while greatly sensitizing cancer cells to existing DNA damaging chemotherapeutic agents.

ACKNOWLEDGEMENTS

I would like to thank my thesis advisor, Dr. Cyrus Vaziri, for his direction through the course of my dissertation. The experience I have gained throughout this process has been invaluable and I am deeply grateful for the multitude of ways he has prepared me for the next steps in my scientific career. Next I express my thanks to the Vaziri Lab members that I have worked with for the past four years for their assistance and insight, especially Dr. Natasha Zlatanou whose encyclopedic knowledge, thorough experimental design, and inquisitorial nature made for a great collaboration.

I am very grateful for the continued input I have received from my committee members Drs. Dale Ramsden, Ilona Jaspers, Ken Pearce, Jeff Sekelsky, and Gaorav Gupta. I am especially indebted to Drs. Rasmden and Jaspers. Dr. Ramsden's organic pursuit for a greater intellectual understanding of science provided a refreshing reminder of research fundamentals. Dr. Jaspers', is an excellent role model through her ability to simultaneously manage various training entities and lead research facilities while increasing the competitiveness of our program.

I am also incredibly grateful to the friends that I have made along this process (especially those in my toxicology cohort) who shared in the challenges and successes of graduate school.

I cannot fully express the gratitude I have towards my parents (Sheila and Jim) and in-laws (Marlene and Steve) and siblings (Alex, Austin, Christina and Darius) who

have given me limitless encouragement throughout this process. My Aunt Linda—thank

you for paving the way, for your unending advice and continual reassurance. Finally, I

would like to thank my husband, David. You are an inspiration to me, an endless source

of patience, support, and motivation, and I cannot imagine this process without you.

Additional acknowledgments specific to each chapter

Chapter 1

This chapter was written entirely by Elizabeth Mutter-Rottmayer (E.M.R.).

Chapter 2

Chapter 3

experiments were carried out by Raquel Martinez-Chacin, Dennis Goldfarb, Dr. Yang Yang, Dr. Feng Yan, Dr. Ben Major, Dr. Satoshi Tateishi, and Dr. Kenneth Pearce. C.V. wrote the manuscript with input from all authors. Studies presented in this chapter were supported by an R01 ES09558 from the National Institutes of Health to C.V., F31 fellowship CA177179 from the National Institutes of Health to A.M.G. and by a Tier 1 Pilot Award from the University of North Carolina Lineberger Comprehensive Cancer Center to Y.G.

Chapter 4

This chapter was written entirely by E.M.R. Study design and experiments for MAGE proteins were done entirely by E.M.R. Experimental design for HORMAD1 studies was done by Y.G. and E.M.R., with guidance from C.V.. Y.G. conducted HORMAD1 experiments in the H1299 cell line. E.M.R. conducted HORMAD1 survivals in H358, MDAMB436 and MDAMB468 cells. Studies presented in this chapter were supported by an R01 ES09558 from the National Institutes of Health to C.V., a Tier 1 Pilot Award from the University of North Carolina Lineberger Comprehensive Cancer Center to Y.G., and a pre-doctoral award in Pharmacology/Toxicology by the PhRMA Foundation awarded to E.M.R..

Chapter 5

This chapter was written entirely by E.M.R.

TABLE OF CONTENTS

LIST OF FIGURES

LIST OF ABBREVIATIONS AND SYMBOLS

Alt-EJ: Alternative end joining

ATM: Ataxia telangiectasia mutated protein

BPDE: Benzo(a)pyrene diol epoxide

BRCA: Breast Cancer susceptibility protein

CDDP: Cisplatin

CPD: Cyclobutane Pyrimidine Dimers

CPT: Camptothecin

CTA: Cancer-Testis Antigen

DSB: Double Strand Break

DDR: DNA Damage Response

DDT: DNA Damage Tolerance

DOXO: Doxorubicin

E2: Ubiquitin conjugating enzyme

E3: Ubiquitin ligase

ETO: Etoposide

FA: Fanconi Anemia

FANC: Fanconi Anemia Complementation group

HLTF: Helicase-Like Transcription Factor

HR: Homologous Recombination

H2A: Histone 2A

H2AX: Histone 2A Variant X

ICL: Inter-Strand Crosslinks

IR: Ionizing Radiation

kDa: kilo Dalton

MAGE: Melanoma Associated Antigen

MDC1: Mediator of Damage Checkpoint protein 1

MHD: MAGE Homology Domain

MIU: Motif Interacting with Ubiquitin

MMC: Mitomycin C

MMS: Methyl Methanesulfonate

MRN: MRE11-RAD50-NBS1 complex

NHEJ: Nonhomologous End Joining

NSCLC: Non Small Cell Lung Cancer

PBS: Phosphate Buffered Saline

PCNA: Proliferating Cell Nuclear Antigen

Pol: polymerase

RAD: Radiation sensitivity protein

RING: Really Interesting New Gene, zinc finger catalytic domain

RNF: RING finger protein

ROS: Reactive Oxygen Species

SHPRH: SNF2 Histone-linker PHD-finger RING-finger Helicase

SS: Single stranded

TCGA: The Cancer Genome Atlas

TLS: Translesion Synthesis

TNBC: Triple Negative Breast Cancer

Topo: DNA topoisomerase

TS: Template Switching

Ub: Ubiquitination

UBZ: Ubiquitin-binding zinc finger domain

UV: Ultraviolet

ZRANB3: Zinc Finger RANBP2-Type Containing 3

η: Eta

κ: Kappa

ι: Iota

δ: Delta

ε: Epsilon

θ: Theta

α: Alpha

ζ: Zeta

γ: Gamma, indicative of phosphorylation

53BP1: p53 binding protein 1

CHAPTER 1: INTRODUCTION

1.1 DNA damage

Genome instability is a hallmark of cancer and the driving force behind the severe clinical phenotypes seen in many genetic diseases. Genome integrity is maintained cellular processes that process the tens of thousands of DNA damaging events each human cell is thought to experience daily[1]. Genome instability is caused Such DNA damage can be induced by exogenous agents including compounds in food items, chemical additives as well common pollutants such as polycyclic aromatic hydrocarbons, which are byproducts of combustion[2]. There are also several endogenously derived compounds such as formaldehyde or reactive oxygen species (ROS) that are produced during cellular metabolism, that can also have deleterious effects on DNA[3-5].

Not only are genotoxins derived from innumerable sources, they also induce a wide array of lesion types including but not limited to bulky adducts, double-stranded DNA breaks (DSBs) and inter-strand crosslinks (ICL), with each lesion repaired via a distinct mechanism. Briefly, bulky DNA adducts are tolerated through a low fidelity mechanism known as trans-lesion synthesis (TLS) which employs specialized polymerases to synthesize across the damaged template. Bulky lesions can also trigger an error-free

template-switching (TS) mechanism that utilizes information of a nascent sister chromatid as a replication template[6, 7].

Double strand breaks are the full cleavage of the sugar-phosphate backbone of double stranded DNA, yielding terminal DNA end structures which are primarily repaired by non-homologous end-joining (NHEJ) or by homologous recombination (HR). During NHEJ a Ku70/Ku80 heterodimer detects the break and is loaded onto each end, recruiting downstream repair proteins that ultimately result in the ligation of the two ends and restoration of genetic continuity[8, 9]. During HR DSB ends are recognized by the MRE11-RAD50-NBS1 (MRN) complex which activates a signaling cascade to initiate end resection and Rad51-mediated strand invasion. The undamaged sister chromatid or homologous allele is then used as a template for DNA synthesis[10]. Finally, ICLs activate the Fanconi Anemia (FA) pathway proteins, which detect, recruit and coordinate repair factors (including those involved in DSB repair) to ICL[11].

Of note, many repair mechanisms rely on information from an undamaged sister chromatid or homologous chromosome to perform high fidelity repair (TS, HR). Utilizing an undamaged template avoids aberrant alteration of the genetic information, however, undamaged templates are not always available. Thus, template-independent pathways (NHEJ, TLS) often coincide with mutagenesis.

1.2 The DNA Damage Response

1.2.1 DNA Damage Tolerance

Accurate replication of DNA is crucial for cell survival and maintenance of genome stability. Cells have thus developed mechanisms to cope with frequent genotoxic injuries that interfere with DNA synthesis. During DNA replication the double helix must

be unwound to expose single stranded DNA (ssDNA), which is used as a template to synthesize daughter strands. DNA unwinding is carried out by a helicase (MCM2-7 complex) and is strictly coupled with high fidelity replicative DNA polymerases (ε, δ, α) in order to avoid the generation of vulnerable, long stretches of ssDNA. Together these core components form a two-pronged fork structure termed the 'replication fork.' During normal conditions the replicative DNA polymerases (Polε on the leading strand, Polδ and Polα on the lagging strand) are able to rapidly duplicate DNA in an accurate manner. However, these polymerases are unable to bypass most DNA lesions, which can result in 'replication fork stalling'. Left unresolved, fork stalling can lead to replication fork collapse and the formation of the most severe type of DNA lesion, DNA double stranded breaks. Lesions encountered during DNA replication are often tolerated by replication-associated DNA damage tolerance mechanisms. There are two predominant replication-associated DNA damage tolerance mechanisms pathways: error-prone TLS, which uses specialized polymerases to synthesizes across a lesion and TS, which uses a newly synthesized sister chromatid as a template for error-free bypass.

1.2.1.1 Trans-lesion synthesis

During normal DNA synthesis, cells utilize canonical replicative DNA polymerases that are able to rapidly duplicate DNA in an accurate and efficient manner. Damaged DNA, however, can act as a physical barrier that prevents bypass by replicative DNA polymerases. One the mechanisms used to tolerate this obstruction is TLS, which employs trans-lesion DNA polymerases to replicate damaged DNA templates. TLS is initiated when Proliferating Cell Nuclear Antigen (PCNA) is mono-ubiquitinated in

response to DNA damage. PCNA is a homotrimeric protein that acts as a sliding clamp and docking site for DNA polymerases[12-14]. Monoubiquitination ($_m$ub) of PCNA is carried out by one of multiple E3 ubiquitin ligases, although with regards to TLS activation, is thought to be predominantly catalyzed by RAD18. E3 ubiquitin ligase activity requires the cooperation of the appropriate E2 ubiquitin conjugating enzyme and a universally employed E1 ubiquitin activating enzyme[15]. Replication fork stalling causes uncoupling of the helicase and replicative DNA polymerase and generates long stretches of ssDNA. Replication Protein A (RPA) coats the ssDNA, activating the s-phase checkpoint and recruiting RAD18 to the lesion site. RAD18 works as a part of a heterotrimeric complex with its E2 ubiquitin conjugating enzyme RAD6 (RAD18$_2$:RAD6$_1$) to $_m$ub-PCNA and induce a 'polymerase switch' from the replicative polymerases to TLS polymerases (Polη, Polκ, Polι, Polζ and Rev1), which have a higher affinity for the $_m$ub-PCNA substrate[16, 17]. These TLS polymerases have enlarged catalytic sites that are able to accommodate bulky DNA lesions[18].

While TLS is inherently error-prone, trans-lesion polymerases are capable of high-fidelity bypass of so-called 'cognate lesions'. Polη, for example, is able to synthesize across helix-distorting thymine homodimers generated from UV radiation in an error-free manner, where Polκ would be error-prone. Benzo[a]pyrene, a product of combustion, is metabolically activated in cells to generate the DNA-adducting species BPDE, which Polκ, but not Polη, can bypass with high fidelity[16, 19-28].

1.2.1.2 Template switching

Template switching is an error-free post-replication repair mechanism that utilizes a newly synthesized daughter strand as a template to bypass the DNA lesion. Initial work

on TS was generated from a series of studies in yeast showing that poly-ubiquitination of PCNA by RAD5 promoted replication between partially replicated sister chromatids [29-34]. In human, two RAD5 homologs have been identified: helicase-like transcription factor (HLTF) and SNF2 Histone-linker PHD-finger RING-finger Helicase (SHPRH), which can both poly-ubiquitinate PCNA in vitro[35-38]. Interestingly, damage-specific roles for HLTF and SHPRH have also been identified in the high fidelity tolerance of UV and MMS lesions, respectively. HLTF and SHPRH may also have acquired additional function in facilitating choosing correct TLS polymerase in response to various DNA damage[39]. Some studies have also suggested that HLTF translocase activity may contribute to template switching via a fork reversal mechanism in which newly-synthesized strands of DNA are annealed back together, forming a 'chicken foot' structure[40-44]. Fork reversal may also be mediated by ZRANB3, which utilizes poly-ubiquitinated PCNA to locate damage sites in vivo. ZRANB3 deficient cells are sensitive to methyl methanesulfonate (MMS), a potent chemotherapeutic and replication fork-stalling agent, but not Camptothecin, Hydroxyurea, H_2O_2 or UV[45].

It should be noted that the ubiquitin ligase RAD18, previously described as the activator of TLS, is also a key mediator of TS. RAD18 not only $_m$ub-PCNA, allowing for further extension of K63-linked poly-ubiquitin chains by the RAD5 homologs, but also mediates damage-specific responses of HLTF and SHPRH through direct binding[39, 46]. Importantly, RAD18 can exist in both ubiquitinated (non-active) and non-ubiquitinated (active) forms. Ubiquitinated RAD18 lacks the ability to interact with HLTF or SHPRH, is unable to ub-PCNA or form foci and can no longer prevent mutagenesis following exposure to DNA damaging agents[47]. RAD18 can additionally be regulated by

phosphorylation, stabilization and controlled expression, as well as sub-cellular distribution[48-53]. Thus may proteins can alter RAD18 function, significantly impacting DNA damage tolerance and cell fate.

1.2.1.3 Fanconi Anemia pathway

The FA pathway was identified through the investigation of a rare genetic instability disorder by the same name. Patients with FA usually have some combination of aplastic anemia, physical abnormalities and are at a 10-30% increased risk for cancer. The heterogeneity of the disease caused by a defect in one of 19 associated FANC genes that regulate genome maintenance[11].

The first mechanistic details of FA pathway activation were characterized in its response to cross-linking agents. Briefly, FANCM-MHF1-MHF2 identifies the lesion and recruits the FA Core (FANCs A-C, E-G, L, M and associated proteins) and ID2 (FANCI, FANCD2) complexes. Monoubiquitination of the ID2 heterodimer by the core complex is considered an initiating event for FA pathway activation. This modification is catalyzed by the E3 ubiquitin ligase subunit FANCL and its E2 conjugating enzyme FANCT. Depending on the nature of the lesion, the FA can evoke the use of TLS polymerases, nucleotide excision repair, and/ or HR, and has been proposed to directly inhibit NHEJ[11, 54].

The E3 ubiquitin ligase RAD18, which was previously described as an activator of TLS (and TS) via ubiquitination of PCNA, also plays a role in FA pathway activation. RAD18-dependent $_m$ub-PCNA recruits FANCL, promotes its subsequent monoubiquitination of the ID2 complex, and has been shown to also recruit FANCD2 via a direct interaction[55-57].

1.2.2 DNA Damage Repair

Mechanisms for recognition and repair of DNA damage are crucial for maintenance of genomic stability and prevention of carcinogenesis. Double strand breaks (DSBs), the most severe type of DNA damage, can occur in response to a variety of agents including environmental toxicants (e.g. reactive oxygen species formed from smog), and cancer therapies (e.g. ionizing radiation)[58, 59]. Defects in DSB repair can cause diseases with severe clinical phenotypes, as is seen in RIDDLE syndrome, where mutations in the DSB repair signaling protein RNF168 generate severe immunodeficiency, developmental defects, radiosensitivity and a predisposition to cancer. Inability to correctly repair DSBs has also been linked to accelerated aging, infertility and abnormal development of the nervous and immune systems.

Double strand breaks are primarily repaired by the HR and NHEJ pathways. Both HR and NHEJ engage complex signaling cascades, resulting in accumulation of repair proteins, BRCA1 and 53BP1, respectively, to the sites of damage[59, 60]. Upstream DSB repair signaling is initiated by ATM-dependent phosphorylation of histone 2A variant X (known as γH2AX), which binds with MDC1 at the lesion site. MDC1 acts as a DNA damage checkpoint activator and recruits the E3 ubiquitin ligase RNF8 to ubiquitinate γH2AX. Further poly-ubiquitination of γH2AX by RNF168 is needed for appropriate recruitment of BRCA1 or 53BP1 and is thought to potentially contribute to DSB repair pathway choice.

In addition to post-translation modifications, repair pathway choice can be dictated by DNA end resection. End resection is a tightly controlled process that involves the 5' to 3' degradation of DSB ends, producing long stretches of 3' ssDNA, and is initiated by

binding of the MRN complex to the DSB site. NBS1 recruits CtIP (required for MRE11 nuclease activity) to the lesion site. MRE11 generates a nick in the DNA (via endonuclease activity) and subsequently generates short (25-50 nt) 3' overhangs through exonucleolytic 3'-5' degradation that are then engaged by more processive nucleases and helicases such as EXO1, DNA2, and BLM to generate ssDNA stretches spanning multiple kilobases. Negative regulation of end-resection is carried out by a series of proteins including 53BP1 and anti-resection factors[10].

1.2.2.1 Homologous recombination

Homologous recombination is crucial for maintenance of genome integrity through its involvement in both DNA repair and meiotic chromosome segregation. In the context of DNA damage HR can respond to DNA gaps, inter-strand crosslinks and DSBs[10]. HR is a high-fidelity DSB repair mechanism that utilizes a sister chromatid or homologous chromosome as a template for repair. This template-dependence, however, restricts HR activity to the S and G2 phases of the cell cycle[59].

In HR, DSB ends are recognized by the MRN complex, which subsequently activates a signaling cascade to initiate end resection followed by Rad51 mediated strand invasion, D-loop formation, and DNA synthesis across lesion using the undamaged homologous allele as template. Replication intermediates are then resolved to restore the linkage flanking DSB[61].

Bunting et al. were amongst the first researchers to demonstrate the competitive nature between NHEJ and HR when they discovered that 53BP1 prevents HR in BRCA-1 deficient cells by inhibiting resection[62]. Loss of 53BP1 is able to rescue HR defects in

BRCA1-null cells[60]. Similarly, studies have found that RAD18 promotes HR through inhibition of NHEJ, adding to the theory of competition between HR and NHEJ[63, 64].

1.2.2.2 Nonhomologous end-joining

Unlike HR, NHEJ acts in a template-independent manner to ligate ends of the DSB. Since repair by NHEJ does not necessitate sequence homology at the break site, it is able to act during all stages of the cell cycle, but this temporal flexibility comes at the expense of repair fidelity. NHEJ is initiated when the Ku70/80 heterodimer is loaded onto the exposed ends of a DSB. Ku plays a multifunctional role in DSB repair- using lyase activity to remove damaged nucleotides in end-processing, and acting as a docking site for recruitment of other NHEJ proteins (e.g. DNA-PKcs)[65, 66]. DNA-PKcs-Ku binding marks the formation of DNA-PK holoenzyme which acts as a bridge to align broken ends of the DSB, and regulates binding of polymerases and nucleases at the lesion site. The DNA Ligase IV-XRCC4-XLF complex ligates the two ends of the DSB together. Use of NHEJ does not come without its limitations. Repair by NHEJ frequently results in small insertion and deletions that can give rise to mutations. NHEJ is also unable to repair collapsed replication fork lesions as collapsed forks represent a 'one-ended' break and are not accessible to NHEJ[67].

1.2.2.3 Alternative end-joining

Alternative end joining (Alt-EJ) (also, theta-mediated end-joining (TMEJ) or microhomology-mediated end-joining (MMEJ)) is a recently characterized DSB repair pathway. Although not a direct competitor with the canonical DSB repair pathways, alternative end-joining (alt-EJ) is thought to serve and important role in the repair of DSB in cells with defective NHEJ or HR. DNA polymerase theta (Polθ) is the primary

mediator of alt-EJ. Polθ utilizes resected ssDNA tails as a substrate for repair, catalyzing DNA synthesis from microhomologies (small patches of complementary sequence) at the lesion site. These ssDNA tails may result from inappropriately timed end-resection or aborted HR, and could describe the synthetic lethality seen with Polθ and factors that promote HR (e.g. BRCA1) or restrict end-resection (e.g. 53BP1)[68-70].

1.3 Role of the DNA damage response in cancer and disease

Defects in DNA repair and genome maintenance are associated with a variety of diseases, including cancer, that often manifest with severe clinical phenotypes. For example, sunlight-induced skin cancer is increased in patients with *xeroderma pigmentosum*-Variant (XPV), caused by defects in the DNA polymerase Polη. In TLS can replicate DNA templates containing solar UV radiation-induced DNA lesions (i.e. Cyclobutane Pyrimidine Dimers). In-deficient XPV patients, failure to bypass CPDs can lead to replication fork collapse and cell death, or genome instability and cancer [71, 72].

While genotoxic injury is generally negative, scientists have also capitalized on an understanding of mechanisms of DNA damage by using genotoxins such as ionizing radiation, platinating agents and other chemotherapeutics in the treatment of cancer[67, 73, 74]. These agents cause a slew of lesion types including a variety of crosslinks, bulky DNA adducts, single-stranded DNA breaks (SSB), and the most severe type of lesion-DSB. As a whole, DNA damage tolerance is critical for multi-step carcinogenesis, allowing established cancer cells to proliferate, adapt, invade and resist chemotherapy (Fig. 1.1).

1.3.1 Cancer/Testis Antigens

Cancer testis antigens (CTAs) comprise a group of over 250 proteins that are normally germ cells restricted but aberrantly overexpressed in a wide array of cancers[75, 76]. Expression of CTAs has been correlatively linked to chemotherapeutic resistance, tumorigenesis, metastasis, and poor patient prognoses, though the mechanisms by which CTAs contribute to carcinogenic outcomes are not known[77-82].

The first CTA, MAGEA1, was discovered nearly three decades ago when a patient with melanoma who was remarkably responsive to therapy was found to have cytotoxic T cells that recognized autologous cancer cells. MAGEA1 belongs to the Melanoma Antigen (MAGE) family of CTAs, a group of over 45 CTAs that share a MAGE Homology Domain (MHD), a region of ~170 amino acids with two structurally similar Winged Helix A and Winged Helix B motifs. A conserved di-leucine motif in the MHD is part of a partially hydrophobic region and participates in known MAGE protein-protein interactions[81, 83]. Outside of their tumorigenic link, MAGEs have been associated with a variety of cellular and developmental processes implicating them in neurodevelopmental and lung disorders[84].

Since the discovery of MAGEA1, several other types of CTAs have been identified, including HORMAD1. In mammalian germ cells, HORMAD1 has been shown to contribute to recombination and segregation during meiosis. Following the discoveries that HORMAD1 acts as a substrate of ATM that co-localizes with γH2AX and may interact with BRCA1, it has been suggested that HORMAD1 may play a role in DSB processing[85-88]. Identification of a role for HORMAD1 in recombinational repair in cancer cells could have huge implications for mechanisms of chemoresistance. In fact, many

CTAs are being aggressively pursued as targets for cancer treatment due to their absence in normal somatic tissue and association with various cancer endpoints.

Our overall hypothesis is that cancer cells upregulate genome maintenance proteins to aberrantly tolerate endogenous, environmental and therapeutic DNA damaging agents to promote mutagenesis and chemoresistance. We have discovered two unique regulators of RAD18 and replication-associated DNA damage tolerance that are overexpressed in cancer: RNF168 (an apical mediator of double strand break signaling) and MAGEA4 (a cancer cell-specific protein with no known function). We show here that RNF168 is a novel component of the RAD18 complex, facilitating its recruitment to stalled replication forks and promoting damage tolerance following replication stress (Chapter 2). We have also identified the cancer/testis antigen (CTA) MAGEA4 as a stabilizing binding partner of RAD18 that promotes trans-lesion DNA synthesis (Chapter 3). Finally, we show that depletion of several CTAs (MAGEA4, MAGEA10, or HORMAD1) sensitizes non-small cell lung cancer (NSCLC) cells to DNA-damaging therapies. These studies identify novel mechanisms by which NSCLC cells aberrantly overexpress germ cell proteins to alter genome maintenance, offering a cancer cell-specific mechanism by which neoplastic cells acquire chemoresistance and evade therapy (Chapter 4) (Fig. 1.2).
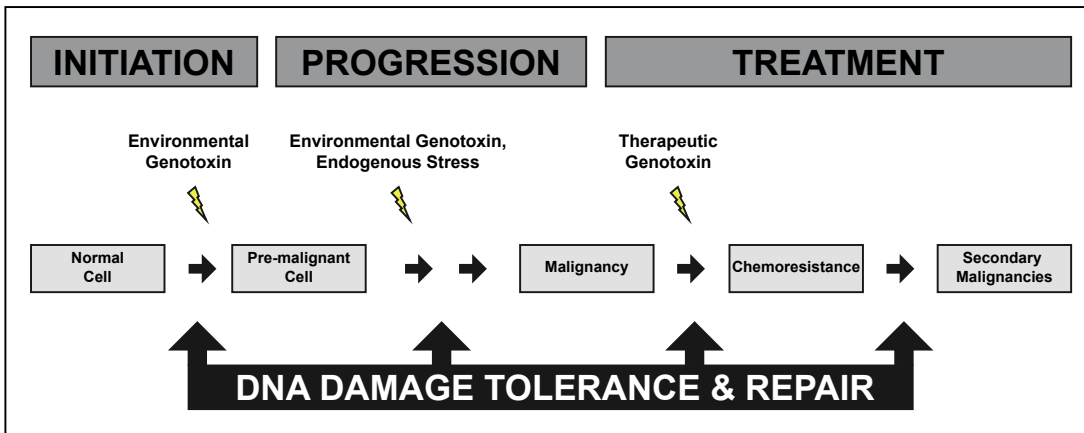
Figure 1.1 Role of DNA damage tolerance and repair in carcinogenesis
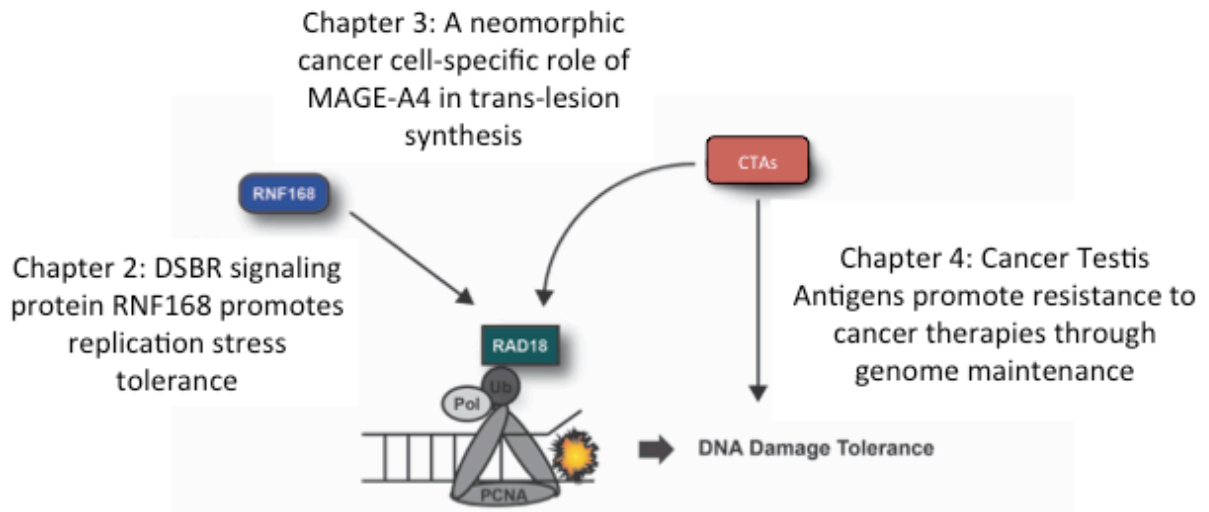
Figure 1.2 RNF168 and Cancer Testis Antigens promote DNA damage tolerance in cancer

REFERENCES

1.   Watson, I. R., et al. (2013). "Emerging patterns of somatic mutations in cancer." Nat Rev Genet **14**(10): 703-718.

2.   Stansbury, K. H., et al. (2000). "Enzyme-mediated dialdehyde formation: an alternative pathway for benzo[a]pyrene 7,8-dihydrodiol bioactivation." Chem Res Toxicol **13**(11): 1174-1180.

3.   Swenberg, J. A., et al. (2013). "Formaldehyde carcinogenicity research: 30 years and counting for mode of action, epidemiology, and cancer risk assessment." Toxicol Pathol **41**(2): 181-189.

4.   Valko, M., et al. (2004). "Role of oxygen radicals in DNA damage and cancer incidence." Mol Cell Biochem **266**(1-2): 37-56.

5.   Halliwell, B. (1991). "Reactive oxygen species in living systems: source, biochemistry, and role in human disease." Am J Med **91**(3C): 14S-22S.

6.   Poole, L. A. and D. Cortez (2017). "Functions of SMARCAL1, ZRANB3, and HLTF in maintaining genome stability." Crit Rev Biochem Mol Biol **52**(6): 696-714.

7.   Branzei, D. (2011). "Ubiquitin family modifications and template switching." FEBS Lett **585**(18): 2810-2817.

8.   Yang, K., et al. (2016). "Non-homologous end joining: advances and frontiers." Acta Biochim Biophys Sin (Shanghai) **48**(7): 632-640.

9.   Shamanna, R. A., et al. (2016). "WRN regulates pathway choice between classical and alternative non-homologous end joining." Nat Commun **7**: 13785.

10.   Heyer, W. D., et al. (2010). "Regulation of homologous recombination in eukaryotes." Annu Rev Genet **44**: 113-139.

11.   Ceccaldi, R., et al. (2016). "The Fanconi anaemia pathway: new players and new functions." Nat Rev Mol Cell Biol **17**(6): 337-349.

12.   Moldovan, G. L. and A. D. D'Andrea (2009). "How the fanconi anemia pathway guards the genome." Annu Rev Genet **43**: 223-249.

13.   Pfander, S., et al. (2007). "Reversible site-specific tagging of enzymatically synthesized RNAs using aldehyde-hydrazine chemistry and protease-cleavable linkers." Nucleic Acids Res **35**(4): e25.

14.   McCulloch, S. D., et al. (2004). "Enzymatic switching for efficient and accurate translesion DNA replication." Nucleic Acids Res **32**(15): 4665-4675.

15. Scheffner, M., et al. (1995). "Protein ubiquitination involving an E1-E2-E3 enzyme ubiquitin thioester cascade." Nature **373**(6509): 81-83.

16. Kannouche, P. L., et al. (2004). "Interaction of human DNA polymerase eta with monoubiquitinated PCNA: a possible mechanism for the polymerase switch in response to DNA damage." Mol Cell **14**(4): 491-500.

17. Watanabe, K., et al. (2004). "Rad18 guides poleta to replication stalling sites through physical interaction and PCNA monoubiquitination." EMBO J **23**(19): 3886-3896.

18. Biertumpfel, C., et al. (2010). "Structure and mechanism of human DNA polymerase eta." Nature **465**(7301): 1044-1048.

19. Bi, X., et al. (2005). "DNA polymerase kappa is specifically required for recovery from the benzo[a]pyrene-dihydrodiol epoxide (BPDE)-induced S-phase checkpoint." J Biol Chem **280**(23): 22343-22355.

20. Bi, X., et al. (2006). "Rad18 regulates DNA polymerase kappa and is required for recovery from S-phase checkpoint-mediated arrest." Mol Cell Biol **26**(9): 3527-3540.

21. Stary, A., et al. (2003). "Role of DNA polymerase eta in the UV mutation spectrum in human cells." J Biol Chem **278**(21): 18767-18775.

22. Wang, Y., et al. (2007). "Evidence that in xeroderma pigmentosum variant cells, which lack DNA polymerase eta, DNA polymerase iota causes the very high frequency and unique spectrum of UV-induced mutations." Cancer Res **67**(7): 3018-3026.

23. Waters, H. L., et al. (1993). "Ultraviolet hypermutability of a shuttle vector propagated in xeroderma pigmentosum variant cells." J Invest Dermatol **101**(5): 744-748.

24. Minko, I. G., et al. (2008). "Role for DNA polymerase kappa in the processing of N2-N2-guanine interstrand cross-links." J Biol Chem **283**(25): 17075-17082.

25. McCulloch, S. D. and T. A. Kunkel (2008). "The fidelity of DNA synthesis by eukaryotic replicative and translesion synthesis polymerases." Cell Res **18**(1): 148-161.

26. Kunkel, T. A., et al. (2003). "Functions of human DNA polymerases eta, kappa and iota suggested by their properties, including fidelity with undamaged DNA templates." DNA Repair (Amst) **2**(2): 135-149.

27. Hendel, A., et al. (2008). "Reduced efficiency and increased mutagenicity of translesion DNA synthesis across a TT cyclobutane pyrimidine dimer, but not a

TT 6-4 photoproduct, in human cells lacking DNA polymerase eta." <u>DNA Repair (Amst)</u> **7**(10): 1636-1646.

28.   Haracska, L., et al. (2001). "Physical and functional interactions of human DNA polymerase eta with PCNA." <u>Mol Cell Biol</u> **21**(21): 7199-7206.

29.   Prakash, L. (1981). "Characterization of postreplication repair in Saccharomyces cerevisiae and effects of rad6, rad18, rev3 and rad52 mutations." <u>Molecular & general genetics : MGG</u> **184**(3): 471-478.

30.   Prakash, S., et al. (1993). "DNA repair genes and proteins of Saccharomyces cerevisiae." <u>Annu Rev Genet</u> **27**: 33-70.

31.   Xiao, W., et al. (2000). "The Saccharomyces cerevisiae RAD6 group is composed of an error-prone and two error-free postreplication repair pathways." <u>Genetics</u> **155**(4): 1633-1641.

32.   Minca, E. C. and D. Kowalski (2010). "Multiple Rad5 Activities Mediate Sister Chromatid Recombination to Bypass DNA Damage at Stalled Replication Forks." <u>Molecular Cell</u> **38**(5): 649-661.

33.   Hofmann, R. M. and C. M. Pickart (1999). "Noncanonical MMS2-Encoded Ubiquitin-Conjugating Enzyme Functions in Assembly of Novel Polyubiquitin Chains for DNA Repair." <u>Cell</u> **96**(5): 645-653.

34.   Broomfield, S., et al. (1998). "MMS2, encoding a ubiquitin-conjugating-enzyme-like protein, is a member of the yeast error-free postreplication repair pathway." <u>Proc Natl Acad Sci U S A</u> **95**(10): 5678-5683.

35.   Motegi, A., et al. (2006). "Human SHPRH suppresses genomic instability through proliferating cell nuclear antigen polyubiquitination." <u>J Cell Biol</u> **175**(5): 703-708.

36.   Motegi, A., et al. (2008). "Polyubiquitination of proliferating cell nuclear antigen by HLTF and SHPRH prevents genomic instability from stalled replication forks." <u>Proc Natl Acad Sci U S A</u> **105**(34): 12411-12416.

37.   Unk, I., et al. (2006). "Human SHPRH is a ubiquitin ligase for Mms2-Ubc13-dependent polyubiquitylation of proliferating cell nuclear antigen." <u>Proc Natl Acad Sci U S A</u> **103**(48): 18107-18112.

38.   Unk, I., et al. (2008). "Human HLTF functions as a ubiquitin ligase for proliferating cell nuclear antigen polyubiquitination." <u>Proc Natl Acad Sci U S A</u> **105**(10): 3768-3773.

39.   Lin, J. R., et al. (2011). "SHPRH and HLTF act in a damage-specific manner to coordinate different forms of postreplication repair and prevent mutagenesis." <u>Mol Cell</u> **42**(2): 237-249.

40. Zeman, M. K. and K. A. Cimprich (2012). "Finally, polyubiquitinated PCNA gets recognized." Mol Cell **47**(3): 333-334.

41. Unk, I., et al. (2010). "Role of yeast Rad5 and its human orthologs, HLTF and SHPRH in DNA damage tolerance." DNA Repair (Amst) **9**(3): 257-267.

42. Fouche, N., et al. (2006). "Replication fork regression in repetitive DNAs." Nucleic Acids Res **34**(20): 6044-6050.

43. Blastyak, A. (2014). "DNA replication: damage tolerance at the assembly line." Trends Biochem Sci **39**(7): 301-304.

44. Neelsen, K. J. and M. Lopes (2015). "Replication fork reversal in eukaryotes: from dead end to dynamic response." Nat Rev Mol Cell Biol **16**(4): 207-220.

45. Weston, R., et al. (2012). "ZRANB3 is a structure-specific ATP-dependent endonuclease involved in replication stress response." Genes Dev **26**(14): 1558-1572.

46. Chiu, R. K., et al. (2006). "Lysine 63-polyubiquitination guards against translesion synthesis-induced mutations." PLoS Genet **2**(7): e116.

47. Zeman, M. K., et al. (2014). "DNA damage-specific deubiquitination regulates Rad18 functions to suppress mutagenesis." J Cell Biol **206**(2): 183-197.

48. Zlatanou, A., et al. (2015). "USP7 is essential for maintaining Rad18 stability and DNA damage tolerance." Oncogene.

49. Gao, Y., et al. (2016). "A neomorphic cancer cell-specific role of MAGE-A4 in trans-lesion synthesis." Nat Commun **7**: 12105.

50. Day, T. A., et al. (2010). "Phosphorylated Rad18 directs DNA polymerase eta to sites of stalled replication." J Cell Biol **191**(5): 953-966.

51. Barkley, L. R., et al. (2012). "c-Jun N-terminal kinase-mediated Rad18 phosphorylation facilitates Poleta recruitment to stalled replication forks." Mol Biol Cell **23**(10): 1943-1954.

52. Masuyama, S., et al. (2005). "Regulated expression and dynamic changes in subnuclear localization of mammalian Rad18 under normal and genotoxic conditions." Genes Cells **10**(8): 753-762.

53. Miyase, S., et al. (2005). "Differential regulation of Rad18 through Rad6-dependent mono- and polyubiquitination." J Biol Chem **280**(1): 515-524.

54. Raschle, M., et al. (2008). "Mechanism of replication-coupled DNA interstrand crosslink repair." Cell **134**(6): 969-980.

55.   Williams, S. A., et al. (2011). "The E3 ubiquitin ligase RAD18 regulates ubiquitylation and chromatin loading of FANCD2 and FANCI." Blood **117**(19): 5078-5087.

56.   Palle, K. and C. Vaziri (2011). "Rad18 E3 ubiquitin ligase activity mediates Fanconi anemia pathway activation and cell survival following DNA Topoisomerase 1 inhibition." Cell Cycle **10**(10): 1625-1638.

57.   Geng, L., et al. (2010). "RAD18-mediated ubiquitination of PCNA activates the Fanconi anemia DNA repair network." J Cell Biol **191**(2): 249-257.

58.   Kelly, F. J. (2003). "Oxidative stress: its role in air pollution and adverse health effects." Occup Environ Med **60**(8): 612-616.

59.   Chapman, J. R., et al. (2012). "Playing the end game: DNA double-strand break repair pathway choice." Mol Cell **47**(4): 497-510.

60.   Panier, S. and S. J. Boulton (2014). "Double-strand break repair: 53BP1 comes into focus." Nat Rev Mol Cell Biol **15**(1): 7-18.

61.   Liu, C., et al. (2014). "A fine-scale dissection of the DNA double-strand break repair machinery and its implications for breast cancer therapy." Nucleic Acids Res **42**(10): 6106-6127.

62.   Bunting, S. F., et al. (2010). "53BP1 inhibits homologous recombination in Brca1-deficient cells by blocking resection of DNA breaks." Cell **141**(2): 243-254.

63.   Kobayashi, S., et al. (2014). "Rad18 and Rnf8 facilitate homologous recombination by two distinct mechanisms, promoting Rad51 focus formation and suppressing the toxic effect of nonhomologous end joining." Oncogene **0**.

64.   Saberi, A., et al. (2007). "RAD18 and poly(ADP-ribose) polymerase independently suppress the access of nonhomologous end joining to double-strand breaks and facilitate homologous recombination-mediated repair." Mol Cell Biol **27**(7): 2562-2571.

65.   Strande, N., et al. (2012). "Specificity of the dRP/AP lyase of Ku promotes nonhomologous end joining (NHEJ) fidelity at damaged ends." J Biol Chem **287**(17): 13686-13693.

66.   Roberts, S. A., et al. (2010). "Ku is a 5'-dRP/AP lyase that excises nucleotide damage near broken ends." Nature **464**(7292): 1214-1217.

67.   Helleday, T., et al. (2008). "DNA repair pathways as targets for cancer therapy." Nat Rev Cancer **8**(3): 193-204.

68. Yu, A. M. and M. McVey (2010). "Synthesis-dependent microhomology-mediated end joining accounts for multiple types of repair junctions." Nucleic Acids Res **38**(17): 5706-5717.

69. Wyatt, D. W., et al. (2016). "Essential Roles for Polymerase theta-Mediated End Joining in the Repair of Chromosome Breaks." Mol Cell **63**(4): 662-673.

70. Wood, R. D. and S. Doublie (2016). "DNA polymerase theta (POLQ), double-strand break repair, and cancer." DNA Repair (Amst) **44**: 22-32.

71. Masutani, C., et al. (1999). "The XPV (xeroderma pigmentosum variant) gene encodes human DNA polymerase eta." Nature **399**(6737): 700-704.

72. Maher, V. M., et al. (1976). "Frequency of ultraviolet light-induced mutations is higher in xeroderma pigmentosum variant cells than in normal human cells." Nature **261**(5561): 593-595.

73. Fuertes, M. A., et al. (2003). "Biochemical modulation of Cisplatin mechanisms of action: enhancement of antitumor activity and circumvention of drug resistance." Chem Rev **103**(3): 645-662.

74. Ward, J. F. (1988). "DNA damage produced by ionizing radiation in mammalian cells: identities, mechanisms of formation, and reparability." Prog Nucleic Acid Res Mol Biol **35**: 95-125.

75. Research, L. I. f. C. (2017). "CT Database." from http://www.cta.lncc.br/.

76. da Silva, V. L., et al. (2017). "Genome-wide identification of cancer/testis genes and their association with prognosis in a pan-cancer analysis." Oncotarget **8**(54): 92966-92977.

77. Zou, C., et al. (2012). "Cancer-testis antigens expressed in osteosarcoma identified by gene microarray correlate with a poor patient prognosis." Cancer **118**(7): 1845-1855.

78. Xie, C., et al. (2016). "Melanoma associated antigen (MAGE)-A3 promotes cell proliferation and chemotherapeutic drug resistance in gastric cancer." Cell Oncol (Dordr).

79. Li, X., et al. (2015). "Evaluation of melanoma antigen (MAGE) gene expression in human cancers using The Cancer Genome Atlas." Cancer Genet **208**(1-2): 25-34.

80. Forghanifard, M. M., et al. (2011). "Cancer-testis gene expression profiling in esophageal squamous cell carcinoma: identification of specific tumor marker and potential targets for immunotherapy." Cancer Biol Ther **12**(3): 191-197.

81. Doyle, J. M., et al. (2010). "MAGE-RING protein complexes comprise a family of E3 ubiquitin ligases." Mol Cell **39**(6): 963-974.

82. Daudi, S., et al. (2014). "Expression and immune responses to MAGE antigens predict survival in epithelial ovarian cancer." PLoS One **9**(8): e104099.

83. Feng, Y., et al. (2011). "When MAGE meets RING: insights into biological functions of MAGE proteins." Protein Cell **2**(1): 7-12.

84. Lee, A. K. and P. R. Potts (2017). "A Comprehensive Guide to the MAGE Family of Ubiquitin Ligases." J Mol Biol **429**(8): 1114-1142.

85. Shin, Y. H., et al. (2010). "Hormad1 mutation disrupts synaptonemal complex formation, recombination, and chromosome segregation in mammalian meiosis." PLoS Genet **6**(11): e1001190.

86. Hill, S. J., et al. (2014). "Systematic screening reveals a role for BRCA1 in the response to transcription-associated DNA damage." Genes Dev **28**(17): 1957-1975.

87. Fukuda, T., et al. (2012). "Phosphorylation of chromosome core components may serve as axis marks for the status of chromosomal events during mammalian meiosis." PLoS Genet **8**(2): e1002485.

88. Fukuda, T., et al. (2010). "A novel mammalian HORMA domain-containing protein, HORMAD1, preferentially associates with unsynapsed meiotic chromosomes." Exp Cell Res **316**(2): 158-171.

CHAPTER 2: DSBR SIGNALING PROTEIN RNF168 PROMOTES REPLICATION STRESS TOLERANCE

2.1 Introduction

Accurate DNA replication is crucial for cell survival and maintenance of genome stability. However, the double-stranded DNA that encodes our genetic information is constantly challenged by endogenous and environmental insults. Cells are particularly vulnerable to DNA damage incurred during DNA synthesis as it can impede replication and generate unstable structures that are prone to rearrangement[1, 2].

During DNA replication, duplex DNA is unwound by helicases and then primed and engaged by the replicative DNA polymerases (Pols ε, δ, and α). Together these core components form a two-pronged fork structure termed the 'replication fork.' This complex additionally includes many other components such as PCNA (proliferating cell nuclear antigen), a DNA sliding clamp protein that serves as a loading platform for replicative polymerases, synthesis initiation and elongation proteins, and fork-protection factors[3]. As the replication fork is progressing through DNA synthesis however, damage or difficult to replicate structures that are encountered must be addressed for faithful replication to proceed.

Replication fork stalling can occur at fragile sites (e.g. stretches of nucleotide repeats), from polymerase-blocking lesions like those induced by methyl methane sulfonate (MMS, an alkylating chemotherapeutic agent) and ultraviolet (UV), via dNTP

pool depletion (e.g. mimicked by Hydroxyurea, a ribonucleotide reductase II inhibitor), and simulated by replication inhibitors (e.g. Aphidocholine, a Polα inhibitor)[4-6]. Failure to resolve stalled replisomes can result in replication fork collapse and the formation of a more severe type of DNA lesion, DNA double-stranded breaks (DSB). Cells have thus developed mechanisms for bypassing DNA damage encountered during replication. These mechanisms include error-prone trans-lesion synthesis (TLS), and error-free template switching (TS)/ fork regression to tolerate genotoxic insults and restore productive synthesis[7].

Post-translational modifications are critical components of the DNA damage response that can significantly alter cell fate. For example, distinct post-translational modifications, like ubiquitination, have been shown to dictate pathway choice in the response to DNA lesions as is observed with the E3 ubiquitin ligases RAD18 (TLS, TS, Fanconi Anemia pathway, homologous recombination), HLTF (TLS and TS), and RNF168 (DSB repair)[8-14].

Consistent with other well-described DNA damage response pathways, choice between TLS and TS is dictated ubiquitin modifications. Following replication fork stalling RAD18 is recruited to sites of RPA-coated single stranded (ss) DNA to mono-ubiquitinate ($_m$ub) PCNA. In its homotrimeric ring state PCNA slides along the DNA, acting as a docking site for polymerases and other signaling molecules. Monoubiquitination of PCNA at K164 induces a 'polymerase switch' from the replicative polymerases to TLS polymerases (η, κ, ι, ζ, and rev1), which have a higher affinity for the ubiquitinated form of PCNA[4, 15]. Unlike the replicative polymerases which have a strict requirement for undamaged bases, TLS polymerases are able to synthesize

across a damaged template and allow for resumption of replication, although mechanisms for damage-specific recruitment of TLS polymerases are not fully understood[16, 17].

In contrast, error-free TS uses the newly synthesized sister chromatid DNA as a template to accurately 'bypass' or 'avoid' lesions on the damaged template. Activation of TS in humans is thought to be mediated by poly-ubiquitination of PCNA by the RAD5 (in S. cerevisiae) homologs: helicase-like transcription factor (HLTF) and SNF2 Histone-linker PHD-finger RING-finger Helicase (SHPRH)[12, 13, 18-20]. A study by Lin et al. identified damage-specific roles for HLTF and SHPRH in high fidelity tolerance of UV and MMS lesions, respectively[8]. This mode of DNA damage tolerance also involves RAD18, which contributes not only mono-ubiquitination of PCNA, allowing for further extension of K63-linked poly-ubiquitin chains by the RAD5 homologs, but also mediates damage-specific responses of HLTF and SHPRH through direct binding[8, 21]. Although recent publications have made headway in identifying novel regulators of DNA damage tolerance, including the influence of additional E3 ubiquitin ligases, but the exact mechanisms determining pathway choice and how it may influence genome instability diseases are not known[22-26].

Defects in genome maintenance mechanisms are responsible for a variety of severe clinical defects associated with many genetic diseases and cancer. Indeed, defects in the E3 ubiquitin ligase and DSB repair signaling protein, RNF168, are responsible for a rare genetic disease known as RIDDLE syndrome in which patients exhibit radiosensitivity, immunodeficiency and have a predisposition to cancer. Here we show that RNF168 localizes to replication factories in a noncanonical manner to promote DNA

synthesis following exposure to fork-stalling DNA damaging agents. RNF168 additionally binds and recruits RAD18 to chromatin, facilitating ubiquitination of PCNA and conferring replication stress tolerance.

2.2 Methods

Cell culture and transfection

hTERT-expressing normal human dermal fibroblasts (NHF) were provided by Dr. William Kaufmann (UNC Chapel Hill). RIDDLE hTERT fibroblast cells stably expressing vector or HA-RNf168, MRC5 and shRNF168- inducible U2OS were provided by Dr. Grant Stewart (University of Birmingham). Immortalized Cancer cell lines H1299, HeLa, U2OS, and 293T were purchased from the American Type Culture Collection (ATCC) and used for the described experiments without further authentication. H1299 RAD18-/- cells were generated by Dr. Yanzhe Gao and previously described[22]. U2OS RNF168 -/- and U2OS RNF8-/- cells were generated by Amélie Fradet-Turcotte and were a gift from the lab of Dr. Daniel Durocher. All cell lines were cultured in DMEM medium supplemented with 10% fetal bovine serum and penicillin–streptomycin (1%). Plasmid DNA and siRNA oligonucleotides were transfected using Lipofectamine 2000 (Invitrogen) according to the manufacturer's instructions, except that concentrations of plasmid DNA and Lipofectamine 2000 used in each transfection reaction were decreased by 50% to reduce toxicity.

Immunoprecipitation and immunoblotting

Lysates of cultured cells were washed three times in ice-cold PBS and lysed in 500 µl of ice-cold cytoskeleton buffer (CSK buffer; 10 mM Pipes pH 6.8, 100 mM NaCl, 300

mM sucrose, 3 mM MgCl2, 1 mM EGTA, 1 mM dithiothreitol, 0.1 mM ATP, 1 mM Na3VO4, 10 mM NaF and 0.1% Triton X-100) freshly supplemented with Protease Inhibitor Cocktail and Phostop (Roche). For subfractionation, lysates were centrifuged at 4,000 RPM for 4 min at 4°C. The supernatant containing a mixture of cytosolic plus nucleosolic proteins was aliquoted and detergent-insoluble nuclear fractions were washed once with 1 ml of CSK buffer. Insoluble (chromatin) fractions were then resuspended in a minimal volume of CSK and sonicated to release chromatin before analysis by SDS–PAGE and immunoblotting.

For all immunoprecipitation experiments, input samples were normalized for protein concentration. Sepharose or magnetic beads containing covalently conjugated antibodies against epitope tags were added to the extracts and incubations were performed overnight at 4°C using rotating racks. Immune complexes were recovered using magnetic stands (magnetic beads) or centrifugation (sepharose beads). The beads were washed five times with 1 ml CSK to remove nonspecifically-bound proteins. The washed immune complexes were boiled in Laemmli buffer for 10 min, to release and denature for SDS–PAGE.

For immunoblotting, cell extracts or immunoprecipitates were separated by SDS-PAGE, transferred to nitrocellulose membranes, blocked in 5% milk in TBST, and incubated overnight with the following primary antibodies: PCNA (sc-56), Chk1 (sc-7898), β-actin (sc-130656), GAPDH (sc-32233), RNF8 (sc-271462), HA.F7 (sc-7392) and GST (sc-53909) from Santa Cruz Biotech; Polη (A301-231A), RAD6 (A300-281A), RAD18 (A301-340A), Polκ (A301-975A), and HLTF (A300-230A) from Bethyl; MYC-Tag (2276) from Cell Signaling; H2A (05-678), γH2AX (05-636), RNF168 (06-1130) from

Millipore; ORC4 (H83120) Transduction Labs; FLAGM2 (F1804) from Sigma-Aldrich; HA.11 (ENZ-ABS118) Enzo Life Sciences; DDDDK–tag magnetic beads (M185-9), MBL International; CldU, AbD Serotec; IdU, Becton Dickinson; BrdU (556028) BD Pharmingen; β-tubulin, AbCam. Antibody dilutions used for immunoblotting were 1:1,000, with exceptions for the following antibodies: RNF168 (1:3000) PCNA (1:500), GAPDH (1:3,000) and γH2AX (1:5,000).

Expression plasmids

Mammalian expression vectors for HA- and MYC-tagged forms of RAD18 have been described previously[15, 27]. FLAG RNF168, GFP-RNF168 and FLAG-RNF8 constructs were provided by Dr. Grant Stewart have been described previously[14]. FLAG-HLTF expression vector was gifted by Dr. Karlene Cimprich.

RNAi

For transfection, two separate tubes were prepared, one containing siRNA and serum-free Optimem, and the other with Lipofectamine 2000 and serum-free Optimem. These separate mixtures were incubated for 5 min at room temperature in the dark before being combined and incubated for an additional 20min, according to Dharmacon and Lipofectamine manufacturer's protocols. Cells were trypsinized and resuspended in antibiotic-free medium and plated directly into the siRNA/Optimem/Lipofectamine solution at 50% confluence to incubate overnight. The following morning media was changed to remove Lipofectamine. Cell lysates were harvested 48 hrs post-transfection. Sequences of siRNA oligonucleotides used here are as follows: control non-targeting siRNA, 5'-UAGCGACUAAACACAUCAA-3' (Thermo Fisher Scientific); RAD18 3'-untranslated region siRNA, 5'-UUAUAAAUGCCCAAGGAAAUU-3-; RNF168 siRNA #1,

27

siGENOME Smartpool Dharmacon (Cat# M-007152-03); RNF168 siRNA #2, 5'-GAGAA UAUGAAGAGGAAAUUU-3'; RNF168 siRNA #3, 5'-GAAGAGUCGUGCCUACUGAUU-3'; and RNF8 siGENOME Smartpool Dharmacon (Cat# M-006900-01).

Genotoxin treatment

For UV treatment, culture medium was removed from cultured cells, which were then irradiated using a UV cross-linker (Stratagene) or left untreated for mock. The UV-C dose delivered to the cells was confirmed with an ultraviolet radiometer (UVP, Inc.). Media was replaced and plates were returned to the incubator and harvested 2 hrs later, unless otherwise indicated. For IR irradiation plates were placed in the Rad Source RS2000 for treatment with X-ray irradiation at the indicated dose and incubated for 1 hr before harvest unless otherwise indicated. The RS2000 machine is calibrated and maintained by the Lineberger Cancer Center. For cisplatin (CDDP) cells were treated with 20 μM CDDP and incubated for 6 hrs in the dark before harvest. For Mitomycin C (MMC) treatment cells were treated with 100nM MMC and incubated for 2hrs prior to harvest. For Hydroxyurea (HU) treatment cells were treated with 2mM HU (immunoblotting) or 1mM (immunofluorescence) and incubated for 24 hrs prior to harvest.

Fluorescence microscopy

MRC5, U2OS WT, U2OS RNF168KO, RIDDLE + vector and RIDDLE +HA-RNF168 cells were transfected with the indicated expression plasmids or siRNA and grown to ~60% confluency on glass cover slips (Thermo Scientific #3422). Twenty-four hrs after plating, cells were treated with the indicated agent (or mock) and harvested at the indicate time points. Cells were pre-extracted, fixed and immunostained with anti-PCNA,

anti-HA, anti-CldU, anti-IdU or detected by click chemistry (EdU), and stained with DAPI (Vectashield). Imaging was done on the Zeiss 710 confocal microscope, in the UNC Microscopy Services Laboratory core facility, as described previously[28].

DNA fiber analysis

DNA fiber analysis was carried out as was described previously [29, 30]. USOS cells transfected with the indicated siRNAs. Twenty-four hrs after treatment cells were plated on coverslips (Thermo Scientific #3422). Cells were pulsed with 250µM CldU for 30min, irradiated with 20J/m2 UV, and pulsed with 250µM IdU for 30min prior to harvest and fiber spreading. For quantification of replication structures, at least 300 structures were counted per experiment. The lengths of red or green labeled tracts were measured using ImageJ (National Institutes of Health; http://rsbweb.nih.gov/ij/) and arbitrary length values were converted into micrometers using the scale bars created by the microscope.

ssDNA assay

RIDDLE cells stably expressing vector or HA-RNF168 cells were pulsed with 250µM IdU for two days. Cells were then treated with mock or UV irradiation (40J/m^2) and 8 hrs later were pulsed with 250µM CldU for 30min before harvest. IdU immunostaining was done under non-denaturing conditions and antibody was fixed prior to denaturing CldU processing. DNA was visualized with DAPI. Data represent mean ± SEM of three independent experiments.

DNA synthesis assay

H1299 cells were treated with siRNA targeting control, RAD18 or RNF168. 24 hours after transfection, cells were re-plated in wells of 24-well plates (in replicate) for 3H

thymidine incorporation and 10cm dishes for immunoblotting, for each time point replicate cultures for each time points. Wells were treated with mock or 5J/m^2 UV irradiation. At the indicated time points cells were then pulsed with 0.5mCi/ml [3H]-methyl thymidine (Perkin Elmer) for 30min. At the indicated time points after re-plating, the amount of radiolabel incorporated into the trichloroacetic acid-insoluble genomic DNA fraction was determined using scintillation counting as described previously[31, 32]. Protein was harvested from the 10cm plates at corresponding times to evaluate relevant proteins. RIDDLE cell experiments were processed as H1299 with the exception of transfection.

Flow cytometry

Cells were labeled with 10 μM BrdU (5-Bromodeoxyuridine) 30 minutes before harvest. Cells were collected by trypsinization, fixed in 35% ethanol for 24 hrs, then stained with anti-BrdU and propidium iodide as previously described[27]. Stained nuclei were analyzed by flow cytometry on an Accuri C6 flow cytometer (BD, Oxford, UK) using the manufacturer's software.

Survival

Replicate cultures of stably-expressing vector or HA-RNF168 RIDDLE patient cells were plated at low density in 6-well plates (3-wells per treatment). 24hrs post-plating cells were treated with UV radiation (0, 5, 10 Jm^{-2}). After two weeks plates are washed with 1xPBS, and fixed and stained with crystal violet. Plates were scanned and the Image J colony counter plugin was used to quantify density[33, 34].

SupF mutagenesis assay

Reporter plasmids harboring UV lesions were transfected into control, RAD18 and RNF168 over-expressing 293T cells, each in triplicate. After 48 hrs plasmids are recovered from cells, transformed into MBM7070 bacteria, and plated on agar containing IPTG and X-Gal. Mutation frequency is determined as the ratio of mutant (white) colonies to the total (white and blue) number of colonies as described previously[22, 35].

2.3 Results

RNF168 localizes to replication fork sites.

RNF168 ligase activity has been canonically associated with ubiquitination of histones H2A/H2AX in the signaling response to DSB. Recent studies suggest that RNF168-dependent chromatin modifications may play a role in altering other cell signaling processes[1, 36, 37]. Interestingly, a study by Raschle et al. found that RNF168 chromatin recruitment was sensitive to inhibition of replication by geminin[1]. Furthermore, several other reports have suggested a role for histone ubiquitination in replication and replication stress[38-41]. To investigate whether RNF168 plays a role in replication-associated activities we wanted to determine if RNF168 was present at replication factories. We looked at co-localization of GFP-RNF168 with PCNA, a key replication fork component in untreated cells or those treated with ultraviolet radiation, which blocks synthesis via the formation of bulky DNA adducts, or HU, which depletes dNTPs in the cells, stalling replication forks. Mock treated cells exhibited minimal localization to sites of replication forks. However, upon treatment with an agent that

induces replication stress (UV or HU), RNF168 co-localized with PCNA foci (Fig 2.1A). Additionally, we found that GFP-RNF168 began to localize at early to mid s-phase PCNA foci at one hour after UV-C irradiation. This colocalization was maintained at 6 and 24 hours, as damaged cells accumulated in late s-phase (Fig. 2.1B).

To determine whether the colocalization of RNF168 with PCNA was indeed at sites of replication forks, we also measured focal localization of RNF168 with EdU (marking sites of newly synthesized DNA) in mock- and HU-treated stably complemented HA-RNF168 h-TERT RIDDLE fibroblasts. Indeed RNF168 also localized at EdU foci following treatment with fork-stalling HU, further demonstrating that RNF168 is recruited to sites of DNA synthesis during replication stress (Fig. 2.9D).

RNF168 associates with RAD18 and promotes its recruitment to chromatin.

After identifying that RNF168 was recruited to replication forks following treatment with fork-stalling agents we next sought to determine whether it was interacting with any known DNA damage tolerance (DDT) components. Fractionated lysates from shRNF168 inducible U2OS cells that were mock or UV irradiated with 20J/m2 were probed for a series of DDT-associated proteins, including the E3 ubiquitin ligase RAD18 (Fig. 2.2A). As expected, UV treatment increased the protein levels of RAD18 (both in total lysate and on the chromatin). Interestingly, however, shRNA-induced silencing of RNF168 diminished RAD18 recruitment to chromatin and abolished the induction of RAD18 on the chromatin usually observed following UV-treatment. RAD18 was instead sequestered in the soluble (cytosolic/ nucleosolic)-component of the harvested lysate.

Consistent with these findings, H1299 lung adenocarcinoma cells treated with siRNAs targeting multiple regions of RNF168 were irradiated with mock or 20J/m^2 UV.

RNF168-depleted cancer cells exhibited substantially decreased recruitment of RAD18 to damaged chromatin. RNF8 (the E3 ubiquitin ligase that has been shown to influence RNF168 recruitment to damaged DNA) depletion reduced levels of both RNF168 and RAD18 on chromatin (Fig. 2.2B). Further, RNF168-depleted cancer cells, RIDDLE patients cells exhibited a similar diminished recruitment of RAD18 to chromatin, which was restored in RIDDLE cells stably-complemented with HA-RNF168(Fig. 2.2C).

To determine whether or not RNF168 alters RAD18 distribution via direct interaction, H1299 cells expressing MYC-RAD18, FLAG-RNF168, or both were subjected to anti-FLAG immunoprecipitation (IP). IP of RNF168 (co-expressed with RAD18) pulled down both RAD18 and its E2 ubiquitin-conjugating enzyme, RAD6 (Fig. 2.2D). Reciprocal IP of ectopically expressed RAD18 in 293T cells also resulted in RNF168 co-immunoprecipitation (Fig. 2.8A). Additionally, size-exclusion chromatography from lysates of cultured cells revealed a ~500 kDa complex containing RAD18, RAD6 and RNF168 (Fig. 2.8E).

RNF168 promotes replication fork progression.

To determine whether RNF168 contributes to replication fork progression we examined rates of DNA synthesis using [3H] thymidine incorporation in RIDDLE patient cells following low-dose UV-treatment. RIDDLE patient cells displayed UV-induced inhibition of DNA synthesis when compared to the isogenic RNF168-complemented RIDDLE cells (Fig. 2.3A). Extending this observation, RNF168-depleted lung cancer cells phenocopied RAD18 depletion in defective recovery of DNA synthesis following UV-induced replication fork stalling (Fig. 2.3C). Chromatin-bound RAD18 is diminished in RNF168-defective cells correlating with defective DNA synthesis rates (Fig. 2.3A-D).

To further determine the impact of RNF168 on replication fork progression we performed DNA fiber analysis in U2OS cells treated with control or RNF168 siRNA, followed by mock or UV irradiation. RNF168-depleted cells showed elevated levels of 1st label termination structures, indicative of fork stalling, compared with control cells, and these were further augmented by UV treatment (Fig. 2.3E). Of note, RNF168 depletion by siRNA does not alter global DNA synthesis rates in U2OS cells as measured by BrdU/PI (Fig. 2.3F).

Replication fork stalling triggers uncoupling of the helicases and replicative polymerases, generating stretches of vulnerable single stranded DNA (ssDNA). We used a thymidine analog ssDNA assay to determine whether or not prolonged fork stalling in the absence of RNF168 coincided with generation of ssDNA. RIDDLE and HA-RNF168 complemented RIDDLE cells were pulsed labeled with IdU two days prior to UV treatment and subsequent 30 minute CldU labeling before harvest. Non-denaturing IdU immunostaining detects ssDNA whereas denaturing CldU immunostaining (following fixation) identifies replicating cells. The amount of single-stranded DNA (ssDNA) generated in RIDDLE cells following UV treatment was significantly higher than that of the stably complemented HA-RNF168 RIDDLE cells, indicating that there were more stalled forks in these cells (Fig. 2.3G-H).

RNF168 promotes ubiquitination of PCNA

Ubiquitination of PCNA is a critical post-translational modification that alters cellular response (and pathway choice) following replication stress. RNF168 expression is able to promote ubiquitination (mono, bi and tri) of PCNA. To determine whether RNF168 overexpression causes global DNA synthesis defects thus leading to $_m$ub (mono-

ubiquitinated)-PCNA, we examined the cell cycle profiles of empty vector and FLAG-RNF168 transfected H1299 lung adenocarcinoma cells. RNF168 over-expressing cells had no change in the s-phase population compared to the non-overexpressing cells measured by BrdU/PI (Fig. 2.4A). Previous reports have shown recombinant RNF8 was able to ubiquitinate PCNA in vitro, however, expression of RNF8 in cells was unable to promote ubiquitination of PCNA. As expected, ubiquitination of γH2AX was increased in RNF168 over-expressing cells, and ub-γH2AX following ionizing radiation was enhanced by both RNF168 and RNF8 overexpression, confirming that the expressed proteins were indeed functional[42](Fig. 2.4B).

To gain further insight into the function of RNF168 in the context of replication stress we made use of a series of RNF168 domain mutants. The catalytic RING (Really Interesting New Gene, zinc finger) domain mutants of RNF168 (ΔRING, C19S- point mutation that diminishes activity) are defective for ub-H2A and recruitment of 53BP1 and BRCA1 following DSB. The MIU (Motif Interacting with Ubiquitin) domain mutants (ΔMIU1, ΔMIU2, ΔMIU 1+2 and A179G/A450G) are required for localization of RNF168 binding to DSBs[14]. We look at the ability of GFP-RNF168 mutants (in U2OS RNF168 -/- cells) to localize at replication factories using PCNA as a replicative marker. Interestingly, the ΔMIU2 mutant, which fails to localize following IR was competent for colocalization with PCNA after UV suggesting a distinct, and novel mechanism for RNF168 recruitment to stalled forks. There also appeared to be some constitutive overlap between GFP-RNF168 ΔRING and PCNA, that was not seen with WT RNF168 (Fig. 2.4C).

Separation of function RNF168

We used FLAG-tagged RNF168 constructs with the same series of mutations to examine the impact on PCNA and RAD18. The contribution of RNF168 to damage tolerance was bifunctional: catalytically-inactive RNF168 (ΔRING, C19S) supported PCNA ubiquitination activity, however, was defective for RAD18 redistribution to chromatin (Fig. 2.5A, 2.5B, 2.8C). Additionally, point mutations in the UBZ (ubiquitin-binding zinc finger) domain of RAD18 were unresponsive to RNF168 (Fig. 2.5C, D). Overall these results suggest that RAD18 recruitment to chromatin following replication stress is mediated by RNF168-dependent chromatin modification, and ub-PCNA is influenced by RNF168 binding to ubiquitinated substrates.

Role for RNF168 in DNA damage tolerance

To determine whether RNF168 directly impacts genome maintenance we a supF mutagenesis assay to measure mutation rates corresponding with lesion bypass of UV-damaged pSP189 supF plasmid. Consistent with previous reports, we showed that ectopic expression of RAD18 suppressed UV-induced mutagenesis[22]. RNF168 was able to phenocopy RAD18 in suppressing mutagenesis of the UV-damaged supF reporter, influencing replicative bypass of ultraviolet-induced DNA lesions (Fig. 2.6A).

As overexpression of RNF168 promoted ubiquitination of PCNA, we also asked whether cells lacking endogenous RAD18, the primary effector of ub-PCNA, would be affected by RNF168 overexpression. Somewhat surprisingly, H1299 RAD18 -/- overexpressing RNF168 displayed a moderate increase in $_m$ub-PCNA, as compared to control. This suggests both that RNF168 promotion of poly-ub-PCNA is primarily

moderated via RAD18 but may also impact RAD18-independent ub-PCNA (Fig. 2.5B, 2.6B).

In response to UV, HLTF binds to RAD18, promotes poly ub-PCNA and high-fidelity bypass of UV lesions[8]. Interestingly, RNF168 depletion decreased HLTF binding to chromatin in UV-damaged cells (Fig. 2.6C). The impact of RNF168 on HLTF was also observed in response to other fork-stalling agents and in RIDDLE cells (Fig. 2.10A-B). We additionally saw that RAD18-HLTF binding was severely reduced in U2OS RNF168 -/- cells as compared to U2OS WT (Fig. 2.6D). Previously published work has shown that HLTF influence binding of RAD18 with trans-lesion polymerase η[8]. Pol η recruitment to chromatin after UV is also diminished following depletion of RNF168 (Fig. 2.6E, 2.3D).

Data from The Cancer Genome Atlas (TCGA) shows that many cancers, including lung squamous cell carcinoma's have elevated levels of RNF168 (Fig. 2.6F). We found that RIDDLE patient cell lines expressing RNF168 exhibited enhanced survival following UV irradiation. Interestingly, levels of RNF168 in the complemented RIDDLE cells are much higher than those in normal human fibroblasts (NHF) (Fig. 2.6G). Taken together these results suggest a role for RNF168 in tolerance of UV-induced replication stress.

2.4 Discussion

RNF168 localizes to replication forks and mediates RAD18 redistribution

Stalled replication forks elicit an elaborate signaling cascade that links cell cycle stage with recruitment of appropriate repair factors. Previous research has shown that depletion of ubiquitin interferes with replication-associated DNA repair without affecting

replication, suggesting that ubiquitination events play a key role in the assembly of DNA damage tolerance complexes at stalled replication forks[1]. Indeed, Vassilev et al. showed that there are not only higher levels of ub-H2A in proliferating cells than non-proliferating but there is also partial co-localization of ub-H2A with PCNA-suggesting a role for ub-H2A in maintenance of DNA replication [41, 43]. We have identified a noncanonical role for the E3 ubiquitin ligase and histone H2A modifier RNF168 in promoting replication-associated damage tolerance.

Following exposure to fork-stalling agents, RNF168 localizes to sites of replication forks (Fig. 2.1A, 2.9D). Additionally, we identified RNF168 as a novel component of RAD18 complexes (Fig 2.2D, Fig 2.8A)- RAD18 is a central regulator of pathway choice in replication-associated DNA damage tolerance. RNF168 depletion severely diminishes RAD18 re-localization to chromatin and abolishes the induction of RAD18 normally observed following replication stress (Fig. 2.2A-C, 2.8B, 2.8D). RAD18 depletion has also been shown to sensitize cells to DNA damage and increase mutation rates in cells[9, 44, 45]. Thus following genotoxic insult RNF168 may alter cellular response and mutagenesis in cells by altering RAD18-dependent signaling.

RNF168 mediates replication fork progression following genotoxic injury

Cells are particularly vulnerable to injury during S-phase of the cell cycle when unrepaired lesions can interfere with DNA synthesis and cell proliferation. We found that RNF168-deficiency impairs recovery from replication fork stalling and recapitulates hallmarks of defective DNA damage tolerance- namely persistent checkpoint signaling and decreased DNA synthesis[28, 46-48]. Both RIDDLE patient cells and H1299 lung adenocarcinoma cells depleted of RNF168 are defective in checkpoint recovery

following low-dose UV-treatment (Fig. 2.3A-D). RNF168-depleted cells showed elevated

of fork stalling by DNA fiber analysis that was further augmented by UV treatment (Fig.

2.3E). Additionally, the amount of vulnerable ssDNA generated in RIDDLE cells

following UV treatment was significantly higher than that of the stably complemented

HA-RNF168 RIDDLE cells (Fig. 2.3H).

RNF168 promotes ubiquitination of PCNA

Ubiquitination of PCNA is a critical post-translational modification that alters cellular

response to replication stress. Interestingly, RNF168 overexpression massively induced

ub-PCNA (Fig. 2.4A, 2.9A-C). Catalytically-inactive RNF168 (ΔRING, C19S), however,

supported PCNA ubiquitination activity, suggesting that RNF168 is not a direct mediator

of ub-PCNA when RAD18 is intact (Fig. 2.5B). Additionally, RNF168-depletion did not

impact $_m$ub-PCNA following treatment with replication-stalling agents (data not shown),

suggesting that RNF168-influenced ub-PCNA may favor poly-ubiquitination. Of note,

mouse embryonic fibroblasts with a double knockout of SHPRH and HLTF (the E3

ubiquitin ligases thought to be responsible for damage-associated poly-ub-PCNA) retain

the ability to poly-ub-PCNA, thus it is possible that under extreme circumstances

RNF168 may adopt PCNA as a substrate[49]. In fact RNF168 does contain a

degenerative PCNA-interacting-protein (PIP) box motif (Fig. 2.9E) [28, 50, 51]. An important

avenue warranting further investigation is whether PCNA can act as a direct substrate

of RNF168 (e.g. via PCNA K164R and ubiquitin K63R mutants)[26].

A previous publication showed that purified RNF8 (the E3 ubiquitin ligase that acts

upstream of RNF168 in DSB repair signaling) induced ub-PCNA *in vitro*[37]. However*, in*

vitro ubiquitination models sometimes reveal activity that isn't relevant *in vivo* and RNF8

ub-PCNA does not appear to be recapitulated in a cell-based system (Fig. 2.4B)[52].

Response of RNF168 to replication stress is distinct from response to DSB

RNF168 accumulation at sites of DSBs is dependent on its MIU domains

(particularly MIU2), which recognize RNF8-catalyzed ub-H2A/H2AX[14]. When trying to

determine the functional requirements for RNF168 in response to replication stress we

expressed a series of GFP-RNF168 mutants in U2OS RNF168 -/- cells and looked at

co-localization with PCNA with and without UV treatment. Interestingly, the ΔMIU2

mutant, which fails to localize following IR, was competent for co-localization with PCNA

after UV (Fig. 2.4C). This suggests that RNF168 recruitment following replication fork

stalling is independent of its canonical recruitment in the context of DSB. None of the

mutants on-hand exhibited severe deficiency in localizing to replication fork sites

following UV irradiation (Fig. 2.5A). This suggests that RNF168 localization to

replication factories following treatment with fork-stalling agents may be mediated

through a third, UMI domain (UIM and MIU-related ubiquitin binding domain). Pinato et

al. found that combined inactivation of all three RNF168 ubiquitin-binding domains

rendered RNF168 unable to localize to DNA damage response foci and unable to form

poly-ubiquitin chains[53]. Thus future studies should investigate a potential role for the

UMI motif in directing RNF168 localization to replisomes following replication stress.

Intriguingly, there appears to be some constitutive overlap between GFP-RNF168

ΔRING and PCNA that is not seen with WT RNF168 (Fig. 2.4C). This could suggest that

the ΔRING mutant is more stable for basal localization to replication factories or

possibly indicates the existence of a scaffold-like protein that recruits non-catalytic RNF168 to replisomes in a damage-free context.

RAD18 localizes to stalled replication forks following RNF168-ubiquitination events

We found that RNF168-dependent recruitment of RAD18 needed the RNF168 catalytic RING domain, suggesting chromatin-modification facilitates RAD18 redistribution (Fig. 2.5A, 2.5B, 2.8C). Indeed, point mutations in the UBZ (ubiquitin-binding zinc finger) domain of RAD18 were unresponsive to RNF168 (Fig. 2.5C, 2.5D). Previous studies have demonstrated a role for RAD18 in DSB repair signaling, especially in promoting homologous recombination (HR) [10, 11, 54, 55]. RAD18 recruitment to sites of DSB appears to be mediated through its UBZ domain, which recognizes ub-H2A, a substrate of RNF168 and RNF8. Indeed RNF8/RNF168 have been shown to be necessary for RAD18/SLF1/SLF2 recruitment to DSB sites. However, SLF1/ SLF2 are not needed for ub-PCNA or polη recruitment, suggesting that the RAD18/SLF1/SLF2 complex promotes function of SMC5/6 in HR and is not required for bypass of replication-blocking lesions[1]. Similarly, Hu et al. found that unlike RNF168, RAD18 specifically competes with 53BP1 for recognition of ubiquitinated histone substrates. Furthermore, the RAD18 ligase activity that is needed for replication stress tolerance is dispensable for its role in HR[11, 56]. Finally, Panier et al. noted that in the DSB response, the ubiquitin-dependent recruitment of RNF168 and RAD18 is 'temporally and genetically distinct'. This group added that the E3 ubiquitin ligase RNF169, a negative regulator of RNF168, was dispensable for the recruitment of RAD18 in the context of DSB. We, however, see that compared to RNF168, RNF169 diminishes recruitment of

RAD18 to chromatin following treatment with a fork-stalling agent[57](Fig. 2.11). Our findings identify a new role for RNF168 in promoting redistribution of RAD18 to stalled replication forks.

RNF168 promotes DNA damage tolerance

Chromatin often serves as a loading platform for various DNA damage signaling, tolerance and repair proteins thus chromatin modifications can significantly alter response fate. We found that the ubiquitin ligase RNF168 is able to promote error-free bypass of UV induced DNA adducts, in a manner similar to RAD18, further cementing a novel role for RNF168 in tolerance of fork stalling lesions (Fig. 2.6A).

Interestingly, RNF168 overexpression in H1299 RAD18-/- cells was able to promote ub-PCNA, although to a far less amount than when over-expressed in the presence of RAD18 (Fig. 2.6B). This suggests both that ub-PCNA promoted by RNF168 is primarily mediated through RAD18 but also that it may, to a lesser extent, contribute to RAD18-independent ub-PCNA. RAD18-independent ub-PCNA could be mediated by CRL4/CDT2, a ubiquitin ligase that promotes degradation of PCNA-bound proteins, which was suggested to $_m$ub-PCNA[26]. However limitations in experimental design suggest that RAD18 could still mediate this ubiquitination activity. Another study by Lin et al. identified a role for HLTF-mediated $_m$ub-PCNA following UV irradiation that promoted recruitment of TLS polymerase η while inhibiting SHPRH function. Intriguingly, the RAD18 UBZ domain required for responsiveness to RNF168 is also required for RAD18-HLTF binding. We found that RNF168 depletion reduced chromatin-bound HLTF and polymerase η, and that RNF168 -/- cells reduced HLTF-RAD18 binding (Fig. 2.3D, 2.6C-E, 2.10A-B). RAD18 ligase activity is carried out in its

heterotrimeric state (RAD18$_2$:RAD6) and thus doesn't necessitate competition between HLTF and RNF168 for the RAD18 UBZ[9].

In addition to its ligase activity, HLTF can also act as an annealing helicase and mediate fork reversal- a proposed mechanism for template switching that allows lesion bypass by providing access to a newly synthesized sister chromatid [2, 24]. Further work by Cimprich group found that treatment with methyl methanesulfonate (MMS), a potent chemotherapeutic and replication fork-stalling agent, promotes HLTF degradation and SHPRH/RAD18 interaction with TLS polymerase κ[8]. Taking these studies into account, future experiments should explore roles for RNF168 in fork reversal as well as damage-specific TLS polymerase recruitment and lesion tolerance that may ultimately contribute to the severe clinical manifestations seen in RIDDLE patients.

Delicate balance of RNF168 and DNA damage tolerance

In general, DNA damage tolerance pathways need to be tightly regulated. For example, RAD18 deficiency can increase mutation rates and induce DNA damage sensitivity. Overexpression of RAD18 can also be detrimental, disrupting recruitment of repair proteins and promoting error-prone TLS polymerases in the absence of DNA damage, that contribute to mutagenesis and cancer [48, 58-61]. RNF168 regulation suffers a similar fate: loss of RNF168 is responsible for the radiosensitivity, immunodeficiency and increased risk of cancer observed in RIDDLE syndrome patients, but RNF168 is also overexpressed in many cancers (Fig. 2.6F). RIDDLE patient cells complemented with RNF168 were shown to display enhanced tolerance of UV-radiation by cell survival assays, where levels of RNF168 are much higher than those in normal human fibroblasts (NHF) (Fig. 2.6G). This supports a gain-of-function role for RNF168 in

promoting DNA damage tolerance and carcinogenesis when it is over-expressed in

cancer. Taken together these results identify a role for RNF168 in tolerance of

replication stress and enforce the delicate balance DNA damage tolerance pathways

require to maintaining genome integrity (Fig. 2.7).
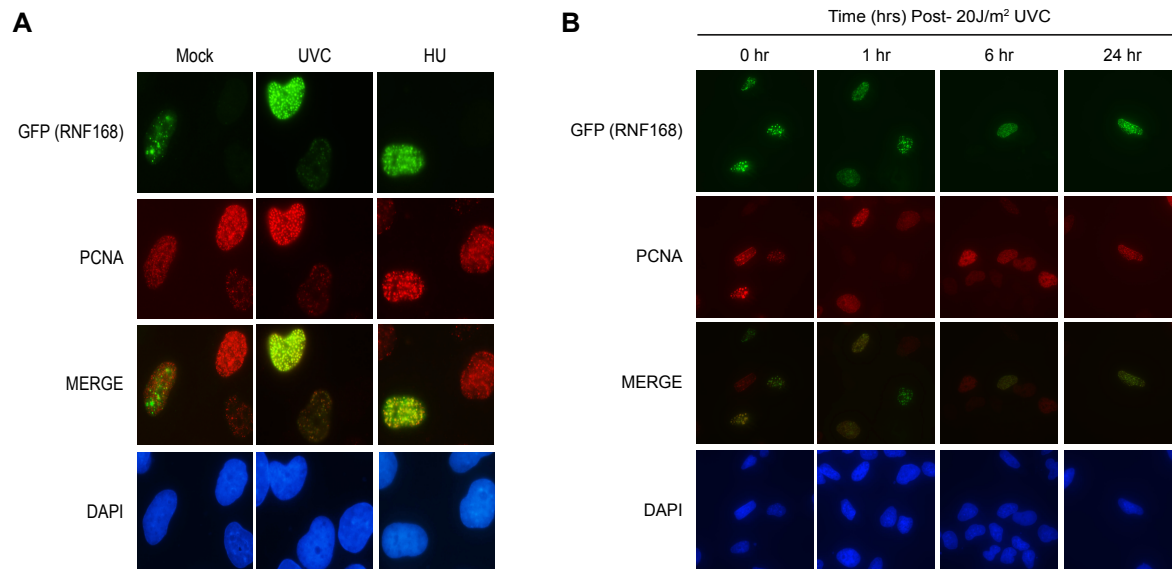
Figure 2.1 RNF168 localizes to replication forks

(A) MRC5 cells expressing GFP-RNF168 were left untreated or treatment Hydroxyurea (1mM) or UV radiation (20J/m2). Cells were fixed and processed for GFP fluorescence and PCNA immunofluorescence. DNA was stained with DAPI.
(B) MRC5 cells were either irradiated with 20J/m2 or mock treated. At the indicated time points cells were fixed and processed for GFP fluorescence and PCNA immunofluorescence. DNA was stained with DAPI.
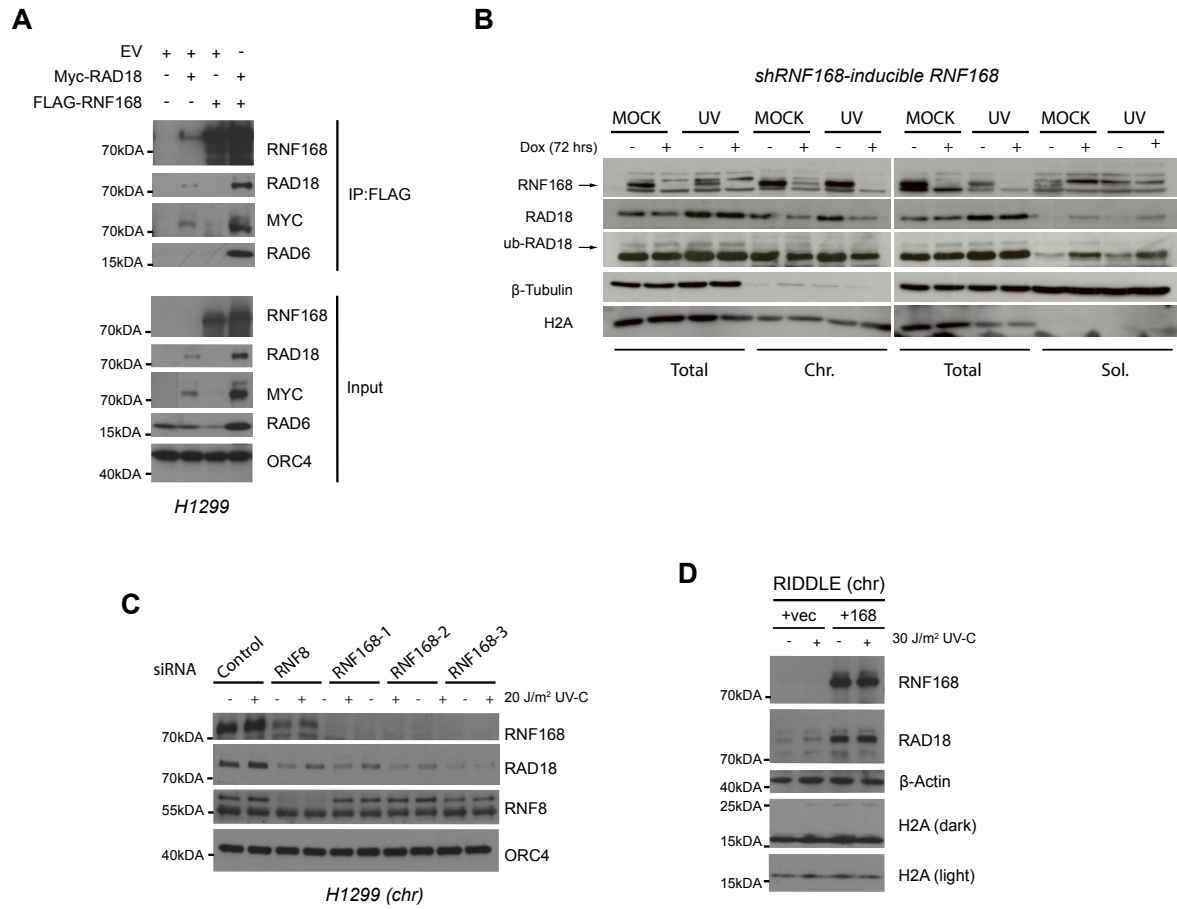
Figure 2.2 RNF168 associates with RAD18 and facilitates its recruitment to chromatin

(A) H1299 cells were transiently transfected with control empty vector (EV), Myc-RAD18, FLAG-RNF168, or both. After 48 hrs FLAG-RNF168 was immunoprecipitated with anti-FLAG beads. Input and immunocomplexes were immunoblotted with the indicated antibodies.

(B) U2OS cells were treated with vehicle or Doxycycline to induce shRNA silencing of RNF168. 72 hrs after induction cells were irradiated with 20J/m2 or mock treated and harvested for immunoblotting with the indicated antibodies.

(C) H1299 cells were treated with the indicated siRNAs and 48 hrs after were subjected to 20J/m2 UV or mock irradiated, and harvested for immunoblotting with the indicated antibodies.

(D) RIDDLE patient cells stably expressing vector or HA-RNF168 were subjected to 30J/m2 UV or mock irradiated and processed as in (C).
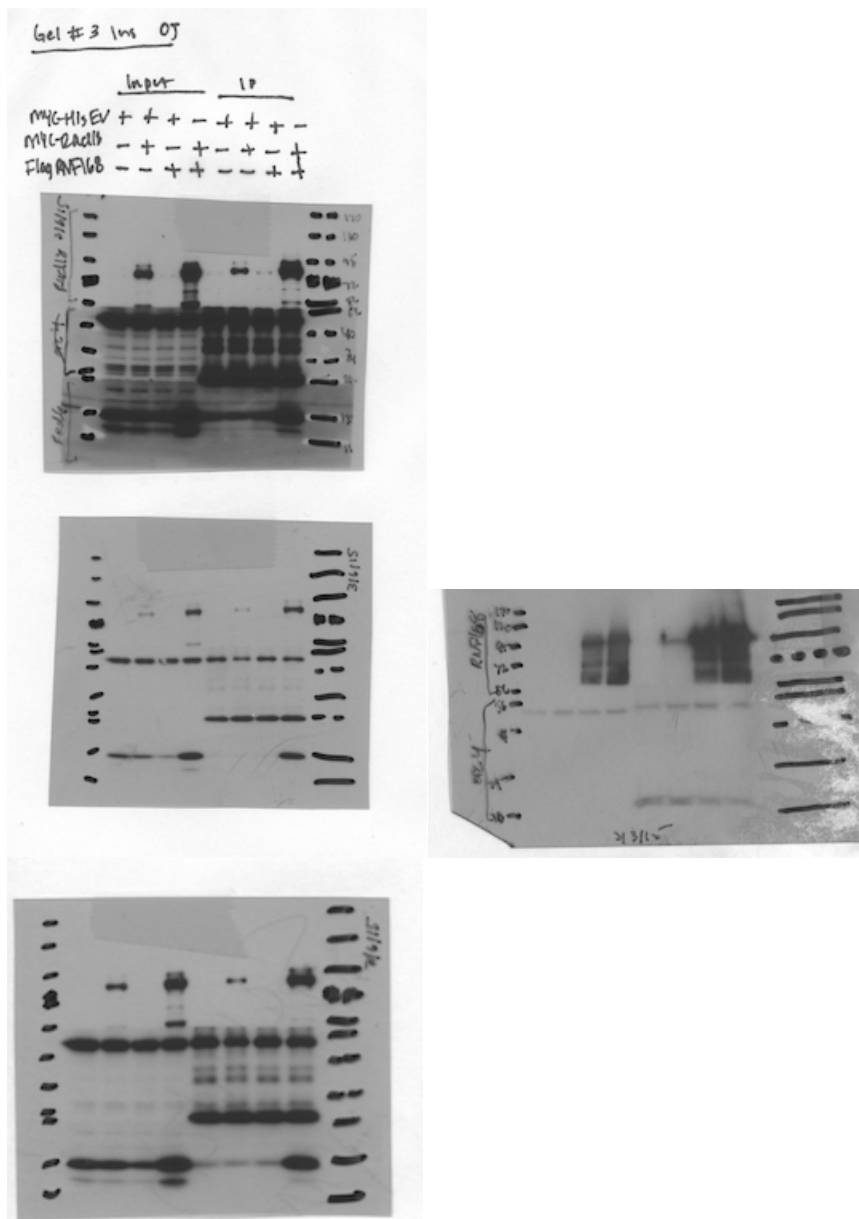
Figure 2 (A) uncropped blot
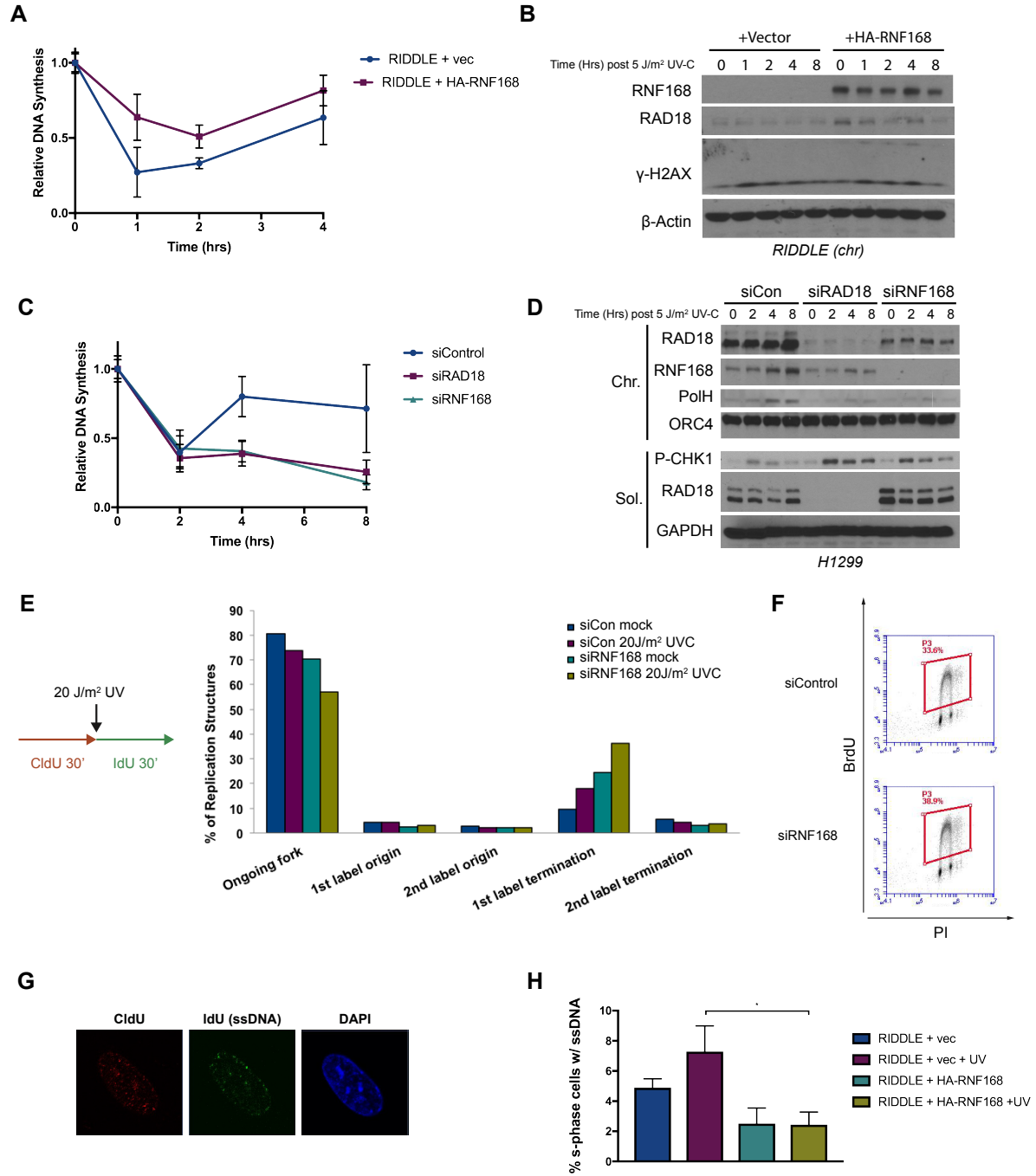
Figure 2.3 RNF168 promotes replication fork progression

Figure 2.3 RNF168 promotes replication fork progression

(A) RIDDLE cells stably expressing vector or HA-RNF168 were plated in triplicate for each time point and treated 5J/m2 UV. Cells were then pulsed with 3H thymidine for 30min at each time point and harvested to measure rates of incorporation by scintillation counter.
(B) Time course immunoblot corresponding to samples in (A).
(C) H1299 cells were treated with the indicated siRNA and plated in triplicate for each time point. 48 hrs after siRNA treatment samples were then processed as in (A).
(D) Time course immunoblot corresponding to samples in (C).
(E) Schematic of treatment for replication fiber analysis (left). DNA fiber analysis of USOS cells transfected with the indicated siRNAs. Cells were pulsed with CldU, irradiated with 20J/m2 UV, and pulsed with IdU. The percentages of ongoing forks, first-label (bidirectional) origins, new origins (IdU-labeled only), first-label terminations (CldU-labeled only) and second label terminations were quantified using imageJ (n=1).
(F) U2OS cells treated with siControl or siRNF168 were pulse labeled with 10 µM BrdU for 30min and analyzed by flow cytometry to quantify S phase–positive populations.
(G) Representative images of staining in RIDDLE fibroblasts used for analyzing the amount of s-phase cells with ssDNA.
(H) RIDDLE cells stably expressing vector or HA-RNF168 cells were pulsed with IdU for two days. Cells were then treated with mock or UV irradiation (40J/m2) and 8 hrs later were pulsed with CldU for 30min before harvest. IdU immunostaining was done under non-denaturing conditions and antibody was fixed prior to denaturing CldU processing. DNA was with DAPI. Data represent mean ± SEM of three independent experiments. * indicates significant difference by one-way ANOVA with Bonferroni multiple comparisons test at 90% confidence (p<0.1).
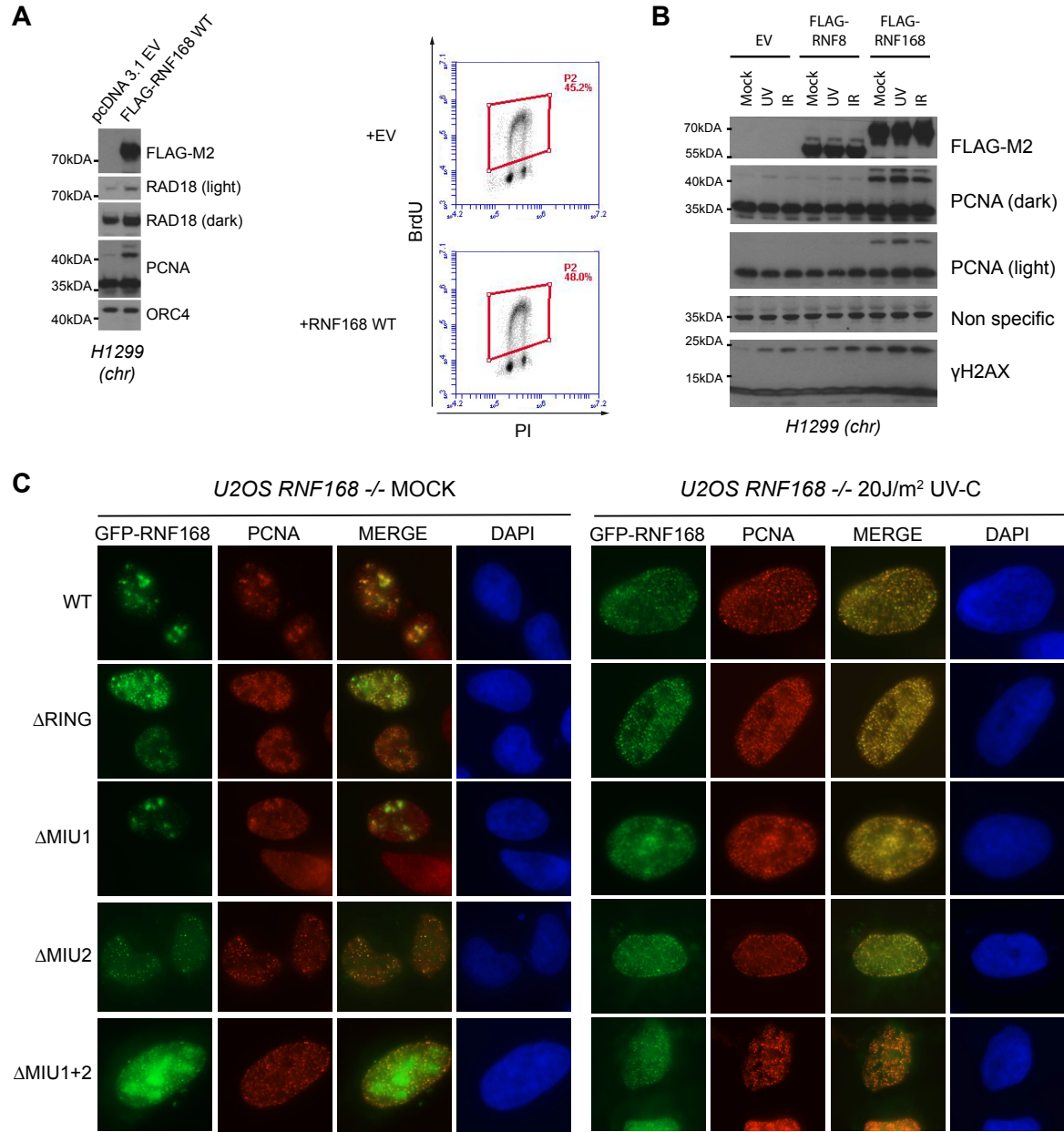
Figure 2.4 RNF168 promotes ubiquitination of PCNA and its association with replication factories is distinct from its canonical role in DSBR.

Figure 2.4 RNF168 promotes ubiquitination of PCNA and its association with replication factories is distinct from its canonical role in DSBR.

(A) H1299 cells were transfected with EV and FLAG-RNF168 WT for 24 hrs before harvest for immunoblot analysis with the indicated antibodies. One replicate plate was pulse labeled with 10 µM BrdU for 30min and analyzed by flow cytometry to quantify S phase–positive populations.

(B) H1299 cells were transfected with EV, FLAG-RNF8 and FLAG-RNF168 for 24hr before mock, UV or IR irradiation. Lysates were harvested and analyzed by immunoblot with the indicated antibodies.

(C) U2OS RNF168 -/- cells transfected with the indicated GFP-RNF168 expression vectors were mock or UV-irradiated. 6 hrs post-irradiation cells were fixed and processed for GFP fluorescence and PCNA immunofluorescence. DNA was stained with DAPI.
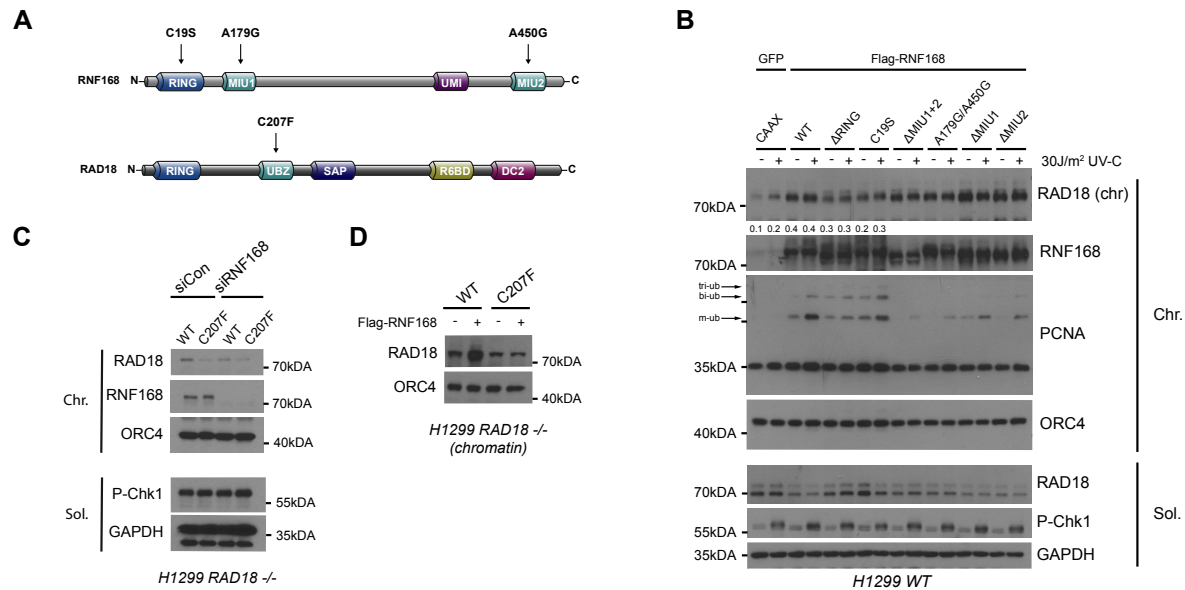
Figure 2.5 Separation of function for RNF168
(A) Schematic of domains and point mutation mutants in RNF168 and RAD18 proteins.
(B) H1299 WT cells were transfected with control plasmid or FLAG-RNF168 mutants. Samples were mock treated or irradiated with 30J/m2 UV and harvested for analysis by western blot with indicated antibodies.
(C) H1299 RAD18 -/- cells were transfected with RAD18 WT or RAD18 C207F mutant plasmids and subsequently treated with siRNA targeting control or RNF168. Cells were harvested for analysis by western blot with indicated antibodies.
(D) H1299 RAD18 -/- cells were transfected with RAD18 WT or RAD18 C207F mutant plasmids and subsequently transfected with FLAG-RNF168 plasmid and processed as in (C).
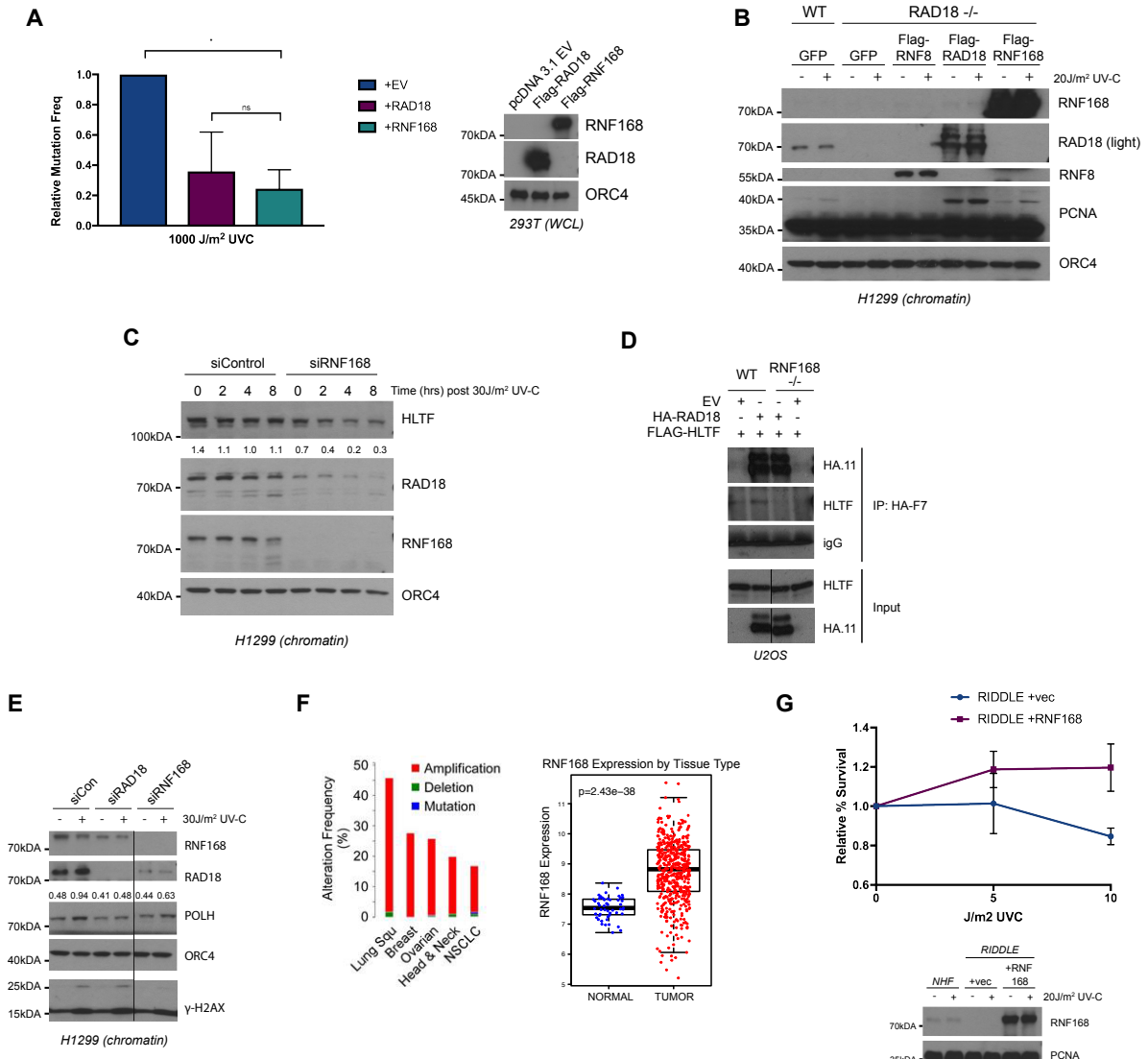
Figure 2.6 Role of RNF168 in DNA damage tolerance

Figure 2.6 Role of RNF168 in DNA damage tolerance

(A) 293T cells were co-transfected with UV-treated pSP189 reporter plasmid and RAD18 or RNF168 expression vectors. Forty-eight hours later, 293T cell extracts were collected for validation of RAD18 and RNF168 expression by western blot (right). Recovered pSP189 plasmid was transformed into electro-competent MBM7070 bacteria and pSP189 mutation rates were determined by enumerating blue and white bacterial colonies. Data represent mean ± SEM of two independent experiments each performed in triplicate. P-values were calculated using a two-tailed Student's t-test. *p=0.0133

(B) H1299 WT or RAD18 -/- cells were transfected with EV, FLAG-RNF8, FLAG-RAD18 or FLAG-RNF168 plasmids as indicated. 24 hrs post-transfection samples were mock or UV irradiated (20J/m2) and harvested for analysis by western blot with indicated antibodies.

(C) H1299 WT cells were treated with control or RNF168 siRNA. 48 hrs post-transfection samples were mock or UV irradiated (20J/m2) and harvested as in (B). Relative levels of HLTF compared to total sample loaded were quantified by densitometry.

(D) U2OS WT and RNF168 -/- cells were transiently transfected with control empty vector (EV), HA-RAD18, FLAG-HLTF, or both, as indicated. After 24 hrs HA-RAD18 was immunoprecipitated with anti-HA beads. Input and immunocomplexes were immunoblotted with the indicated antibodies.

(E) H1299 WT cells were treated with control, RAD18 or RNF168 siRNA. 48 hrs post-transfection samples were mock or UV irradiated (30J/m2) and harvested as in (B).

(F) Expression of RNF168 in normal and Lung Squamous Cell Carcinoma tumors from the TCGA data base.

(G) RIDDLE + vector and RIDDLE + HA-RNF168 cells were plated at low density in 6-well plates (3-wells per treatment). 24h post-plating cells were damaged with UV and let to grow for two weeks before harvesting and staining with crystal violet .Data represent mean ± SEM of two independent experiments (left). NHF, RIDDLE + vector and RIDDLE + HA-RNF168 cells were mock or UV irradiated (20J/m2) and harvested to analyze relative levels of RNF168 (right).
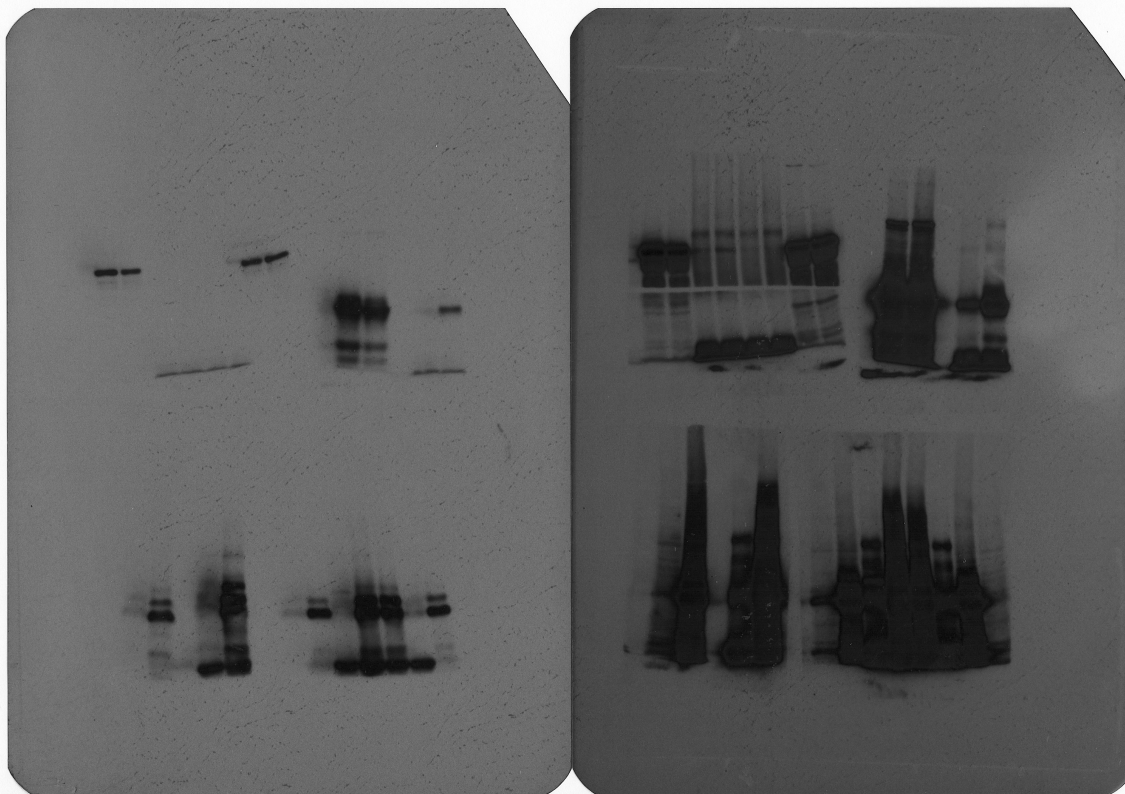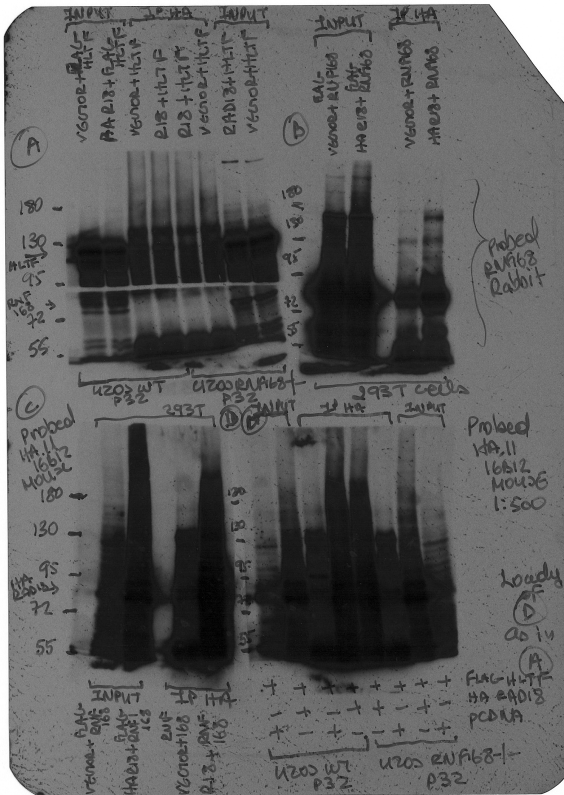
Figure 2.6 (D) and 2.8 (A) uncropped blots
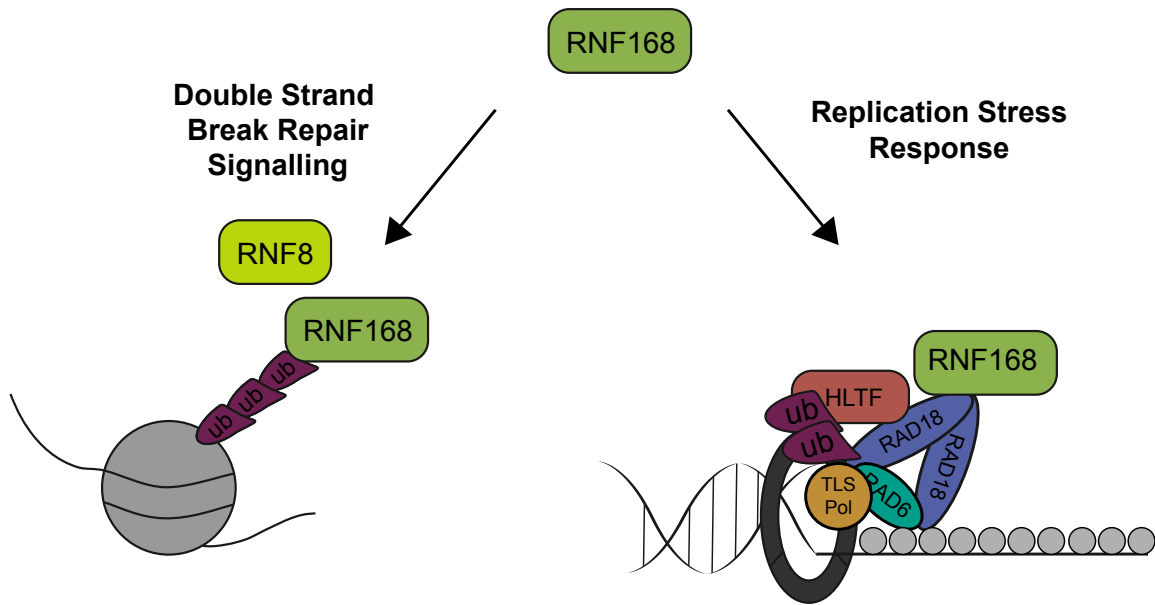
Figure 2.7 Hypothetical model for RNF168 in replication stress and DNA damage tolerance
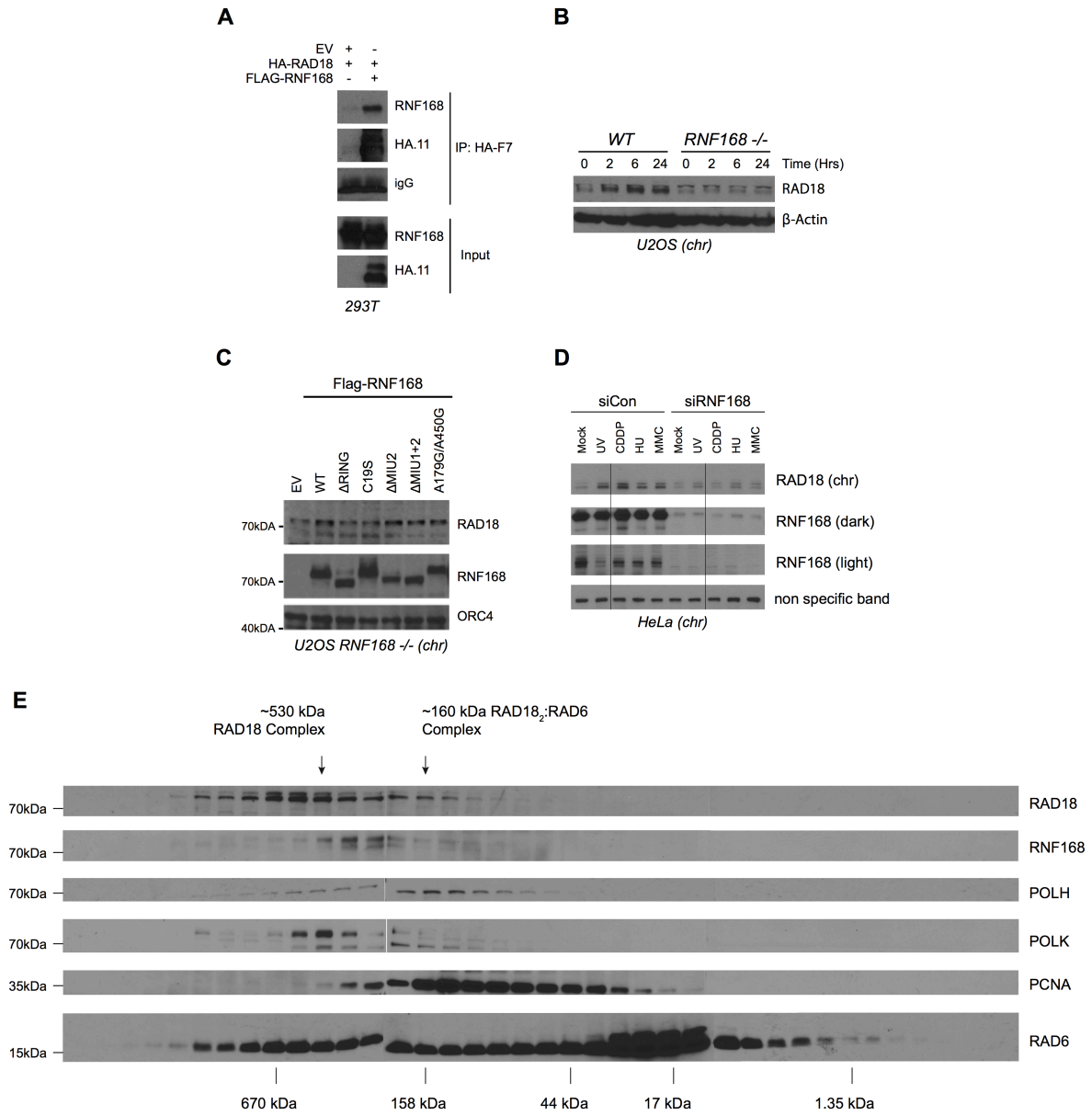
Figure 2.8 Supplemental characterization of RNF168-RAD18 association

Figure 2.8 Supplemental characterization of RNF168-RAD18 association

 (A) 293T cells were transiently transfected with control empty vector (EV), HA-RAD18, FLAG-RNF168, or both, as indicated. After 24 hrs HA-RAD18 was immunoprecipitated with anti-HA beads. Input and immunocomplexes were immunoblotted with the indicated antibodies.

 (B) U2OS WT and RNF168 -/- cells were mock or UV irradiated (20J/m2) and harvested for analysis by western blot at various time points with indicated antibodies.

 (C) U2OS RNF168-/- were transiently transfected with EV or FLAG-RNF168 WT or mutant constructs. 24 hrs post-transfection samples were UV irradiated (20J/m2) and harvested for analysis by western blot with indicated antibodies.

 (D) HeLa cells were transfected with control or RNF168 siRNAs. 48hrs post-transfection cells were treated with the UV, Cisplatin, Hydroxyurea, Mitomycin C or mock treated and harvested for immunoblot with the indicated antibodies.

 (E) Size fractionation of RAD18, RAD6, and RNF168 complexes in cultured cells. Exponentially-growing cultures of 293T cells were lysed in 300 µl of CSK without sucrose and supplemented with 1 µg/ml (25,000 units/ml) of Benzonase. Lysates were incubated at room temperature for 15 minutes to digest chromatin, then centrifuged at 21,000g for 20 min. 250 µl of each clarified cell lysate (~2.0 mg) was loaded onto a 25ml Sephadex 200 gel filtration column. The column was eluted with sucrose-free CSK. 0.5 ml fractions were collected and 30 µl of each fraction was analyzed by SDS-PAGE and immunoblotting with antibodies against RAD18, RAD6 and MAGE-A4.
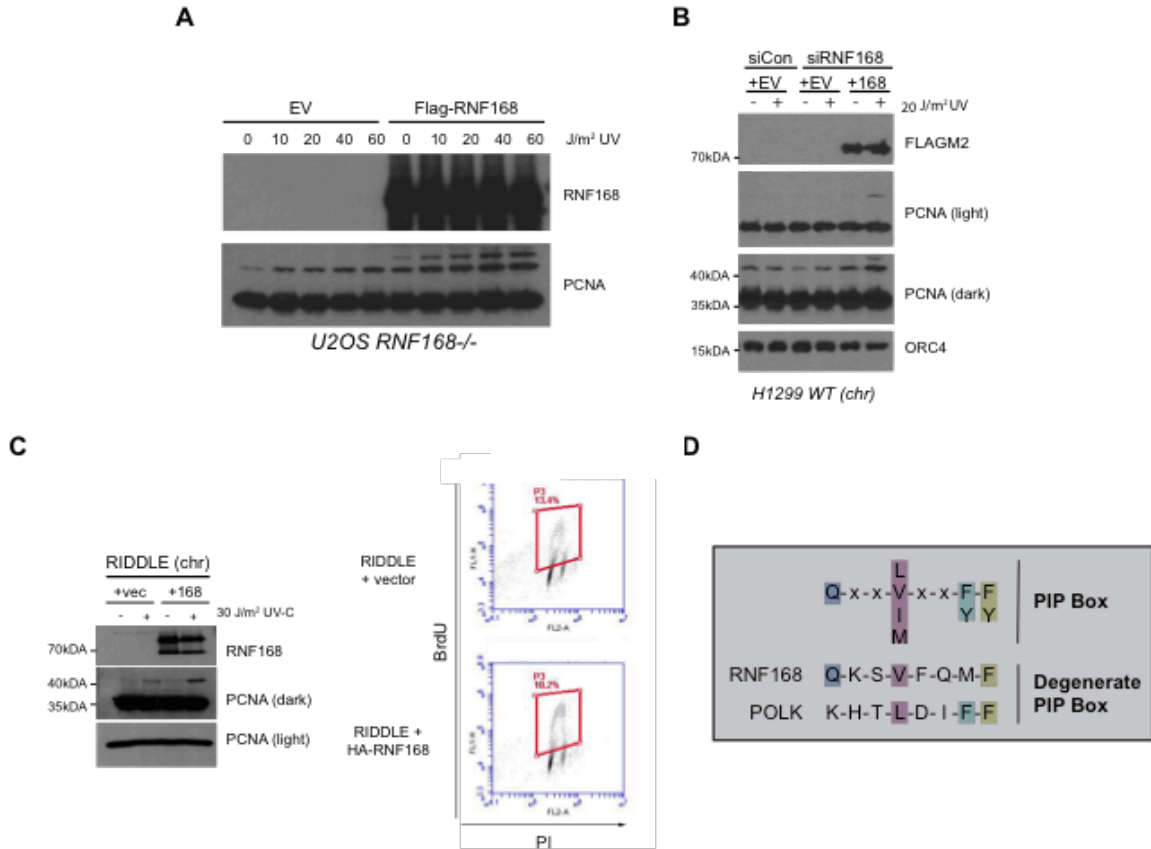
Figure 2.9 Supplemental characterization of RNF168-mediated ub-PCNA

(A) U2OS RNF168-/- were transiently transfected with EV or FLAG-RNF168 WT or mutant constructs. 24 hrs post-transfection samples were UV irradiated with the indicated doses of UV and harvested for analysis by western blot with indicated antibodies.

(B) H199 cells were treated with siControl or siRNF168. 24 hrs later cells were subsequently transfected with EV or siRNA-resistant FLAG-RNF168 for another 24 hrs. Cells were then treated with UV and harvested for analysis by western blot with the indicated antibodies.

(C) RIDDLE cells stably expressing vector or RNF168 were treated with UV and harvested for immunoblot with anti-RNF168 and anti-PCNA antibodies. Additional samples were pulse labeled with 10 µM BrdU for 30min and analyzed by flow cytometry to quantify S phase–positive populations.

(D) Analysis of RNF168 amino acid sequence identifies a degenerative PIP Box motif, as is seen in DNA Pol κ[51].
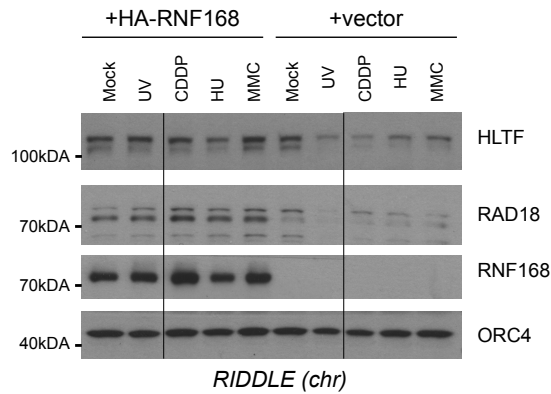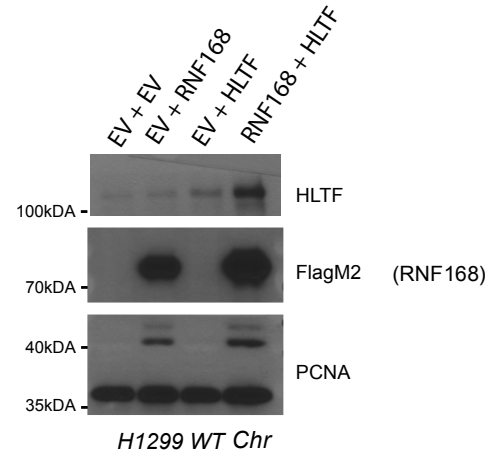
Figure 2.10 RNF168 levels influence chromatin-bound HLTF
(A) RIDDLE cells stably expressing vector or RNF168 were treated with the UV, Cisplatin, Hydroxyurea, Mitomycin C or mock treated and harvested for immunoblot with the indicated antibodies.
(B) H1299 cells were transfected with EV, RNF168 or HLTF plasmids. 24 hrs after transfection, cells were treated with 20J/m2 UV and harvested for immunoblotting with the indicated antibodies.
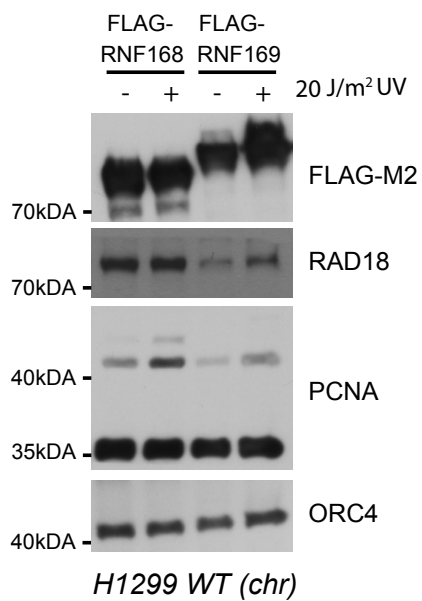
Figure 2.11 Comparison of RNF168 and RNF169 on RAD18 recruitment and ub-PCNA

H1299 cells were transfected with FLAG-RNF168 or FLAG-RNF169. 24 hrs after transfection cells were treated with 20J/m2 UV and harvested for immunoblot analysis with the indicated antibodies.

REFERENCES

1. Raschle, M., et al. (2015). "DNA repair. Proteomics reveals dynamic assembly of repair complexes during bypass of DNA cross-links." Science **348**(6234): 1253671.

2. Zeman, M. K. and K. A. Cimprich (2012). "Finally, polyubiquitinated PCNA gets recognized." Mol Cell **47**(3): 333-334.

3. Leman, A. R. and E. Noguchi (2013). "The replication fork: understanding the eukaryotic replication machinery and the challenges to genome duplication." Genes (Basel) **4**(1): 1-32.

4. Kannouche, P. L., et al. (2004). "Interaction of human DNA polymerase eta with monoubiquitinated PCNA: a possible mechanism for the polymerase switch in response to DNA damage." Mol Cell **14**(4): 491-500.

5. Glover, T. W., et al. (1984). "DNA polymerase alpha inhibition by aphidicolin induces gaps and breaks at common fragile sites in human chromosomes." Hum Genet **67**(2): 136-142.

6. Fu, Y. H., et al. (1991). "Variation of the CGG repeat at the fragile X site results in genetic instability: resolution of the Sherman paradox." Cell **67**(6): 1047-1058.

7. Branzei, D. and M. Foiani (2008). "Regulation of DNA repair throughout the cell cycle." Nat Rev Mol Cell Biol **9**(4): 297-308.

8. Lin, J. R., et al. (2011). "SHPRH and HLTF act in a damage-specific manner to coordinate different forms of postreplication repair and prevent mutagenesis." Mol Cell **42**(2): 237-249.

9. Zeman, M. K., et al. (2014). "DNA damage-specific deubiquitination regulates Rad18 functions to suppress mutagenesis." J Cell Biol **206**(2): 183-197.

10. Palle, K. and C. Vaziri (2011). "Rad18 E3 ubiquitin ligase activity mediates Fanconi anemia pathway activation and cell survival following DNA Topoisomerase 1 inhibition." Cell Cycle **10**(10): 1625-1638.

11. Huang, J., et al. (2009). "RAD18 transmits DNA damage signalling to elicit homologous recombination repair." Nat Cell Biol **11**(5): 592-603.

12. Motegi, A., et al. (2008). "Polyubiquitination of proliferating cell nuclear antigen by HLTF and SHPRH prevents genomic instability from stalled replication forks." Proc Natl Acad Sci U S A **105**(34): 12411-12416.

13. Unk, I., et al. (2008). "Human HLTF functions as a ubiquitin ligase for proliferating cell nuclear antigen polyubiquitination." Proc Natl Acad Sci U S A **105**(10): 3768-3773.

14. Stewart, G. S., et al. (2009). "The RIDDLE syndrome protein mediates a ubiquitin-dependent signaling cascade at sites of DNA damage." Cell **136**(3): 420-434.

15. Watanabe, K., et al. (2004). "Rad18 guides poleta to replication stalling sites through physical interaction and PCNA monoubiquitination." EMBO J **23**(19): 3886-3896.

16. Betous, R., et al. (2009). "Role of TLS DNA polymerases eta and kappa in processing naturally occurring structured DNA in human cells." Mol Carcinog **48**(4): 369-378.

17. Biertumpfel, C., et al. (2010). "Structure and mechanism of human DNA polymerase eta." Nature **465**(7301): 1044-1048.

18. Unk, I., et al. (2006). "Human SHPRH is a ubiquitin ligase for Mms2-Ubc13-dependent polyubiquitylation of proliferating cell nuclear antigen." Proc Natl Acad Sci U S A **103**(48): 18107-18112.

19. Unk, I., et al. (2010). "Role of yeast Rad5 and its human orthologs, HLTF and SHPRH in DNA damage tolerance." DNA Repair (Amst) **9**(3): 257-267.

20. Motegi, A., et al. (2006). "Human SHPRH suppresses genomic instability through proliferating cell nuclear antigen polyubiquitination." J Cell Biol **175**(5): 703-708.

21. Chiu, R. K., et al. (2006). "Lysine 63-polyubiquitination guards against translesion synthesis-induced mutations." PLoS Genet **2**(7): e116.

22. Gao, Y., et al. (2016). "A neomorphic cancer cell-specific role of MAGE-A4 in trans-lesion synthesis." Nat Commun **7**: 12105.

23. Weston, R., et al. (2012). "ZRANB3 is a structure-specific ATP-dependent endonuclease involved in replication stress response." Genes Dev **26**(14): 1558-1572.

24. Poole, L. A. and D. Cortez (2017). "Functions of SMARCAL1, ZRANB3, and HLTF in maintaining genome stability." Crit Rev Biochem Mol Biol **52**(6): 696-714.

25. Ciccia, A., et al. (2012). "Polyubiquitinated PCNA recruits the ZRANB3 translocase to maintain genomic integrity after replication stress." Mol Cell **47**(3): 396-409.

26.   Terai, K., et al. (2010). "CRL4(Cdt2) E3 ubiquitin ligase monoubiquitinates PCNA to promote translesion DNA synthesis." Mol Cell **37**(1): 143-149.

27.   Day, T. A., et al. (2010). "Phosphorylated Rad18 directs DNA polymerase eta to sites of stalled replication." J Cell Biol **191**(5): 953-966.

28.   Durando, M., et al. (2013). "A non-catalytic role of DNA polymerase eta in recruiting Rad18 and promoting PCNA monoubiquitination at stalled replication forks." Nucleic Acids Res **41**(5): 3079-3093.

29.   Higgs, M. R., et al. (2015). "BOD1L Is Required to Suppress Deleterious Resection of Stressed Replication Forks." Mol Cell **59**(3): 462-477.

30.   Petermann, E., et al. (2010). "Hydroxyurea-stalled replication forks become progressively inactivated and require two different RAD51-mediated pathways for restart and repair." Mol Cell **37**(4): 492-502.

31.   Liu, P., et al. (2008). "The SPARC-related factor SMOC-2 promotes growth factor-induced cyclin D1 expression and DNA synthesis via integrin-linked kinase." Mol Biol Cell **19**(1): 248-261.

32.   Liu, P., et al. (2006). "The Chk1-mediated S-phase checkpoint targets initiation factor Cdc45 via a Cdc25A/Cdk2-independent mechanism." J Biol Chem **281**(41): 30631-30644.

33.   Guzman, C., et al. (2014). "ColonyArea: an ImageJ plugin to automatically quantify colony formation in clonogenic assays." PLoS One **9**(3): e92444.

34.   Franken, N. A., et al. (2006). "Clonogenic assay of cells in vitro." Nat Protoc **1**(5): 2315-2319.

35.   Machida, Y., et al. (2012). "Spartan/C1orf124 is important to prevent UV-induced mutagenesis." Cell Cycle **11**(18): 3395-3402.

36.   Ramaekers, C. H., et al. (2014). "RNF8-independent Lys63 poly-ubiquitylation prevents genomic instability in response to replication-associated DNA damage." PLoS One **9**(2): e89997.

37.   Zhang, S., et al. (2008). "PCNA is ubiquitinated by RNF8." Cell Cycle **7**(21): 3399-3404.

38.   Hung, S. H., et al. (2017). "Monoubiquitylation of histone H2B contributes to the bypass of DNA damage during and after DNA replication." Proc Natl Acad Sci U S A **114**(11): E2205-E2214.

39.   Northam, M. R. and K. M. Trujillo (2016). "Histone H2B mono-ubiquitylation maintains genomic integrity at stalled replication forks." Nucleic Acids Res **44**(19): 9245-9255.

40. Trujillo, K. M. and M. A. Osley (2012). "A role for H2B ubiquitylation in DNA replication." <u>Mol Cell</u> **48**(5): 734-746.

41. Vassilev, A. P., et al. (1995). "The levels of ubiquitinated histone H2A are highly upregulated in transformed human cells: partial colocalization of uH2A clusters and PCNA/cyclin foci in a fraction of cells in S-phase." <u>J Cell Sci</u> **108 (Pt 3)**: 1205-1215.

42. Huen, M. S., et al. (2007). "RNF8 transduces the DNA-damage signal via histone ubiquitylation and checkpoint protein assembly." <u>Cell</u> **131**(5): 901-914.

43. Vissers, J. H., et al. (2008). "The many faces of ubiquitinated histone H2A: insights from the DUBs." <u>Cell Div</u> **3**: 8.

44. Friedl, A. A., et al. (2001). "Deletion of the SRS2 gene suppresses elevated recombination and DNA damage sensitivity in rad5 and rad18 mutants of Saccharomyces cerevisiae." <u>Mutat Res</u> **486**(2): 137-146.

45. Tateishi, S., et al. (2003). "Enhanced genomic instability and defective postreplication repair in RAD18 knockout mouse embryonic stem cells." <u>Mol Cell Biol</u> **23**(2): 474-481.

46. Yang, Y., et al. (2013). "Cell cycle stage-specific roles of Rad18 in tolerance and repair of oxidative DNA damage." <u>Nucleic Acids Res</u> **41**(4): 2296-2312.

47. Bi, X., et al. (2005). "DNA polymerase kappa is specifically required for recovery from the benzo[a]pyrene-dihydrodiol epoxide (BPDE)-induced S-phase checkpoint." <u>J Biol Chem</u> **280**(23): 22343-22355.

48. Bi, X., et al. (2006). "Rad18 regulates DNA polymerase kappa and is required for recovery from S-phase checkpoint-mediated arrest." <u>Mol Cell Biol</u> **26**(9): 3527-3540.

49. Krijger, P. H., et al. (2011). "HLTF and SHPRH are not essential for PCNA polyubiquitination, survival and somatic hypermutation: existence of an alternative E3 ligase." <u>DNA Repair (Amst)</u> **10**(4): 438-444.

50. Warbrick, E. (1998). "PCNA binding through a conserved motif." <u>Bioessays</u> **20**(3): 195-199.

51. Choe, K. N. and G. L. Moldovan (2017). "Forging Ahead through Darkness: PCNA, Still the Principal Conductor at the Replication Fork." <u>Mol Cell</u> **65**(3): 380-392.

52. Iconomou, M. and D. N. Saunders (2016). "Systematic approaches to identify E3 ligase substrates." <u>Biochem J</u> **473**(22): 4083-4101.

53. Pinato, S., et al. (2011). "UMI, a novel RNF168 ubiquitin binding domain involved in the DNA damage signaling pathway." Mol Cell Biol **31**(1): 118-126.

54. Inagaki, A., et al. (2011). "Human RAD18 interacts with ubiquitylated chromatin components and facilitates RAD9 recruitment to DNA double strand breaks." PLoS One **6**(8): e23155.

55. Kobayashi, S., et al. (2014). "Rad18 and Rnf8 facilitate homologous recombination by two distinct mechanisms, promoting Rad51 focus formation and suppressing the toxic effect of nonhomologous end joining." Oncogene **0**.

56. Hu, Q., et al. (2017). "Mechanisms of Ubiquitin-Nucleosome Recognition and Regulation of 53BP1 Chromatin Recruitment by RNF168/169 and RAD18." Mol Cell **66**(4): 473-487 e479.

57. Panier, S., et al. (2012). "Tandem protein interaction modules organize the ubiquitin-dependent response to DNA double-strand breaks." Mol Cell **47**(3): 383-395.

58. Helchowski, C. M., et al. (2013). "A small ubiquitin binding domain inhibits ubiquitin-dependent protein recruitment to DNA repair foci." Cell Cycle **12**(24): 3749-3758.

59. Wong, R. P., et al. (2012). "Elevated expression of Rad18 regulates melanoma cell proliferation." Pigment Cell Melanoma Res **25**(2): 213-218.

60. Zhou, J., et al. (2012). "Overexpression of DNA polymerase iota (Poliota) in esophageal squamous cell carcinoma." Cancer Sci **103**(8): 1574-1579.

61. Xie, C., et al. (2014). "RAD18 mediates resistance to ionizing radiation in human glioma cells." Biochem Biophys Res Commun **445**(1): 263-268.

CHAPTER 3: A NEOMORPHIC CANCER CELL-SPECIFIC ROLE OF MAGE-A4 IN TRANS-LESION SYNTHESIS

3.1 Introduction

Eukaryotic cells are exposed to many intrinsic and exogenous sources of DNA damage. The S-phase of the cell cycle is particularly vulnerable to genotoxins, because error-prone replication of damaged DNA can lead to mutagenesis, a 'hallmark and enabling characteristic' of cancer[1]. To mitigate the genome destabilizing consequences of DNA damage in S-phase, DNA replication forks that encounter lesions trigger a network of signal transduction pathways collectively termed the DNA damage response (DDR). The different effector arms of the DDR cooperate to facilitate S-phase recovery and resumption of normal cell cycle progression following genotoxic insult[2]. Failure to integrate DNA replication with DNA repair and cell cycle progression leads to reduced viability, compromised genome stability and a predisposition to cancer.

Trans-lesion synthesis (TLS) is one of the main effector pathways of the DDR and is important for normal recovery from DNA replication fork stalling[3]. The conventional DNA polymerases that duplicate most of the genome every cell cycle cannot replicate DNA templates harboring bulky lesions. Therefore, following acquisition of DNA damage, a 'polymerase switch' replaces replicative DNA polymerases at stalled replication forks with specialized TLS DNA polymerases that can accommodate bulky lesions.

The Y-family TLS polymerases include DNA polymerase eta (Polη), DNA polymerase kappa (Polκ), DNA polymerase iota (Polι) and REV1[3, 4]. Collectively, Y-family TLS polymerases enable cells to maintain DNA synthesis using damaged genomes. In TLS-deficient cells, checkpoint kinase signaling persists, leading to a protracted S-phase arrest and accumulation of DNA double-stranded breaks (DSBs)[5-7].

TLS can be error-free or error-prone depending on the nature of the DNA damage and the particular TLS polymerase(s) selected for lesion bypass[3, 4]. Polη is the default TLS polymerase recruited to stalled replication forks and performs error-free replication of DNA templates containing its cognate lesions (including ultraviolet-induced cyclo-butane pyrimidine dimers), thereby suppressing mutagenesis. However, when Polη is absent, error-prone compensatory lesion bypass by other Y-family DNA polymerases leads to mutations[8], a mechanism that explains the ultraviolet sensitivity and skin cancer propensity of Polη-deficient xeroderma pigmentosum-Variant patients[9]. TLS must be regulated strictly and used sparingly to ensure genomic stability.

Mono-ubiquitination of the DNA polymerase processivity factor proliferating cell nuclear antigen (PCNA) is important for TLS activation and lesion bypass[10, 11]. In response to DNA damage, the E3 ubiquitin ligase RAD18 is recruited to stalled replication forks where it mono-ubiquitinates PCNA at the conserved residue K164[12, 13]. K164 mono-ubiquitination promotes interactions between PCNA and Y-family TLS polymerases (which possess ubiquitin-binding zinc fingers and ubiquitin-binding motifs) at stalled replication forks[14].

RAD18 overexpression can increase PCNA mono-ubiquitination and promote recruitment of TLS polymerases to replication forks, even in the absence of DNA damage[5]. Conversely, in RAD18-deficient cells, Y-family TLS polymerases are not recruited efficiently to sites of DNA replication stalling[5, 15, 16] and overall lesion bypass is reduced[17]. Moreover, RAD18 deficiency recapitulates the defective S-phase recovery phenotypes of Polη and Polκ-deficient cells after genotoxin exposure[5], supporting a major role for RAD18 in TLS.

Although RAD18 is important for TLS polymerase recruitment to stalled replication forks, the basis for lesion-specific selection of the correct TLS polymerase is not yet fully understood. All TLS polymerases preferentially associate with mono-ubiquitinated PCNA relative to unmodified species. Clearly, relative expression levels and activities of RAD18 and the Y-family DNA polymerases are likely to have an impact on the overall TLS capacity and accuracy, determining mutagenic outcomes. Recent sequencing efforts have demonstrated that cancer cell genomes contain tens to hundreds of thousands of nucleotide substitutions and other mutations[18]. Mutation rates of untransformed cells are insufficient to explain the large numbers of mutations found in cancer cells. Therefore, cancer may be associated with a 'mutator phenotype' that generates large numbers of driver and passenger mutations during tumor progression[19, 20]. Owing to its pivotal role in error-prone DNA synthesis, RAD18-mediated TLS has the potential to contribute to the mutational burden of cancer genomes. Neoplastic cells experience various oncogene-induced forms of DNA damage and replication stress (including oxidative DNA damage from reactive oxygen species (ROS) and re-replication) throughout tumor progression. The ATR/CHK1 branch of the DDR may help

pre-neoplastic cells endure oncogenic stress, thereby promoting tumorigenesis[21]. Similarly, the RAD18–TLS pathway is in essence a DNA-damage tolerance mechanism that could help maintain viability in the face of oncogene-induced replication stresses[22]. Therefore, RAD18–TLS has the potential to have an impact on tumorigenesis by promoting error-prone DNA synthesis and by conferring oncogenic stress tolerance. However, whether dysregulation of the TLS pathway has an impact on genome maintenance mechanisms and phenotypes of cancer cells is unknown. Most of our understanding of the mammalian RAD18–TLS signaling pathway stems from studies performed in cultured cancer cell lines. Remarkably, however, it is unknown whether RAD18 and TLS are differentially regulated in cancer cell lines and untransformed cells.

In this report we identify a cancer cell-specific protein, the cancer/testes antigen (CTA) melanoma antigen-A4 (MAGE-A4), as a novel binding partner and stabilizing factor for RAD18. CTA proteins are ordinarily germ line restricted, yet can be aberrantly expressed at high levels in many cancers[23]. The MAGE represent a subclass of CTA[24], some of which were recently shown to associate with and activate specific RING E3 ubiquitin ligases[25], thereby providing a new mechanism by which ubiquitin signaling is deregulated in cancer cells. Here we show that MAGE-A4 contributes to TLS pathway activation, DNA-damage tolerance and genome maintenance in cancer cells. These results suggest a mechanism by which cancer genomes are impacted via reprograming of ubiquitin signaling.

3.2 Methods

Cell culture and transfection

hTERT-expressing human dermal fibroblasts were provided by Dr. William Kaufmann (UNC Chapel Hill). Primary mouse embryonic fibroblasts were derived from E13.5 embryos of WT C57/BL6 mice. Cancer cell lines H1299, A549, HeLa, U2OS, H157, H650, HCT116 and 293T were purchased from the American Type Culture Collection (ATCC) and used for the described experiments without further authentication. It is noteworthy that the H157 squamous cell lung carcinoma cell line is on the International Cell Line Authentication Committee (ICLAC) misidentified cell list. According to the ATCC, H157 is identical to the H1264 squamous cell lung carcinoma cell line. In the experiments shown in Fig. 3.13, H157 cells were used solely as one (of several) example of independent cancer cell lines in which RAD18 expression is MAGE-A4 dependent. All cell lines tested negative for mycoplasma contamination using the ATCC Universal Mycoplasma Detection Kit (ATCC 301012K). All cell lines were cultured in DMEM medium supplemented with 10% fetal bovine serum and penicillin–streptomycin (1%). Plasmid DNA and siRNA oligonucleotides were transfected using Lipofectamine 2000 (Invitrogen) according to the manufacturer's instructions, except that concentrations of plasmid DNA and Lipofectamine 2000 were used in each transfection reaction were decreased by 50% to reduce toxicity.

Adenovirus construction and infection

Adenovirus construction, purification and infections were performed as described previously[26, 27]. H1299 cells were typically infected with 0.1-1.0 x 10^9 pfu ml^{-1} and titrated to achieve near-endogenous expression levels of RAD18 and other proteins.

Expression plasmids

GST-RAD18, GST-RAD6 and GST-MAGE-A4 were expressed using the pGEX2T vector (GE Healthcare) and purified from BL21 (DE3) Escherichia coli (Invitrogen) as described previously[26]. Hexa-histidine tagged MAGE-A4 was expressed using the pRSET vector (Invitrogen V351-20) and purified from BL21 (DE3) E. coli bacteria. Mammalian expression vectors for HA- and MYC-tagged forms of RAD18 have been described previously[26, 28]. To generate MAGE-A4 expression vectors, the MAGE-A4 open reading frame was PCR amplified from H1299 genomic DNA and subcloned into the pcDNA3.1(-) expression plasmid. MAGE-A4 mutants harboring internal deletions and individual nucleotide substitutions were derived by PCR using conventional methods. The primers used to make MAGE-A4 mutants are: 5'-F WT (5'-CGCGGATC CGCCACCATGTCTTCTGAGCAGAAGAGTCAGCAC-3'), 3'-R WT (5'-AACAAGCTTTC AGACTCCCTCTTCCTCCTCTAACAAAG-3'); 5'-F HelixB (5'-CGCGGATCCGCCACCA TGGATGGCCTGCTGGGTAATAATCAG-3'), 5'-F Helix A + B (5'-CGCGGATCCGCCAC CATGTCCTTGTTCCGAGAAGCACTCAGTAAC-3'); ΔWHA-F (5'-GCCTTTCCTATGGT CCAAGGGC-3'), ΔWHA-R (5'-GCCCTTGGACCATAGGAAAGGC-3'); ΔWHA-F (5'-TG ACGCAGAGGATGGCCTGC-3'), ΔWHA-R (5'-GCAGGCCATCCTCTGCGTCA-3'); ΔWHB-F (5'-GCCTTTCCTATGGTCCAAGGGC-3'), ΔWHB-R (5'GCCCTTGGACCATA GGAAAGGC-3'); ΔMage-F (5'-GACGCAGAGGGTCCAAGGGC-3'), ΔMage-R (5'-GCC CTTGGACCCTCTGCGTC-3'); L121/2A-F (5'-CTCATTTTGCGGCCCGCAAG-3'), L121/ 2A-R (5'-CTTGCGGGCCGCAAAATGAG-3'); S90A-F (5'-GTTCCAGCGCCCAAGAAGA GG-3'), S90A-R (5'-CCTCTTCTTGGGCGCTGGAAC-3'); and S90D-F (5'- GGGTTCCAGCGATCAAGAAGAGG-3'), S90D-R (5'-CCTCTTCTTGATCGCTGGAACC

C-3'). The identities of all complementary DNA inserts were confirmed by sequencing. MYC–TRIM69 was a gift from Dr. Angelique Whitehurst (UT Southwestern) and expression plasmids encoding FLAG-tagged MAGE-A4, MAGE-A12, MAGE-B10 and MAGE-A1 were obtained from the UNC Tissue Culture Core Facility Orfeome collection.

RNA interference

siRNAs were incubated with Lipofectamine 2000 and serum free Optimem for 15 min at room temperature in the dark. Cells were then trypsinized and resuspended in 1 ml of medium and plated directly into the siRNA/Optimem/Lipofectamine solution at 50% confluence and incubated for 72 h. Sequences of siRNA oligonucleotides used here are as follows: control non-targeting siRNA, 5'-UAGCGACUAAACACAUCAA-3' (Thermo Fisher Scientific); RAD18 3'-untranslated region siRNA, 5'-UUAUA AAUGCCCAAGGAAAUU-3-; MAGE-A4 siRNA #1, 5'-AGUGUGAAUUCACCGUGAA - 3', MAGE-A4 siRNA #2 (targeting the 3'-untranslated region), 5'-GUGAAAUAGGU GAGAUAAAUU-3'; and USP7, 5'-AAGCGUCCCUUUAGCAUUAUU-3'. For MAGE-A4 depletions, siRNA#1 was used unless otherwise indicated.

Genotoxin treatment

For ultraviolet C (UVC) treatment, growth medium was removed from cultured cells and replaced with PBS. The resulting culture dishes plates were irradiated using an ultraviolet cross-linker (Stratagene) or left untreated for control. The UVC dose delivered to the cells was confirmed with an ultraviolet radiometer (UVP, Inc.). Following ultraviolet or sham irradiation, cells were re-fed with complete growth medium and returned to the incubator. For CPT treatments, cells were treated with 2 µM CPT and incubated for 2 h.

Fluorescence microscopy

H1299 cells were grown to ~60% confluency on glass bottom plates (Mat-tek) and then transfected with a CFP-RAD18-WT expression plasmid. Twenty hours after transfection, cells were ultraviolet irradiated ($20 \, Jm^{-2}$) or sham treated and fixed 6 h later for staining with anti-MAGE-A4 and fixed-cell imaging on a Zeiss 710 confocal microscope, in the UNC Microscopy Services Laboratory core facility, as described previously[29].

Immunoprecipitation and immunoblotting

To prepare extracts containing soluble and chromatin-associated proteins, monolayers of cultured cells typically in 60 mm plates were washed three times in ice-cold PBS and lysed in 500 µl of ice-cold cytoskeleton buffer (CSK buffer; 10 mM Pipes pH 6.8, 100 mM NaCl, 300 mM sucrose, 3 mM $MgCl_2$, 1 mM EGTA, 1 mM dithiothreitol, 0.1 mM ATP, 1 mM Na_3VO_4, 10 mM NaF and 0.1% Triton X-100) freshly supplemented with Protease Inhibitor Cocktail and Phostop (Roche). Lysates were centrifuged at 1,000 g for 2 min, to remove the CSK-insoluble nuclei. Supernatants were removed and further centrifuged at 10,000 g for 10 min, to obtain a clarified fraction containing a mixture of cytosolic plus nucleosolic proteins. The detergent-insoluble nuclear fractions were washed once with 1 ml of CSK buffer and then resuspended in a minimal volume of CSK before analysis by SDS–PAGE and immunoblotting.

For all immunoprecipitation experiments, input samples were normalized for protein concentration. Magnetic beads containing covalently conjugated antibodies against epitope tags were added to the extracts and incubations were performed overnight at 4°C using rotating racks.

Immune complexes were recovered using magnetic stands. The beads were washed five times with 1 ml CSK (5–10 min per wash), to remove nonspecifically associated proteins. The washed immune complexes were boiled in protein loading buffer for 10 min, to release and denature for SDS–PAGE.

For immunoblotting, cell extracts or immunoprecipitates were separated by SDS-PAGE, transferred to nitrocellulose membranes, and incubated overnight with the following primary antibodies: PCNA (sc-56), Chk1 (sc-7898), β-actin (sc-130656), cyclin E (sc-198), GAPDH (sc-32233), MAGE-A4 (sc-292429), Pan-MAGE-A (sc71537) and GST (sc-53909) from Santa Cruz Biotech (Santa Cruz, CA); Polη (A301-231A), Polι (A301-304A), RAD6 (A300-281A), RAD18 (A301-340A) and USP7 (A300-033A) from Bethyl Laboratories (Montgomery, TX); p42 MAPK (9107) and MYC-Tag (2276) from Cell Signaling; γH2AX (05-636) from Millipore; and Cdc45 rat monoclonal antibody as previously described[30]. Antibody dilutions used for immunoblotting were 1:1,000, with exceptions for the following antibodies: PCNA (1:500), GAPDH (1:2,000) and γH2AX (1:2,000).

In vitro protein-binding assays with lysate

Mammalian cells were transfected with 2 μg of plasmid and incubated for 48 h. Cell lysate was collected in CSK buffer and centrifuged at 13,300 r.p.m. to clear lysate. Recombinant GST–RAD18 fragments (100 ng) were incubated in 1 ml CSK with 100 μg cleared lysate for 2 h at 4°C. Fifty microlitres of Glutathione Sepharose beads (GE Healthcare 17-0756-01) was added to the solution and incubated for 2 h more at 4°C. Beads and complexes were collected by centrifugation and washed three times in CSK + 1% BSA, then resuspended in water and 4 x Laemmli buffer and boiled for 10 min.

In vitro RAD18–MAGE-A4 recombinant protein binding assay

Recombinant 6 x His–MAGE-A4 (1 µg) was incubated in 1 ml of CSK + 1% BSA with either GST or GST–RAD18 (0.3 µg) for 2 h at 4°C. Fifty microlitres of Glutathione sepharose beads (GE Healthcare 17-0756-01) was added to the solution and incubated for 2 h more at 4°C. Beads and complexes were collected by centrifugation and washed three times in CSK + 1% BSA, then resuspended in water and 4 x Laemmli buffer and boiled for 10 min.

In vitro degradation of RAD18

HA–RAD18 was expressed alone or in combination with MAGE-A4 in 293T cells. Cells were collected using CSK buffer. HA–RAD18 complexes were isolated by immunoprecipitation using anti-HA magnetic beads (MBL Intl M-1329) for 2 h at 4°C. Beads were washed with CSK and incubated for 1 h at 37°C in 2 mM MgCl2, 1 mM creatine phosphate, 25 U ml^{-1} creatine phosphokinase (FisherSci, ICN10050990), PBS and 1 mg ml^{-1} of rabbit reticulocyte lysate, untreated (L4151), from Promega, as a source of ubiquitination factors and proteasome activity, as described by Hernandez-Pigeon et al.[31].

Flow cytometry

Cells were labeled with 10 µM BrdU immediately before harvest. Cells were collected by trypsinization, fixed in 35% ethanol for 24 h, then stained with anti-BrdU and propidium iodide as previously described[26]. Stained nuclei were analyzed by flow cytometry on an Accuri C6 flow cytometer (BD, Oxford, UK) using the manufacturer's software.

In vitro PCNA ubiquitination assay

Recombinant RAD18–RAD6 complex was purified from baculovirus-infected Sf9 cells and incubated with recombinant PCNA in the presence of E1, ubiquitin and an ATP-regenerating system as described previously[32].

SupF mutagenesis assay

293T cells were co-transfected with a ultraviolet-irradiated (500 Jm^{-2}) pSP189 reporter plasmid[33] and control, RAD18 or MAGE-A4 expression vectors using Lipofectamine 2000. Forty-eight hours later, pSP189 was recovered from the 293T cells using a DNA miniprep kit (Qiagen, Hilden, Germany). Purified plasmid DNA was DpnI digested and electroporated into the MBM7070 bacterial strain. The mutation frequency in the supF coding region was determined by enumerating the ratios of blue (WT) and white (mutant) colonies.

Mass spectrometry

PBS-washed cell pellets from HA-RAD18-expressing (and control) cells were lysed with CSK and digested with 1,000 U ml^{-1} of RNasefree DNase I (Roche) at 25°C for 30 min. The resulting mixtures were sonicated to dissociate the nuclei. Insoluble material was removed by centrifugation at 10,000 g for 10 min. The resulting supernatant (containing cytosol, nucleosol and solubilized chromatin proteins) was used for immunoprecipitation of RAD18 complexes.

Anti-HA-conjugated magnetic beads (MBL Intl, M-1329) were incubated with HA–RAD18-containing supernatant for 4°C for 3 h. Following incubation, beads were washed in CSK. The protein complexes were digested directly off of the beads using FASP Protein Digestion Kit (Protein Discovery #44250).

Peptides were separated by reversed-phase nano-high-performance liquid chromatography with a nanoAquity UPLC system (Waters Corp.). Peptides were first trapped in a 2-cm trapping column (75-μm inside diameter (ID), Michom Magic C18 beads of 5.0-μm particle size, 200-Å pore size) and then separated on a self-packed 25-cm column (75-μm ID, Michom Magic C18 beads of 5.0-μm particle size, 100-Å pore size) at room temperature. The flow rate was 350 nl min^{-1} over a gradient of 1% buffer B (0.1% formic acid in acetonitrile) to 30% buffer B in 200 min. Next, a following wash raised buffer B to 70%. The identity of the eluted peptides was determined with an in-line LTQ-Orbitrap Velos mass spectrometer (Thermo Scientific). The ion source was operated at 2.0–2.4 kV with the ion transfer tube temperature set at 250°C. Full MS scan (300 to 2,000 m/z) was acquired in Orbitrap at 60,000 resolution setting; datadependent MS2 spectra were acquired in LTQ by collision-induced dissociation with the 15 most intense ions. Precursor ions were selected on the basis of charge states (2 or 3) and intensity thresholds (above 5,000) from the full scan; dynamic exclusion (one repeat every 30 s, with a 60-s exclusion time window) was also taken into account. The polysiloxane lock mass of 445.120030 was used throughout spectral acquisition.

Protein identification, quantification and filtering. Raw data were analyzed using Sorcerer-SEQUEST (build 5.1.1, SageN Research) and the Transproteomic Pipeline (TPP v4.7.1). MS/MS spectra were searched against the human UniProtKB/ Swiss-Prot sequence database (downloaded February 2015) supplemented with common contaminants, that is, porcine (Swiss-Prot P00761) and bovine (P00760) trypsin, and further concatenated with its reversed copy as a decoy. Search parameters used were a precursor mass between 400 and 4,500 amu, up to 2 missed cleavages, precursor-ion

tolerance of 3 amu, accurate mass binning within PeptideProphet, semi-tryptic digestion, a static carbamidomethyl cysteine modification and variable methionine oxidation. False discovery rates were determined by ProteinProphet and minimum protein probability cutoffs resulting in a 1% false discovery rate were selected individually for each experiment. The resulting spectral count data from controls and HA–RAD18-WT APMS experiment were input into the Spotlite web application using SAINTexpress (version 3.1.0), to determine protein–protein interaction probabilities by modeling the expected spectral count distribution of true and false interactions. In addition, raw data were re-searched and signal intensity was quantified using the MaxQuant LFQ algorithm with the identical sequence database and search parameters, except a 20-p.p.m. precursor mass tolerance, fully tryptic digestion and match between runs were used.

3.3 Results

MAGE-A4 is a component of the RAD18–RAD6 complex.

To identify new regulators of the TLS pathway we defined the RAD18 protein interaction network in H1299 adenocarcinoma cells using label-free affinity purification and shotgun mass spectrometry (APMS). As a control we also investigated the protein interaction network of a TLS-compromised RAD18 Δ402-444 mutant, which lacks a domain involved in mediating binding to Polη[26, 28] and other partners[34] (Fig. 1a). RAD18 interaction networks were defined for HA–RAD18 wild type (WT) and HA–RAD18 Δ402-444 complexes isolated from undamaged cells and from genotoxin (ultraviolet or Camptothecin (CPT))-treated cultures.

Co-complexed proteins were separated from background contaminants and false positives using the SAINT (significance analysis of interactome) algorithm. Top-scoring proteins included well-known RAD18 interactors such as RAD6A and RAD6B (E2 ubiquitin-conjugating enzymes), PCNA (a RAD18 substrate) and MSH2, a reported regulator of RAD18 ([35]; Fig. 3.1B). As expected from previous work[29], PCNA binding to RAD18 Δ402-444 was decreased or undetectable (Fig. 3.1C). One of the highest confidence and abundant novel RAD18 interactors we identified was the CTA MAGE-A4 (Fig. 3.1C).

The presence of MAGE-A4 in the RAD18 complexes was unaffected by ultraviolet or CPT, genotoxins that activate the distinct TLS and DSB repair effector pathways of RAD18, respectively. Comparison of relative MAGE-A4 abundance between RAD18 WT and RAD18 Δ402-444 APMS revealed that MAGE-A4 association does not depend on the Polη-binding domain of RAD18.

As the association of RAD18 with MAGE-A4 provided a potentially important new relationship between DNA-damage tolerance and cancer, we validated and further characterized the RAD18–MAGE-A4 interaction. First, we confirmed the RAD18–MAGE-A4 interaction in H1299 cells by performing independent co-immunoprecipitation (co-IP) and immunoblotting experiments (Fig. 3.1D).

A genome-wide screen previously detected MAGE-A4 as a binding partner of the E3 ubiquitin ligase TRIM69[36], a mitotic regulator[37]. For the purpose of comparison with a known MAGE-A4 partner, we expressed MYC epitope-tagged RAD18 and TRIM69 at similar levels in H1299 cells and examined levels of MAGE-A4 associated with each E3 ligase by co-IP. In a side-by-side comparison, RAD18 immune complexes contained

more MAGE-A4 than was present in TRIM69 immunoprecipitates (Fig. 3.1E). Other E3 ubiquitin ligases we tested (HLTF1, SHPRH, RNF8 and RNF168) failed to co-IP with MAGE-A4 (not shown). We conclude that MAGE-A4 is a specific and constitutive component of the RAD18 complex in H1299 lung carcinoma cells.

MAGE-A4 associates with the RAD6-binding domain of RAD18.

E3 ubiquitin ligases share many common sequence motifs. However, for the known MAGE-interacting RING-domain E3 ligases, no single consensus sequence or domain of the E3 is sufficient to mediate MAGE binding[24, 25]. Therefore, we performed experiments to map the MAGE-A4-interacting domain of RAD18. We expressed the different functional domains of the RAD18 protein as individual in-frame fusions with glutathione S-transferase (GST) (Fig. 3.2A), then performed 'pull-down' assays to identify the MAGE-A4-binding domain(s) of RAD18. As shown in Fig. 3.2B, the GST–RAD18 267-402 fragment, specifically recovered MAGE-A4 from H1299 cell lysates. In reciprocal 'pull-down' experiments, GST–MAGE-A4 also recovered RAD18 from H1299 and 293T cell lysates (Fig. 3.2C).

Interestingly, GST–RAD18 (267–402) contains the RAD6- binding domain (amino acids 340–395) previously defined by Watanabe et al.[28]. Similar to MAGE-A4, RAD6 was only recovered from cell lysates with GST–RAD18 (267–402) (Fig. 3.2B). To determine whether the RAD6-binding domain is also involved in RAD18–MAGE-A4 complex formation in cells, we determined the effect of internal deletion of amino acids 340–395 on the RAD18–MAGE-A4 association. Using transient transfection, HA–RAD18 (WT) and HA–RAD18 D340–395 (Fig. 3.2D) were expressed at similar levels in H1299 cells (Fig. 3.2E). However, in co-IP and immunoblotting experiments, MAGE-A4

and RAD6 only associated with WT RAD18 (Fig. 3.2E). We conclude that the RAD6-binding domain is necessary for RAD18–MAGE-A4 interactions *in vitro* and in cells.

We considered the possibility that the association of MAGE-A4 with RAD18 might be indirect and mediated via RAD6. However, in pull-down experiments recombinant GST–RAD6 did not recover MAGE-A4 from H1299 cell lysates (Fig. 3.2F). To more carefully evaluate a role for RAD6 (or other factors) in mediating the RAD18–MAGE-A4 interaction, we performed binding studies using purified MAGE-A4 and GST–RAD18 (267–402). As shown in Fig. 3.2G, we detected specific association of RAD18 (267–402) with MAGE-A4 in the absence of RAD6. Using AlphaScreen-based protein proximity assays[38], we validated the association of isolated MAGE-A4 (and of RAD6) with RAD18 (267–402) (Fig. 3.8). Interestingly, recombinant unlabeled RAD6 competed with epitope-tagged MAGE-A4 for RAD18 binding both in vitro and in cells (Fig. 3.8A–D). However, gel filtration chromatography experiments show that most of the cellular RAD6 is free and monomeric (Fig 3.8E–H). Moreover, from quantitative immunoblotting, RAD6 levels in H1299 cells exceed MAGE-A4 by 28-fold and exceed RAD18 levels by 114-fold (Fig. 3.9). Therefore, MAGE-A4 is not sufficiently abundant in H1299 cells to outcompete RAD6 for RAD18 association. We conclude that MAGE-A4 is a specific binding partner of RAD18 and associates with the RAD6-binding domain (as also reported for p95/NBS1)[39].

MAGE-A4 promotes RAD18 stability.

Reportedly, several MAGE family members directly activate their partner E3 ligases to promote substrate ubiquitination[25]. Therefore, we performed in vitro ubiquitin ligase assays using recombinant proteins, to determine the effect of MAGE-A4 on RAD18-

directed PCNA mono-ubiquitination. As shown in Fig. 3.3A, recombinant MAGE-A4 did not stimulate RAD18-dependent PCNA mono-ubiquitination under experimental conditions where other MAGE proteins stimulate catalytic activities of their cognate E3 ligases[25]. Interestingly, MAGE-A4 was ubiquitinated by RAD18 (Fig. 3.3A). High molar ratios of MAGE-A4:RAD18 led to decreased PCNA mono-ubiquitination in vitro (Fig. 3.3A). The apparent mild inhibition of PCNA mono-ubiquitination by MAGE-A4 in vitro results from substrate competition when MAGE-A4 is in vast excess of PCNA (Fig. 3.3A, lanes 9–12).

The major substrate and distal effector of RAD18-mediated ubiquitination in DNA damage tolerance is the sliding clamp PCNA, which is present on replicating chromatin in the nucleus.

Although PCNA and RAD18 were present in both chromatin and soluble fractions, MAGE-A4 was primarily soluble (Fig. 3.3B). Moreover, in ultraviolet-irradiated H1299 cells, RAD18 but not MAGE-A4 redistributed to nuclear foci representing sites of DNA replication stalling (Fig. 3.3C). Taken together, the results of Fig. 3.3A-C suggest that MAGE-A4 may not function as an allosteric activator of RAD18 or respond directly to replication fork stalling. Accordingly, we investigated alternative roles for MAGE-A4 in RAD18 regulation.

Proteins often stabilize their binding partners. Therefore, we determined the effect of MAGE-A4 depletion on RAD18 levels. As shown in Fig. 3.3D, we attained ~90% depletion of MAGE-A4 in H1299 cells using two independent transiently transfected small interfering RNAs (siRNAs). Interestingly, both MAGE-A4- directed siRNAs led to substantial (92% and 73% decreases in RAD18 expression in H1299 cells). Neither

MAGE-A4-directed siRNA affected RAD18 levels in 293T cells, which lack detectable

MAGE-A4 expression (Fig. 3.3D). Using cycloheximide treatment to block new protein

synthesis, we measured RAD18 decay rates in control and MAGE-A4-depleted cultures.

In control (MAGE-A4 replete) H1299 cells, RAD18 was stable for at least 24 hrs (the

duration of this experiment, see Fig. 3.3E). In MAGEA4-depleted cells, RAD18

expression was reduced and its half-life decreased when compared with MAGE-A4-

replete cells (Fig. 3.3E). RAD18 depletion did not affect the half-life of MAGE-A4 (Fig.

3.3F). However, we note that MAGE-A4 levels exceed those of RAD18 by ~3-fold in

H1299 cells (Fig. 3.9). Moreover, most of the cellular MAGE-A4 is not nuclear (Fig.

3.3C) or in the same complex as RAD18 (Fig. 3.8f–h), explaining why RAD18 does not

influence the overall MAGE-A4 pool.

Figure 3.3D–F suggested that MAGE-A4 stabilizes RAD18. In previous work,

proteasomal degradation of RAD18 (in USP7-depleted cells) was partially prevented by

treatment with the proteasome inhibitor MG132[40]. Therefore, we determined the effect

of MG132 treatments on RAD18 stability in control (MAGE-A4 replete), MAGE-A4-

depleted and USP7-depleted H1299 cells. RAD18 levels were unaffected by MG132 in

MAGE-A4-replete H1299 cells in which RAD18 is stable and has a half-life ($t_{1/2}$)

exceeding 24 hrs (Fig. 3.3E). However, the reduced RAD18 stability in USP7- or

MAGE-A4-depeleted H1299 cells was partially rescued by MG132 treatment (Fig. 4.4A).

MG132-induced poly-ubiquitin laddering of RAD18 was also decreased by ectopically

expressed MAGE-A4 in 293T cells, which lack endogenous MAGE-A4 (Fig. 3.10). To

further test the effect of MAGE-A4 on RAD18 stability, we reconstituted the ubiquitin-

coupled proteolysis of RAD18 in a cell-free rabbit reticulocyte lysate and compared the

degradation of immunopurified HA–RAD18 complexes from control and MAGE-A4-expressing cells. As shown in Fig. 3.4B, HA–RAD18 derived from MAGE-A4 co-expressing 293T cells was degraded less efficiently when compared with RAD18 from control cultures lacking endogenous MAGE-A4. Taken together Figs 3.3A–F and 3.4A,B show that MAGE-A4 protects RAD18 from ubiquitin-coupled proteolysis.

The results of Fig. 3.2 suggest that MAGE-A4 increases RAD18 expression via direct binding. Therefore, we compared the stabilizing effects of co-transfected MAGE-A4 on HA–RAD18 WT and the MAGE-A4-interaction-deficient HA–RAD18 Δ340–395 mutant. As shown in Fig. 3.4C, levels of HA–RAD18 WT were increased by co-expressed MAGE-A4. HA–RAD18 Δ402–444 (which is defective for Polη interaction but binds MAGE-A4) was also stabilized by co-expressed MAGE-A4. However, levels of HA–RAD18 Δ340–395 (indicated by the white arrowhead in Fig. 3.4C) were insensitive to MAGE-A4.

The MAGE-A4-interaction-deficient RAD18 mutant also lacks RAD6-binding activity. Therefore, we considered the possibility that failure of MAGE-A4 to stabilize RAD18 Δ340–395 was secondary to impaired ubiquitin ligase activity. However, a catalytically inactive RAD18 C28F mutant was stabilized by co-expressed MAGE-A4 (Fig. 3.4C). We conclude that MAGE-A4 stabilizes RAD18 via direct interactions with the RAD6-binding motif and independently of RAD18 E3 ligase activity.

Next we asked whether stabilization of associated E3 ligases represents a general mechanism for modulation of ubiquitin signaling by MAGE-A4. We determined the effect of MAGE-A4 expression on TRIM69 levels. As shown in Fig. 3.4D, MAGE-A4 expression was inversely correlated with TRIM69 levels. Therefore, the stabilizing effect

of MAGE-A4 on RAD18 expression is relatively specific. Other MAGE-A4-associated E3 ligases have not been identified but eventually it will be interesting to elucidate the basis for the differential effects of MAGE-A4 on stability of its (putative) other E3 ligase partners.

Structural basis for MAGE-induced RAD18 stability.

Previous investigators have used deletion and truncation mutants to isolate separable functional domains of MAGE proteins (albeit for effectors other than RAD18)[41, 42]. Therefore, we performed structure–function analyses to define MAGE-A4 residues and domains that are important for stabilizing RAD18. We generated MAGE-A4 deletion mutants lacking or retaining the winged-helix (WH)-A and WH-B regions of the MAGE-homology domain, as illustrated in Fig. 3.5A. In addition, we generated a MAGE-A4 LL4AA mutant harboring alanine substitutions in a di-Leucine motif (L121 and L122) that is conserved between MAGE proteins and is generally necessary for their interactions with E3 ubiquitin ligase partners. We also generated a MAGE-A4 mutant with an alanine substitution at Serine 90, a phosphorylated residue present in RAD18-associated MAGE-A4. In transient transfections, the MAGE-A4 mutants were expressed with different efficiencies in 293T cells. Most notably, mutants lacking the WH-A and WH-B domains expressed poorly when compared with full-length MAGE-A4 (Fig. 3.5B and Fig. 3.11). We compared the various MAGE-A4 mutants for RAD18-stabilizing activity. As expected, WT MAGEA4 extended the half-life of RAD18 from ~24 to >50 h in 293T cells (Fig. 3.5C,D). MAGE-A4 S90A retained RAD18-stabilizing activity, indicating that MAGE-A4 S90 phosphorylation is dispensable for regulating RAD18

expression levels (Fig. 3.11). MAGE-A4 LL4AA did not affect RAD18 levels, suggesting that MAGE-A4–RAD18 interactions are necessary for MAGE-A4 to stabilize RAD18.

All MAGE-A4 deletion mutants (including MAGE-A4 mutant AB, which retains a pro-apoptotic carboxy-terminal domain of MAGE-A4 previously shown to bind gankyrin[41, 42]) failed to stabilize RAD18. We conclude that the individual WH-A or WH-B domains, or the entire MAGE-homology domain and its flanking sequences alone are insufficient to confer RAD18 stability. Instead, it is most likely to be that multiple regions of the MAGE-A4 protein act in a concerted non-separable manner to stabilize RAD18.

The MAGE family members are highly conserved and may, in some cases, have overlapping functions in activating their E3 ligase partners[25]. It was of interest to determine the extent to which other MAGE family members stabilized RAD18. We were able to ectopically express MAGE-A12, MAGE-B10 and MAGE-A1 in 293T cells (Fig. 3.6A) and therefore these particular CTAs were tested for RAD18-stabilizing activity. Unexpectedly, despite the high conservation of primary sequences and domains between different MAGE family members, only MAGE-A4 stabilized RAD18 (Fig. 3.6B,C). Interestingly, these cycloheximide stability experiments also showed that MAGE-A4 has a long half-life (>48 hrs) when compared with MAGE-B10, MAGE-A1 and MAGE-A12. Therefore, MAGE-A4 is highly stable compared with other MAGE family members and specifically stabilizes RAD18.

MAGE-A4 promotes PCNA mono-ubiquitination and TLS.

Increased expression of RAD18 can substantially enhance both basal and genotoxin-induced PCNA mono-ubiquitination[5]. Therefore, we determined whether MAGE-A4 contributes to RAD18-dependent TLS pathway activation in cancer cells. As

shown in Fig. 3.7A and Fig. 3.12, siRNA-mediated MAGE-A4 knockdown in H1299 cells led to an attenuation of ultraviolet-inducible PCNA mono-ubiquitination. The reduced PCNA ubiquitination of MAGE-depleted cells was rescued by co-transfection of siRNA-resistant MAGE-A4 (Fig. 3.7A). 5-Bromodeoxyuridine (BrdU) labeling and fluorescence activated cell sorting analyses revealed no effect of MAGE-A4 depletion on DNA synthesis or cell cycle parameters (Fig. 3.7B). Therefore, the reduced PCNA mono-ubiquitination of MAGEA4-depleted cells was not secondary to cell cycle changes.

As MAGE-A4 depletion led to reduced PCNA monoubiquitination in H1299 cells, we also asked whether forced expression of MAGE-A4 in cells lacking the protein endogenously was sufficient to induce PCNA mono-ubiquitination. As shown in Fig. 3.7C, ectopic overexpression of MAGE-A4 in A549 cells enhanced PCNA mono-ubiquitination in response to low ultraviolet doses. Overexpressed MAGE-A4 did not affect PCNA mono-ubiquitination in H1299 cells (which already express high levels of endogenous MAGE-A4). MAGE-A4 also induced PCNA mono-ubiquitination when ectopically expressed in non-transformed mouse embryonic fibroblasts and human dermal fibroblasts. MAGE-A4 expression did not induce PCNA monoubiquitination in RAD18 -/- cells, demonstrating that the stimulatory effect of MAGE-A4 on PCNA mono-ubiquitination was RAD18 dependent.

As MAGE-A4 promotes RAD18-mediated PCNA monoubiquitination (Fig. 3.7A–C), we determined the potential contribution of MAGE-A4 to replication of damaged DNA. RAD18-depleted cells fail to recover appropriately from DNA damage-induced inhibition of DNA synthesis[5]. Interestingly, MAGE-A4 depletion partially phenocopied the defective S-phase recovery of RAD18-depleted H1299 cells from ultraviolet induced

88

replication arrest (Fig. 3.7D). Moreover, co-depletion of RAD18 and MAGE-A4 did not have additive inhibitory effects on S-phase recovery after ultraviolet treatment (Fig. 3.7D). Similar to phenotypes described in RAD18-depleted cells, the defective recovery of MAGE-A4-depleted cells from S-phase arrest was associated with persistence of γH2AX (Fig. 3.7E). RAD18 expression was also MAGE-A4 dependent in H157 and H650 adenocarcinoma cells and in U2OS osteosarcoma cells (which express endogenous MAGE-A4; see Fig. 3.13A,B). Similar to H1299 cells, MAGE-A4 depletion led to an attenuation of PCNA mono-ubiquitination and increased γH2AX after ultraviolet treatment in U2OS cells (Fig. 3.13C). Taken together, the results of Fig. 3.7C–E indicate a role for MAGEA4 in facilitating TLS and recovery from DNA damage-induced replication fork stalling.

To determine whether MAGE-A4 impacts RAD18-mediated genome maintenance we used an established assay in which RAD18 promotes error-free bypass of an ultraviolet-damaged pSP189 reporter plasmid, thereby suppressing mutagenesis[43]. As shown in Fig. 3.7F, ectopic expression of RAD18 in 293T cells suppressed mutagenesis of the ultraviolet-damaged supF reporter by 40%, consistent with previous reports[43]. Interestingly, MAGE-A4 expression alone led to a 31% decrease in mutagenesis. When co-expressed with RAD18, MAGE-A4 further enhanced the suppressive effect of RAD18 on mutagenesis. As expected, MAGE-A4 induced the expression of endogenous and ectopically co-expressed RAD18 coincident with suppression of mutagenesis (Fig. 3.7F). MAGE-A4 overexpression did not affect DNA synthesis rates or ultraviolet-checkpoint recovery of 293T cells (Fig. 3.14). Therefore, MAGE-A4 can

specifically influence replicative bypass of ultraviolet-induced DNA lesions, further

consistent with its novel role in regulating RAD18 levels and TLS activity in cancer cells.

3.4 Discussion

Potts and colleagues[25] made the seminal discovery that many MAGE proteins bind

and activate E3 ubiquitin ligases, contributing to deregulated ubiquitin signaling in

cancer cells. Our work identifies RAD18 as a target of MAGE-A4 and provides a new

potential mechanism by which genome maintenance and genome stability can be

altered in cancer cells.

There are interesting similarities and differences in the relationship between MAGE-

A4 and RAD18 when compared with previously described MAGE-E3 ligase

associations. For example, the conserved di-leucine motif required by other MAGE

family members to activate their cognate E3 ligases[25] is also necessary for MAGE-A4 to

stabilize RAD18. However, although other MAGEs are allosteric activators of their

associated E3 ligases[25], MAGE-A4 does not stimulate catalytic activity of purified

recombinant RAD18 under defined in vitro conditions. Instead MAGE-A4 stabilizes

RAD18 to confer increased PCNA mono-ubiquitination and TLS. Therefore, this study

provides a new paradigm for MAGE induced reprograming of ubiquitin signaling via

altered E3 ligase stability in cancer cells.

It is possible that MAGE-A4–RAD18 signaling also occurs during normal mammalian

development and in non-pathological situations. Similar to MAGE proteins, Rad18 is

expressed at high levels in germ cells and male rad18-/- mice have impaired

spermatogenesis and fertility[44]. However, in preliminary experiments we have not

detected Mage-A4 (or other Mage proteins) in anti-RAD18 immunoprecipitates from mouse testes extracts. Therefore, we favor the hypothesis that RAD18 binding is a 'neomorphic' activity of aberrantly expressed MAGE-A4 in cancer cells.

Remarkably, although several MAGE-E3 ubiquitin ligase complexes have been characterized[25], no conserved sequence motifs (on MAGE-A4 family member or E3 ligases) mediate these protein–protein associations. Thus, the mechanism of association appears to be different for every MAGE-E3 ligase complex. Our structure–function analyses show that MAGE-A4 binds and stabilizes RAD18 via the RAD6-binding domain. Reportedly, p95/NBS1 also associates with the RAD6-binding domain of RAD18[39]. Physiologically, RAD18 exists as an asymmetric hetero-trimer comprising two RAD18 molecules in complex with one molecule of RAD6[45]. Therefore, we hypothesize that one RAD18 molecule in the [RAD18]2–RAD6 heterotrimer has a 'free' RAD6-binding domain that is available to interface with MAGE-A4, p95 and perhaps additional proteins. This hypothesis predicts that MAGE-A4 and p95 (or other proteins) may compete for RAD18 binding in cancer cells, and that such competition may have an impact on genome maintenance events involving RAD18–p95 associations. MAGE-A4 lacks the RAD6-like β-sheet and therefore interacts with RAD18 via a distinct mechanism. Clearly, biophysical and crystallographic studies will be necessary to fully characterize the putative [RAD18]$_2$–RAD6–MAGE-A4 complex that exists in cancer cells.

The only other documented E3 ligase-binding partner of MAGE-A4 is TRIM69 and the mechanism of MAGE-A4– TRIM69 association has not been studied. Other known effectors of MAGE-A4 are the transcription factor Miz1[42] and the liver oncoprotein

gankyrin[41], which both bind a C-terminal region of MAGE-A4. We show here that the minimal MAGE-A4 C-terminal region (AB) that regulates Miz1 and gankyrin is insufficient to stabilize RAD18. Indeed, none of the major conserved MAGE-A4 domains retain RAD18-stabilizing activity in isolation. Therefore, RAD18 binding is probably not a modular interaction mediated by individual MAGE-A4 domains. Instead, the overall tertiary structure adopted by MAGE-A4 is likely to be involved in the formation of the MAGE-A4–[RAD18]$_2$–RAD6 complex. The finding that all MAGE-A4 mutants failed to stabilize RAD18 may further support the idea that multiple regions of the MAGE-A4 are required for its RAD18 association. Other MAGE family members with a MAGE-A4-related domain organization do not share RAD18-stabilizing activity, further suggesting that unique or specific tertiary structural determinants are required for MAGE-A4 to bind and stabilize RAD18.

Regardless of the mechanism of MAGE-A4–RAD18 interaction, we show here that endogenous MAGE-A4 confers RAD18 stability and expression in cancer cells. TLS is generally assumed to be a housekeeping genome maintenance mechanism and it has not been suggested that expression or activities of core TLS pathway components are significantly different between cell types. However, expression levels of RAD18 and other TLS proteins (including Polη, Polι and PCNA) vary greatly between different cultured cell lines (Fig. 3.15). What then are the possible consequences of variable RAD18 and TLS polymerase expression on genome stability and carcinogenesis? RAD18-deficient cells do not recruit TLS polymerases to replication forks[5, 16] and exhibit reduced lesion bypass activity[17]. Conversely, RAD18 overexpression stimulates PCNA ubiquitination, recruits Y-family polymerases to replication forks, promoting TLS[5, 46].

Therefore, the repertoire of Y-family DNA polymerases and the degree to which different TLS polymerases respond to RAD18 and PCNA monoubiquitination may have enormous impact on genome stability when RAD18 is present at aberrantly high levels. For example, HeLa cells express unusually high levels of Polι compared with H1299 cells (Fig. 3.15). Polι has exceptionally low fidelity, misincorporating dGTP more frequently than the correct dATP across 'T' on undamaged templates[47]. Therefore, increased RAD18 expression in a cell with aberrantly high Polι levels cell will probably have a severe effect on replication fidelity. Polk overexpression in cultured cells leads to insertions and deletions[48]. Consequently, Polk activation in response to aberrant RAD18 overexpression might cause elevated frequency of indel mutations. Moreover, TLS polymerases have low processivity compared with replicative DNA polymerases. Therefore, elevated RAD18 expression and PCNA monoubiquitination could lead to rampant recruitment of Y-family polymerases to undamaged DNA, causing replication fork slowdown and/or other defects that result in 'fork collapse' and compromise genome stability due to DSB formation. A potential role for MAGE-A4–RAD18 as a mutagenic driver or source of genomic instability in cancer cells owing to inappropriate TLS polymerase activation is highly likely.

Maiorano and colleagues[46] recently showed that ectopic RAD18 overexpression can lead to DNA damage tolerance. Potentially, MAGE-A4-induced RAD18 expression might contribute to tumorigenesis by enhancing DNA-damage tolerance via TLS (and perhaps additional RAD18-mediated DNA repair pathways such as homologous recombination[49] and cross-link repair[34]). Neoplastic cells must endure endogenous stresses including ROS-induced DNA damage and other forms of DNA replication

stress[50]. Collectively, TLS polymerases can perform bypass of oxidative lesions (such as 8-oxo-dG and AP sites) potentially conferring tolerance of oncogene-induced ROS. In addition, TLS polymerases can facilitate ongoing DNA synthesis in cells undergoing oncogene-induced re-replication[22] (one of the earliest responses to oncogene activation in untransformed cells[51]). Therefore, increased TLS capacity afforded by MAGE-A4– RAD18 may contribute to tolerance of spontaneously arising DNA damage and replication stress, thereby facilitating neoplastic cell survival and tumor progression.

Clearly, future experiments are necessary to determine the potential contribution of MAGE-A4 and RAD18 to genome destabilization and tolerance of oncogenic stress. In addition to promoting tolerance of intrinsic oncogene-induced sources of stress (such as ROS and re-replication), RAD18 confers tolerance of chemo/radiotherapy[52, 53]. Therefore, the MAGE-A4–RAD18 signaling axis may represent an attractive therapeutic target that, when inhibited, could be innocuous to normal cells but selectively sensitize cancer cells to intrinsic and therapy-induced DNA damage and replication stress.
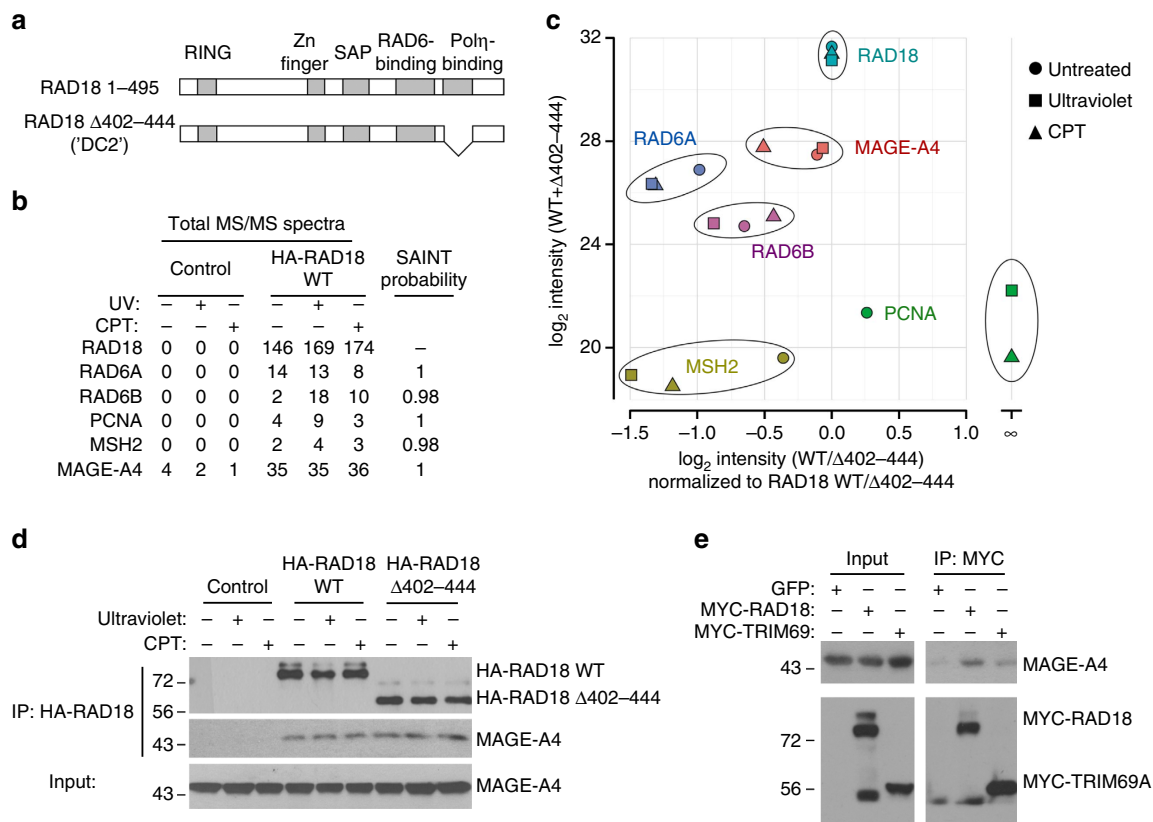
a

RAD18 1–495 — RING, Zn finger, SAP, RAD6-binding, Polη-binding

RAD18 Δ402–444 ('DC2')

b

Total MS/MS spectra

	Control			HA-RAD18 WT			SAINT probability
UV:	–	+	–	–	+	–	
CPT:	–	–	+	–	–	+	
RAD18	0	0	0	146	169	174	–
RAD6A	0	0	0	14	13	8	1
RAD6B	0	0	0	2	18	10	0.98
PCNA	0	0	0	4	9	3	1
MSH2	0	0	0	2	4	3	0.98
MAGE-A4	4	2	1	35	35	36	1

c

log$_2$ intensity (WT/Δ402–444) normalized to RAD18 WT/Δ402–444 — log$_2$ intensity (WT+Δ402–444)

● Untreated ■ Ultraviolet ▲ CPT

RAD18, RAD6A, MAGE-A4, RAD6B, PCNA, MSH2

d

IP: HA-RAD18 — HA-RAD18 WT, HA-RAD18 Δ402–444, MAGE-A4

Input: MAGE-A4

e

Input / IP: MYC — MAGE-A4, MYC-RAD18, MYC-TRIM69A

Figure 3.1: MAGE-A4 is a novel component of the RAD18 complex in cancer cells

(A) Domain organization of full-length RAD18 and RAD18 Δ402-444 (which harbors an internal deletion removing the Polη-binding domain). **(B)** Spectral counts and estimated probability of true interaction by SAINT analysis for selected proteins identified HA-RAD18-WT and Control (HA) APMS experiments. **(C)** Total protein signal intensity versus relative abundance between HA-RAD18-WT and HA-RAD18 Δ402-444 APMS. Signal intensity was normalized to the corresponding experiment's bait intensity (x axis). **(D)** H1299 cells were infected with adenoviruses encoding WT HA-RAD, HA-RAD18 Δ402-444 or with an 'empty' control adenovirus. Infected cells were treated with CPT (2 µM) or UVC (20 Jm^{-2}). Two hours (h) later, cell extracts were prepared and immunoprecipitated with anti-HA antibody- conjugated magnetic beads. The resulting immune complexes and input fractions were analyzed by immunoblotting with anti-HA and anti-MAGE-A4 antibodies. **(E)** Expression vectors encoding MYC–RAD18, MYC–TRIM69 or green fluorescent protein (GFP) (for control plasmid) were transiently transfected into H1299 cells. Extracts from the resulting cells were immunoprecipitated with an anti-MYC antibody and the resulting immune complexes (or input fractions) were analyzed by immunoblotting with antibodies against MAGE-A4 and MYC.
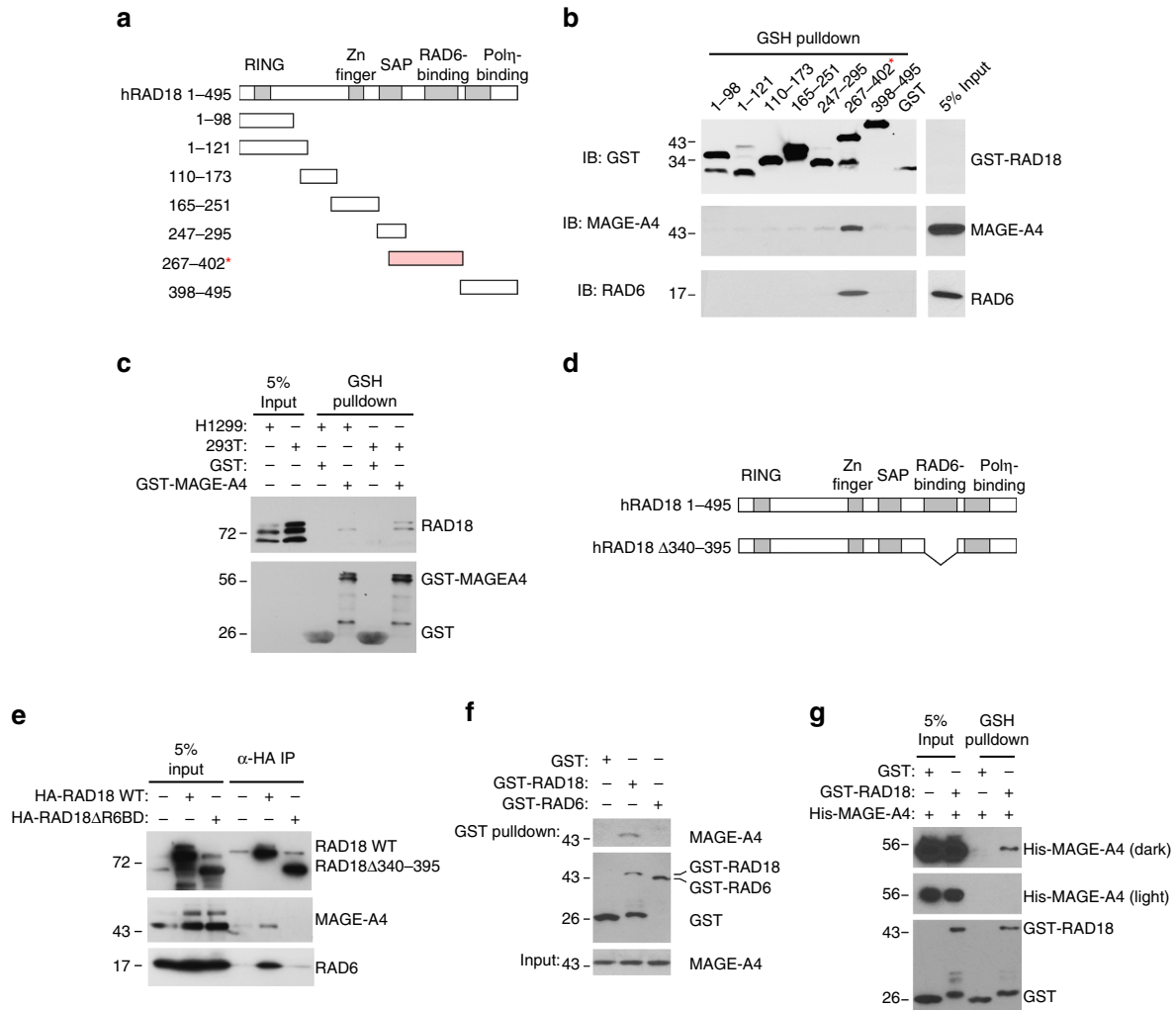
95

Figure 3.2: MAGE-A4 associates with the RAD6-binding domain of RAD18.

Figure 3.2: MAGE-A4 associates with the RAD6-binding domain of RAD18.
(A) The indicated RAD18 fragments were expressed as GST fusions in E. coli. The RAD6-binding domain spanning residues 267–402 is highlighted in red. **(B)** GST–RAD18 fragments were incubated with H1299 cell extracts. After 'pull-down' with GSH-sepharose beads, the recovered GST–RAD18 fusions and 5% of 'input' H1299 cell lysate were analyzed by immunoblotting with antibodies against GST, MAGE-A4 and RAD6. **(C)** GST–MAGE-A4 or GST was incubated with extracts from H1299 or 293T cells. After pulldown with GSH-sepharose beads, the recovered GST proteins (and 5% of input cell extract) were analyzed by immunoblotting with antibodies against GST and RAD18. **(D)** Domain organization of full-length RAD18 and the RAD18 D340–395 (ΔR6BD) mutant harboring an internal deletion that removes the RAD6-binding domain. **(E)** H1299 cells were transiently transfected with expression plasmids encoding HA–RAD18 and HA–RAD18 D340–395 (ΔR6BD) or with an empty vector control. Lysates from the resulting cells were immunoprecipitated with anti-HA antibodies. Anti-HA immune complexes and inputs (20 mg) were analyzed by immunoblotting with antibodies against RAD18, MAGE-A4 and RAD6. **(F)** Recombinant GST, GST–RAD18 267–402 or GST–RAD6 were incubated with H1299 cell extracts then pulled down with GSH-sepharose beads. The recovered GST proteins were analyzed by immunoblotting with antibodies against MAGE-A4 and GST. **(G)** Recombinant GST and GST–RAD18 267–402 were incubated with full-length recombinant Hexa-histidine-tagged MAGE-A4 (His-MAGE-A4). GST proteins were recovered using GSH-sepharose beads. Recovered GST proteins (and 5% of input) were analyzed by immunoblotting with antibodies against GST and MAGE-A4.
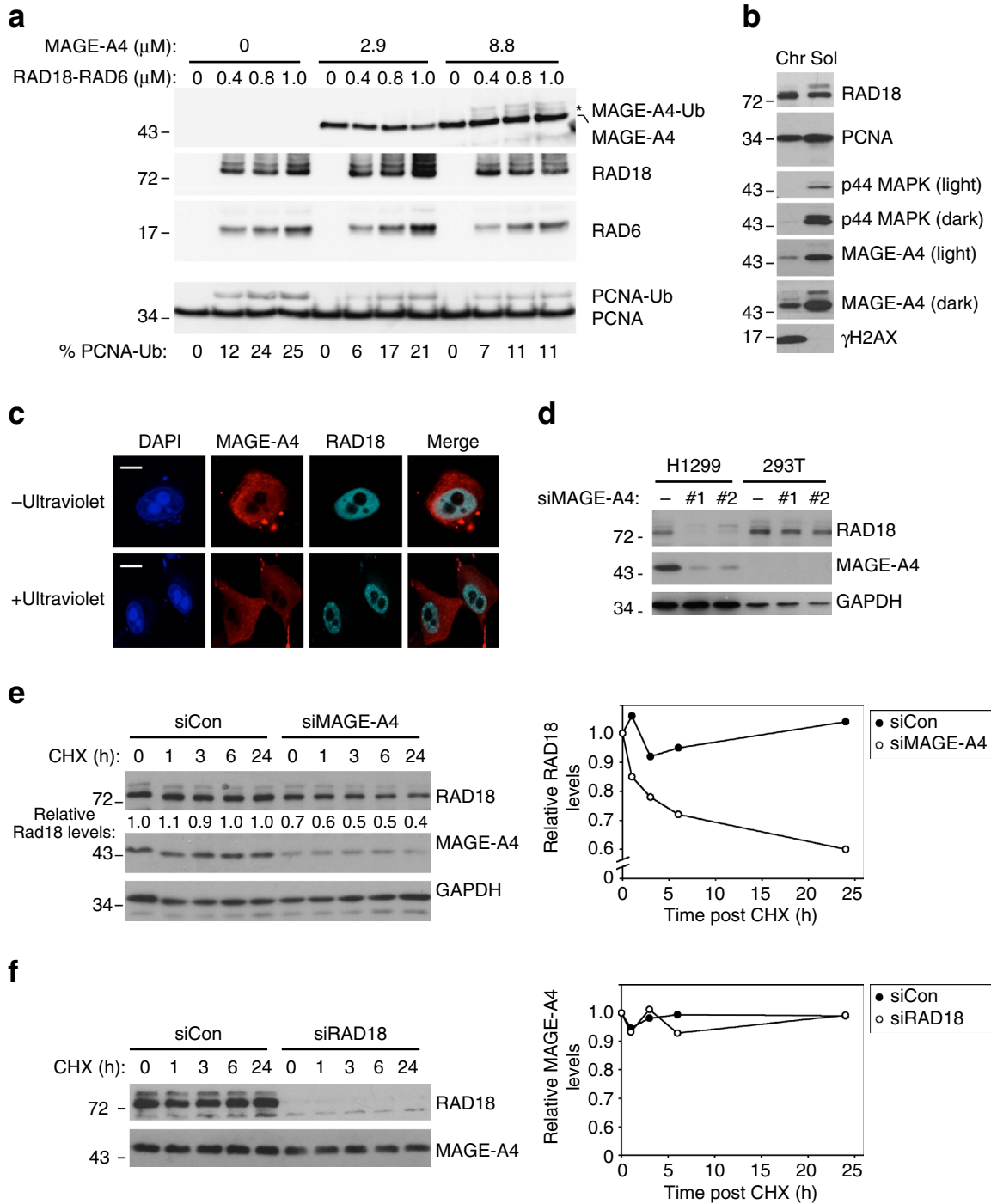
Figure 3.3 MAGE-A4 promotes RAD18 stability.

Figure 3.3 MAGE-A4 promotes RAD18 stability.

(A) Recombinant RAD18–RAD6 complex (0, 0.27, 0.54 and 0.82 µM) was incubated with E1, ubiquitin and purified PCNA. Reaction products were analyzed by immunoblotting with antibodies against the indicated proteins. **(B)** Soluble and chromatin fractions from H1299 cells were analyzed by SDS–PAGE (20 µg per lane) and immunoblotting with antibodies against the indicated proteins. **(C)** H1299 cells were transiently transfected with an expression plasmid encoding CFP-RAD18 (or empty vector for control), ultraviolet irradiated (20 J m^{-2}) and processed for immunofluorescence microscopy after 6 h. Scale bar, 10 µm. **(D)** H1299 and 293T cells were transfected with two independent siRNAs targeting MAGE-A4 or with control non-targeting siRNA oligonucleotides. After 72 h, extracts from the siRNA-transfected cells were analyzed by immunoblotting with antibodies against the indicated proteins. **(E,F)** H1299 cells were transfected with siRNA oligonucleotides against MAGE-A4, RAD18 or control non-targeting siRNA as indicated. Forty-eight hours later, cells were treated with cycloheximide (CHX, 100 µg ml^{-1}) and collected at different time points for immunoblot analysis.
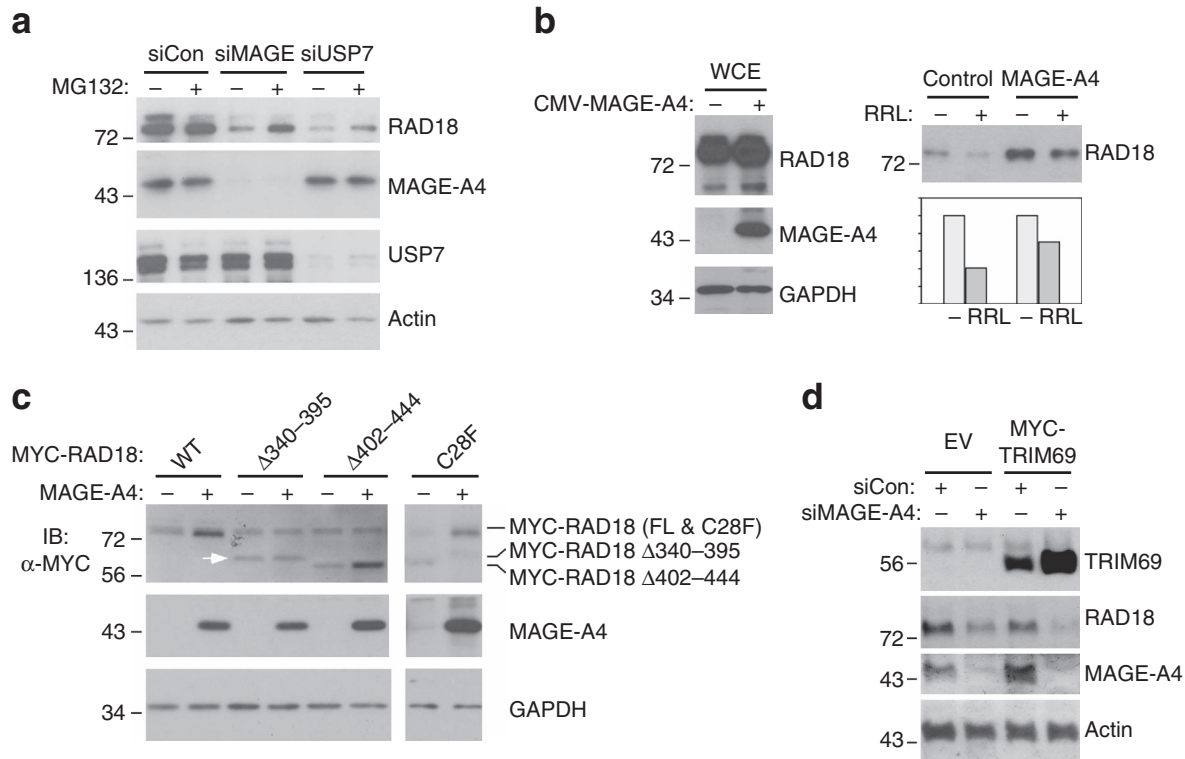
Figure 3.4 MAGE-A4 protects RAD18 from ubiquitin-mediated proteolysis.

(A) Replicate plates of H1299 cells were transfected with siRNA against MAGE-A4, USP7 or with non-targeting control siRNA. After 48 h, one plate of each replicate was treated with 10 µM MG132 for 16 h. Extracts from control and MG132-treated cells were analyzed by immunoblotting with antibodies against the indicated proteins. **(B)** 293T cells were co-transfected with an HA–RAD18 expression vector in combination with a CMV-MAGE-A4 plasmid or an empty vector for control. After 48 h, RAD18 complexes were immunoprecipitated with anti-HA antibodies. The resulting immune complexes were incubated in a rabbit reticulocyte lysate (RRL) to reconstitute ubiquitin-coupled proteolysis in vitro. Relative levels of RAD18 and MAGE-A4 were determined by immunoblotting and quantified using densitometry. **(C)** H1299 cells were transiently co-transfected with WT or mutant HA–RAD18 expression plasmids in combination with a MAGE-A4 expression vector (or empty vector control). Forty-eight hours later, cells were harvested for immunoblot analysis of RAD18 and MAGE-A4. The white arrowhead indicates the RAD18Δ340–395 mutant protein band that is insensitive to MAGE-A4. **(D)** Replicate cultures of H1299 cells were transfected with an expression vector encoding MYC–TRIM69 or with an empty vector plasmid for control. Sixteen hours later, the cells were transfected with siRNA against MAGE-A4 or with a scrambled control siRNA and incubated for an additional 48 h before immunoblot analysis.
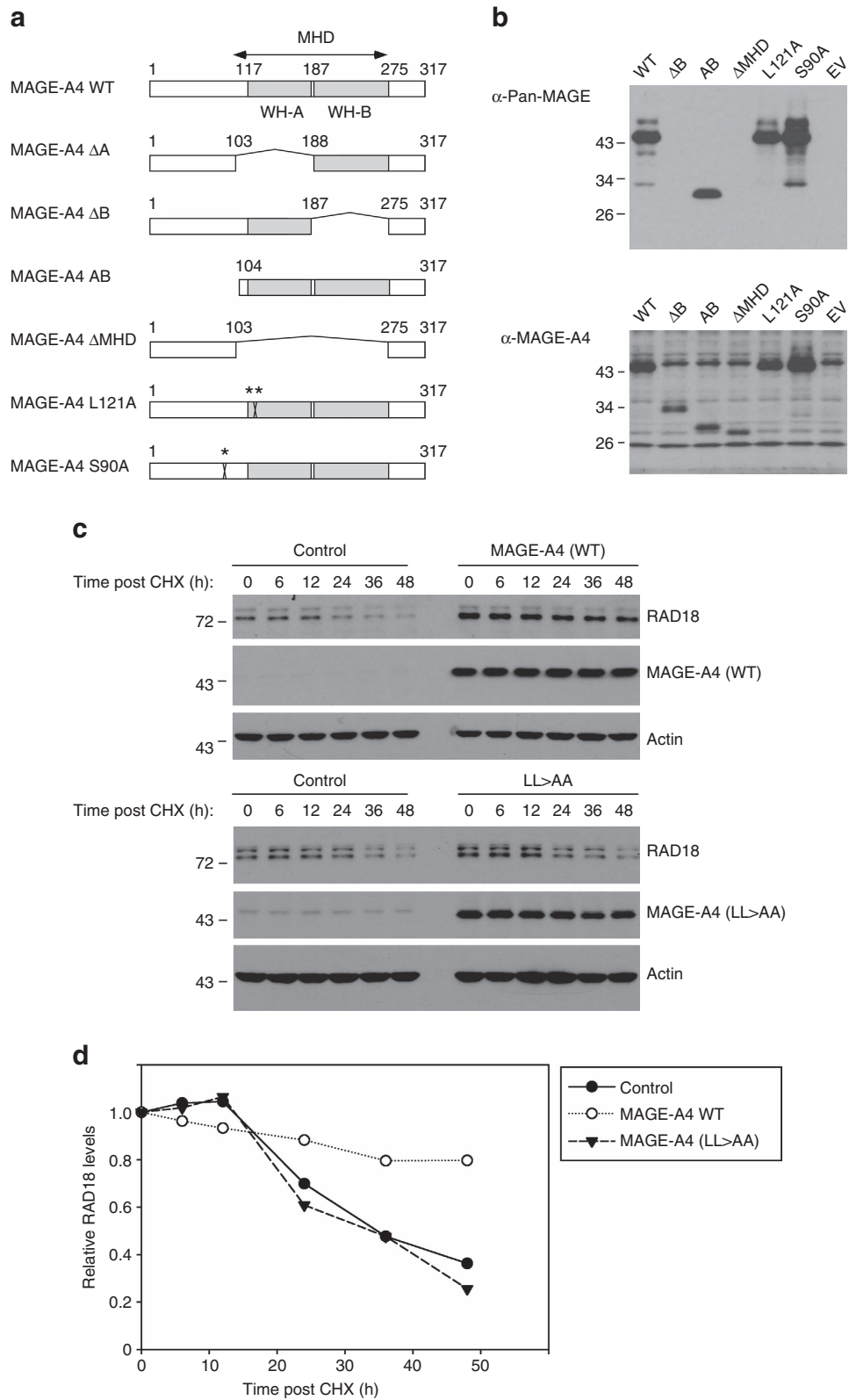
Figure 3.5: Mutational analyses to define structural requirements for MAGE-A4-induced RAD18 stabilization.

Figure 5: Mutational analyses to define structural requirements for MAGE-A4-induced RAD18 stabilization.

(A) Domain structure of full-length MAGE-A4 and MAGE-A4 mutants used in this study. The MAGE-homology domain (MHD) is conserved between MAGE family members and comprises juxtaposed WH-A and WH-B regions. **(B)** 293T cells were transiently transfected with expression vectors encoding the MAGE-A4 mutants shown in **A** or with an empty vector (EV). After 48 h, extracts from the resulting cells were analyzed by immunoblotting with anti-Pan-MAGE-A (which recognizes an epitope in the WH-B domain) or with anti-MAGE-A4 (which recognizes a C-terminal epitope of MAGE-A4 in residues 275–317). **(C)** Replicate plates of 293T cells were transiently transfected with expression vectors encoding WT or mutant forms of MAGE-A4. Forty-eight hours post transfection, cells were treated with cycloheximide (CHX) and then harvested at different times post CHX. Cell extracts were analyzed by immunoblotting with antibodies against RAD18, MAGE-A4 and actin. **(D)** RAD18 levels in each lane of immunoblots in c were quantified by densitometry with ImageJ software. The graph indicates the levels of RAD18 remaining at each time point following CHX treatment in control and MAGE-A4-expressing cells.
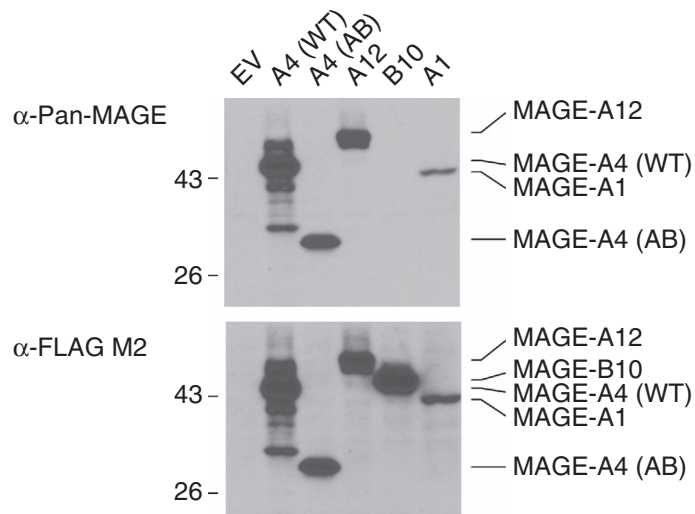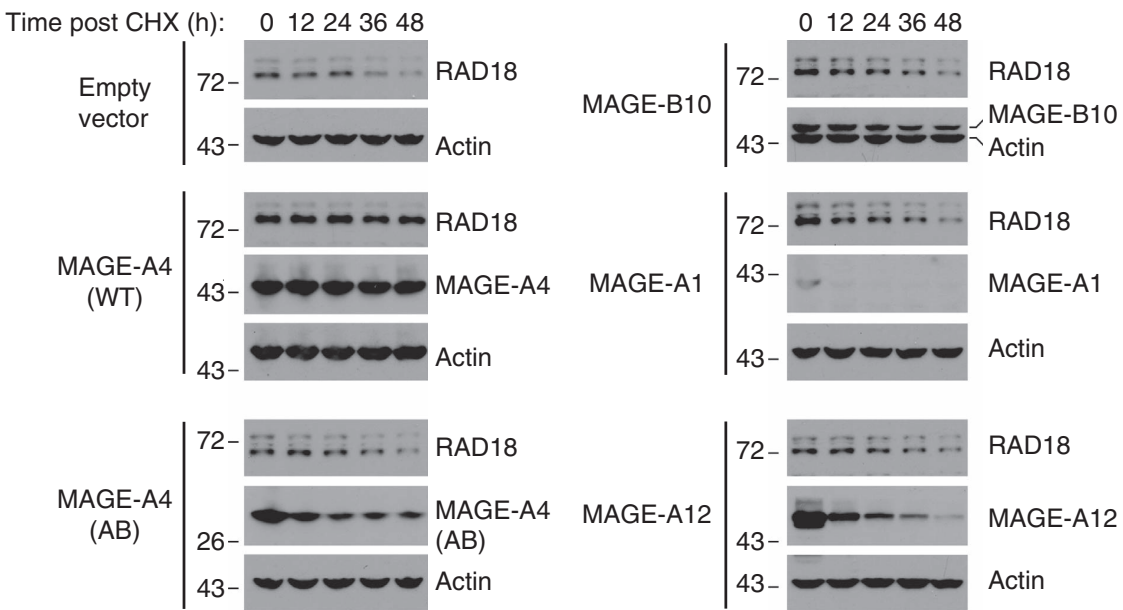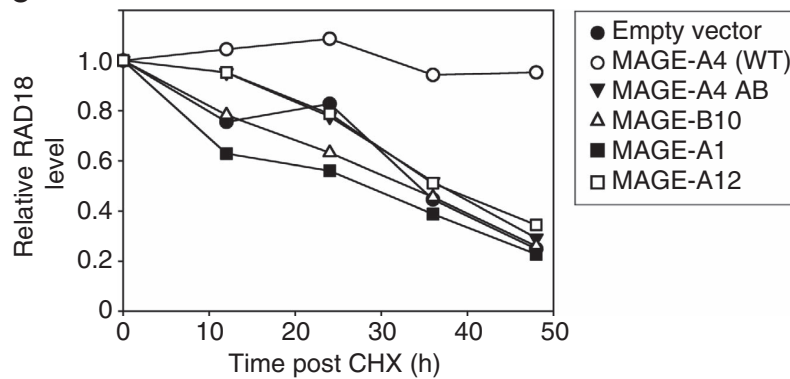
Figure 3.6: Effect of MAGE family members on RAD18 stability.

Figure 3.6: Effect of MAGE family members on RAD18 stability.

(A) 293T cells were transfected with expression vectors encoding FLAG-tagged forms of WT MAGE-A4, MAGE-A4 AB (see Fig. 5a), MAGE-A12, MAGE-B10 and MAGE-A1. After 48 h, extracts were prepared from the transfected cells and analyzed by immunoblotting with anti-Pan-MAGE and anti-FLAG antibodies. **(B)** Replicate plates of 293T cells were transiently transfected with expression vectors encoding WT MAGE-A4, MAGE-A4 AB, MAGE-A12, MAGE-B10 and MAGE-A1. Forty-eight hours post transfection, cells were treated with cycloheximide (CHX) and then harvested at different times post CHX. Cell extracts were analyzed by immunoblotting with antibodies against RAD18, FLAG and actin. **(C)** RAD18 levels in each lane of immunoblots in b were quantified by densitometry with ImageJ software. The graph indicates the levels of RAD18 remaining at each time point following CHX treatment in control and MAGE-expressing cells.
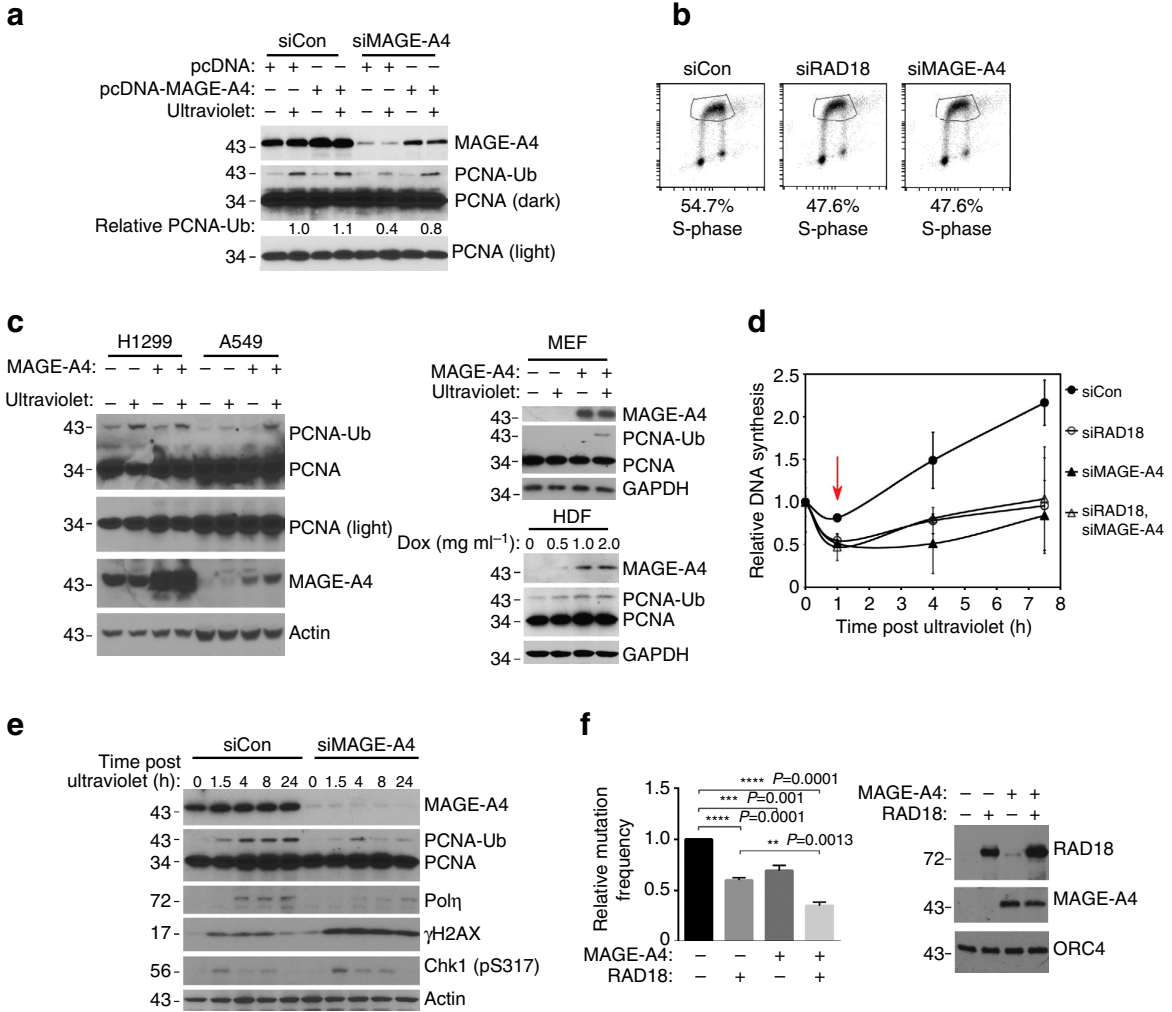
Figure 3.7 MAGE-A4 promotes TLS and DNA-damage tolerance.

Figure 3.7 MAGE-A4 promotes TLS and DNA-damage tolerance.

(A) H1299 cells were transiently transfected with MAGE-A4 or non-targeting siRNAs. After 16 h, cells were transfected with a siRNA-resistant MAGE-A4 expression plasmid (or empty vector control). Forty-eight hours later, cells were sham or ultraviolet irradiated (20 Jm^{-2}) and harvested for immunoblot analysis after 2 h. **(B)** H1299 cells were transfected with siRNA against RAD18, MAGE-A4 or non-targeting siRNA. Forty-eight hours later, cells were pulsed labeled with BrdU (10 µM) for 1 h and collected for flow cytometry. **(C)** H1299, A549 or mouse embryonic fibroblast (MEF) cells were transfected with a MAGE-A4 expression plasmid or empty vector. After 48 h, cells were sham or ultraviolet irradiated (20 Jm^{-2}) and extracted 2 h later for immunoblotting. Human dermal fibroblasts (HDFs) stably transduced with a pINDUCER-MAGE- A4 were treated with indicated doxycycline concentrations for 48 h and then collected for immunoblotting. **(D)** H1299 cells were transfected with siRNA against RAD18 and MAGE-A4 (or with non-targeting oligonucleotides). Twenty-four hours post transfection, cells were re-plated in 24-well dishes and ultraviolet irradiated (5 Jm^{-2}) 48 h later. DNA synthesis rates were measured immediately before and at different times after ultraviolet treatment. **(E)** H1299 cells were transfected with siRNA against MAGE-A4 or with non-targeting siRNA. Seventy-two hours post transfection, cells were sham or ultraviolet irradiated (5 Jm^{-2}) and harvested at different times for immunoblotting. **(F)** 293T cells were co-transfected with ultraviolet-damaged pSP189 reporter plasmid and MAGE-A4 or RAD18 expression vectors. Forty-eight hours later, 293T cell extracts were collected for immunoblot analysis of MAGE-A4 and RAD18 (right). Recovered pSP189 plasmid was transformed into electro-competent MBM7070 bacteria and pSP189 mutation rates were determined by enumerating blue and white bacterial colonies. Data represent means ± s.e.m. of four independent experiments each performed in triplicate. P-values were calculated using a two-tailed Student's t-test. Baseline mutation rates for the experiments ranged from 5.6 to 9.6%.
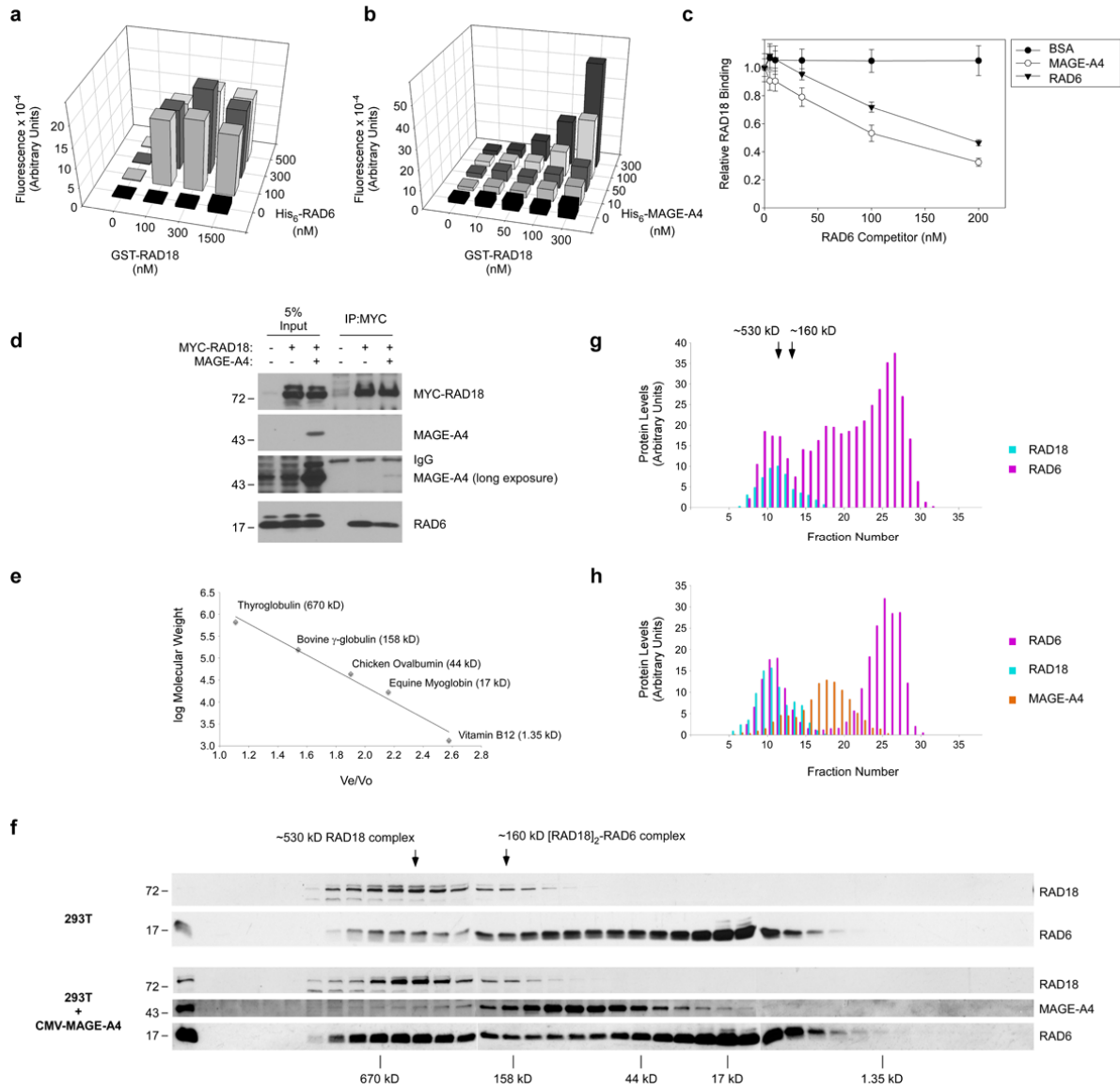
Figure 3.8 RAD6 and MAGE-A4 associate with the RAD6-binding domain of RAD18.

107

Figure 3.8 RAD6 and MAGE-A4 associate with the RAD6-binding domain of RAD18.

 (A) Amplified Luminescent Proximity Homogeneous Assay AlphaScreen assay showing association of RAD18 and RAD6. The indicated concentrations of purified recombinant GST- RAD18 335-400 and His-tagged full-length RAD6 were incubated in 384-well plates (16 replicate wells for each experimental condition) in a reaction volume of 6 µl for 1 hr at room temperature in the dark. Next, 3 µl of nickel chelate acceptor beads (Perkin Elmer 6760619C) were added to give a concentration of 20 µg/ml and incubations were continued for 1 hr. Finally 3 µl of glutathione donor beads (Perkin Elmer 6765300) were added (20 µg/ml final concentration) and incubations were continued for one more hour. Plates were analyzed using the Perkin Elmer Envision plate reader to excite at 680 nm and detect fluorescence at 520 nm.
(B) The AlphaScreen assay was used to detect the association of GST-RAD18 335-400 with His-tagged full-length MAGE-A4, exactly as described for RAD18-RAD6 association in **(A)** above. Note that the binding curves in **(A)** and **(B)** cannot be compared directly because in AlphaScreen assays the magnitude of signal for each unique protein-protein interaction is determined by specific protein conformations and tag proximities.
(C) AlphaScreen assay was used to detect competition between RAD6 and MAGE-A4 for RAD18-binding. In separate reactions His-RAD6 (25 nM) or His-MAGE-A4 (200 nM) were incubated with equimolar GST-RAD18 in the presence of different concentrations (0-200 nM) of untagged competitor RAD6 (or BSA for control). Donor and acceptor beads were added to the reactions and plates were analyzed as described in **(A)** above. To plot the data, the effect of untagged RAD6 (or BSA) on fluorescence was normalized to emission signals obtained in the RAD18/His-RAD6 and RAD18/His-MAGE-A4 reactions without added protein. Error bars represent the mean of 16 replicate wells +/- SEM for each experimental condition.
(D) Effect of MAGE-A4 expression on RAD18-associated RAD6 in cultured cells. 293T cells were transfected with expression vectors encoding MYC-RAD18 and MAGE-A4 (or empty vector for control). Cell lysates were prepared 48 hrs after transfection, and RAD18 was immunoprecipitated using anti-MYC beads. Levels of RAD18-associated RAD6 were determined by SDS-PAGE and immunoblotting. Note that in this experiment, levels of ectopically-expressed RAD18 were very high and no longer sensitive to co-expressed MAGE- A4.
(E)-(H) Size fractionation of RAD18, RAD6 and MAGE-A4 complexes in cultured cells. Exponentially-growing cultures of 293T cells were transfected with empty vector, CMV-GFP, or with a CMV-MAGE-A4 expression plasmid. 48 hrs later GFP fluorescence was used to confirm efficient (~90%) transfection efficiency. Cells were lysed in 300 µl of CSK without sucrose and supplemented with 1 µg/ml (25,000 units/ml) of Benzonase. Lysates were incubated at room temperature for 15 minutes to digest chromatin, then centrifuged at 21,000g for 20 min. 250 µl of each clarified cell lysate (~2.0 mg) was loaded onto a 25ml Sephadex 200 gel filtration column that was calibrated with appropriate molecular weight markers **(E)**. The column was eluted with sucrose-free CSK. 0.5 ml fractions were collected and 30 µl of each

Figure 3.8 RAD6 and MAGE-A4 associate with the RAD6-binding domain of RAD18.

fraction was analyzed by SDS-PAGE and immunoblotting with antibodies against RAD18, RAD6 and MAGE-A4 **(F)**. Relative levels of RAD18, RAD6 and MAGE-A4 between different fractions were determined by densitometry and are plotted in panels **(G)** and **(H)**. The fractions containing the ~160 kDa [RAD18]2-RAD6 complex predicted by biophysical studies and a previously undescribed ~530 kDa RAD18 and RAD6-containing complex are indicated.
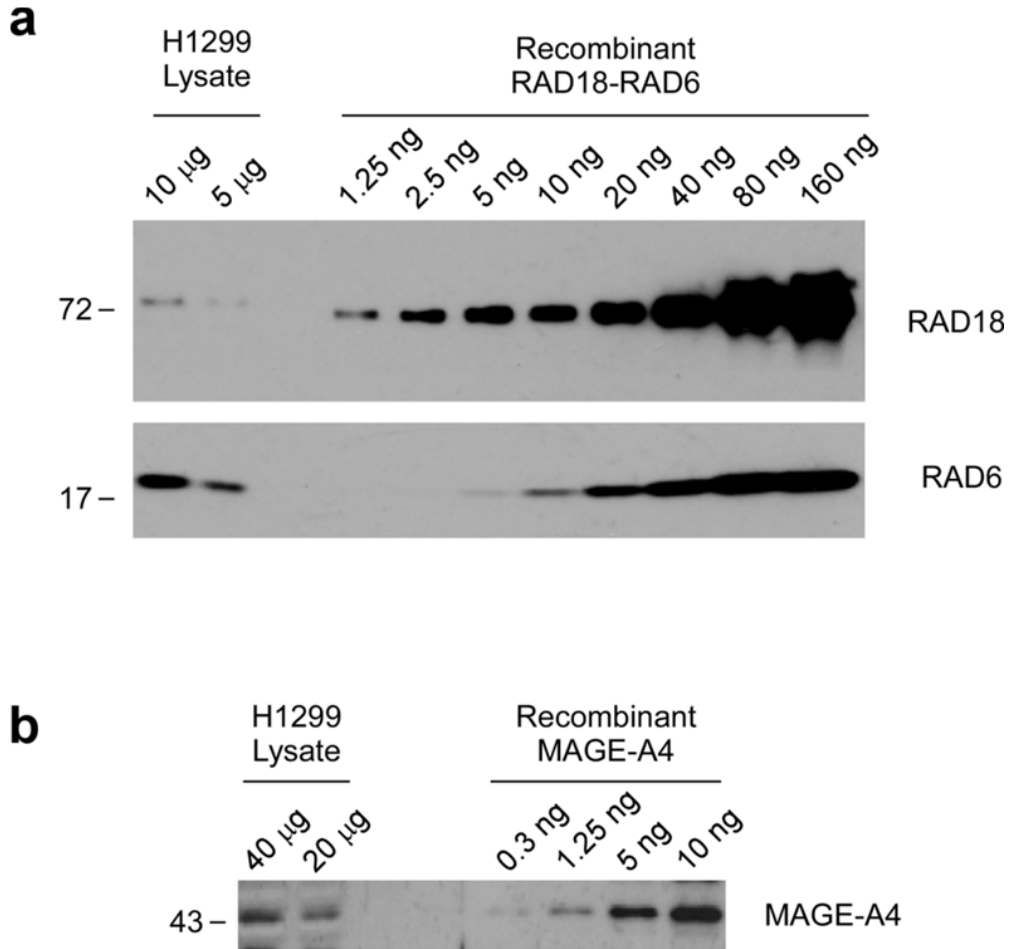
Figure 3.9 Quantitative immunoblot analysis of RAD18, RAD6 and MAGE-A4 expression levels in H1299 cells.

The indicated amounts of H1299 whole cell lysate, recombinant RAD18-RAD6 **(A)**, and MAGE- A4 **(B)** proteins were analyzed by SDS-PAGE and immunoblotting. By comparing expression levels of proteins in cell lysates with defined quantities of purified protein standards we estimate that 1 μg of H1299 cell lysate contains 41 pg (0.74 fmol) of RAD18, 719 pg (42 fmol) of RAD6, and 88 pg (2.5 fmol) of MAGE-A4. Therefore, the RAD18:RAD6:MAGE-A4 stoichiometry in H1299 cells is approximately 1:57:3.

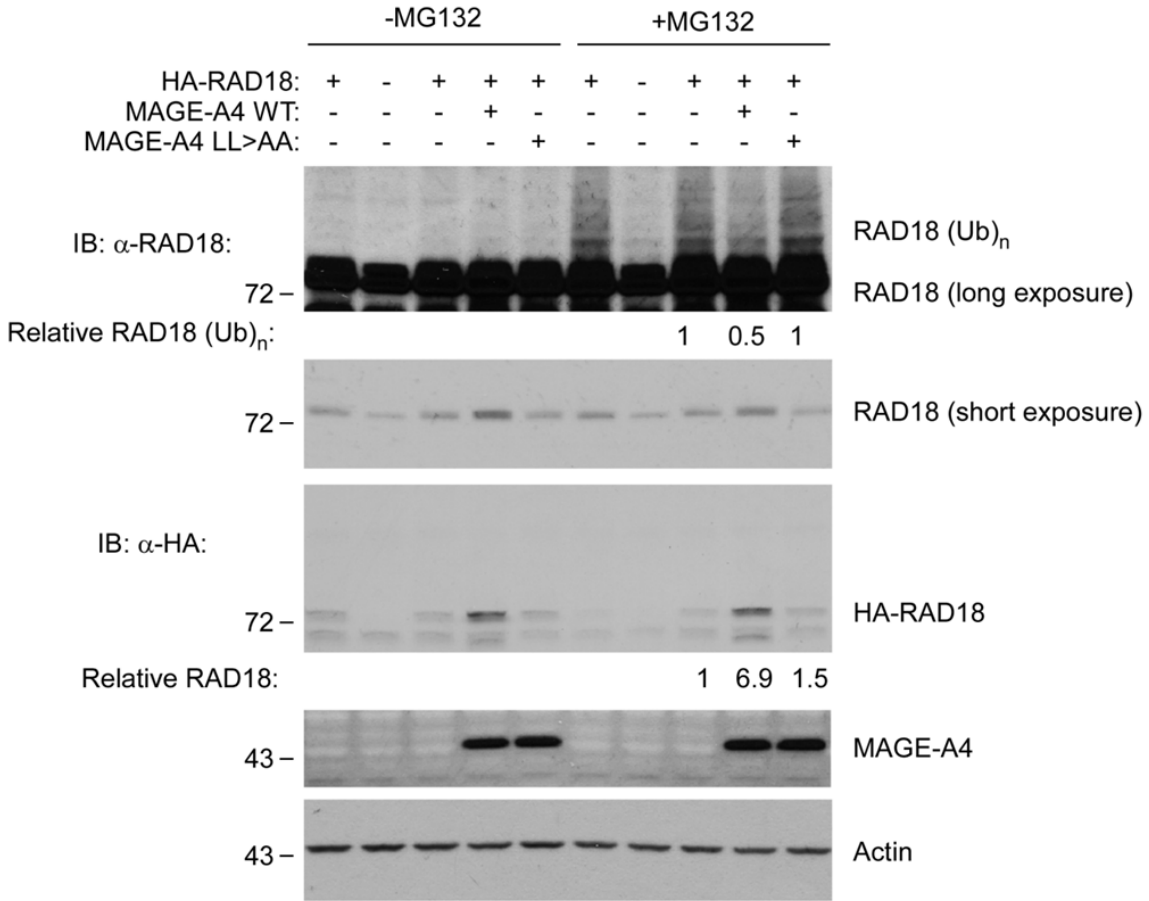**Figure 3.10 Effect of MAGE-A4 on MG132-induced ubiquitin laddering of RAD18 in 293T cells.**

Replicate cultures of exponentially-growing 293T cells were co-transfected with expression vectors encoding HA-RAD18 and MAGE-A4 (WT or LL>AA mutant). 48 hrs later the resulting cultures were treated with MG132 (20 µM) for 4 hrs. Cell lysates were analyzed by immunoblotting with the indicated antibodies.

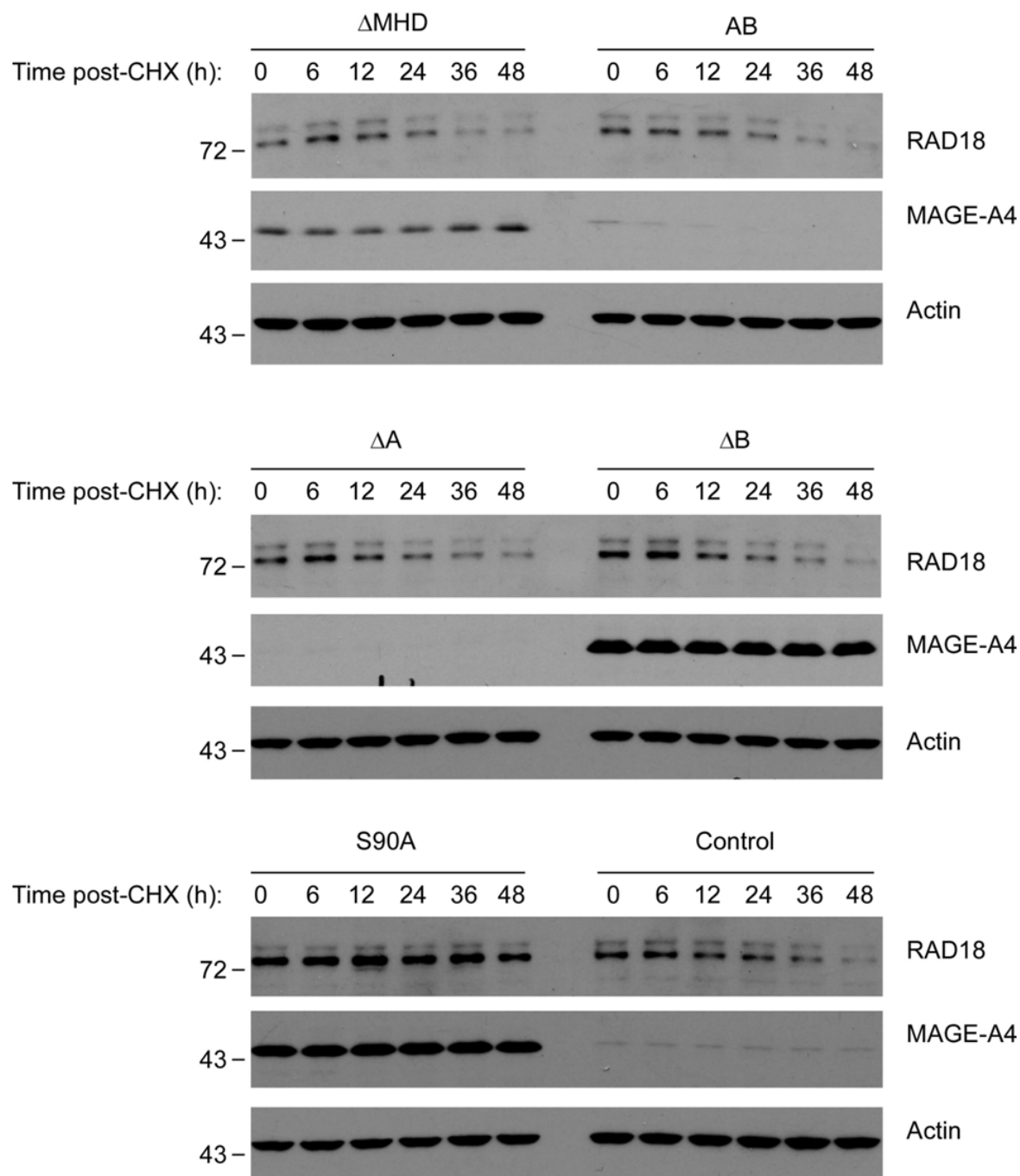**Figure 3.11 Effect of different MAGE-A4 mutants on RAD18 stability.**

Replicate plates of 293T cells were transiently transfected with expression vectors encoding wild-type or mutant forms of MAGE-A4. 48 hrs post-transfection cells were treated with CHX and then harvested at different times post-CHX. Cell extracts were analyzed by immunoblotting with antibodies against RAD18, MAGE-A4, and Actin.
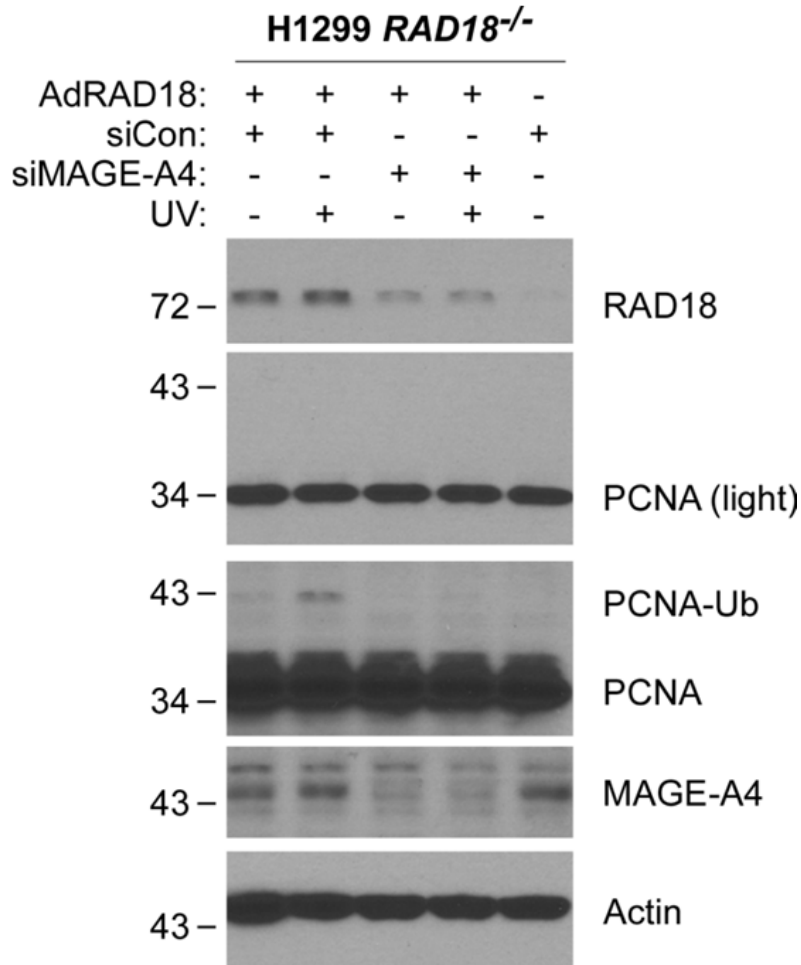
Figure 3.12 MAGE-A4-depletion leads to reduced RAD18 expression and decreased PCNA mono-ubiquitination.

RAD18-/- H1299 cells were transfected with MAGE-A4-directed siRNA or with a non-targeting siRNA control. 24 hrs post-transfection cells were complemented with adenovirally-encoded HA- RAD18. 24 hrs later, cells were UV-irradiated (20 J/m2), or sham-treated for controls. 4 hrs after UV-treatment cells were lysed and extracts were analyzed by SDS-PAGE and immunoblotting with the indicated antibodies.

Figure 3.13 Fig. 7 Effect of MAGE-A4 depletion on RAD18 expression in H157, H650 and U2OS cells.

Figure 3.13 Effect of MAGE-A4 depletion on RAD18 expression in H157, H650 and U2OS cells.

(A) Exponentially-growing H157 and H650 cells were transfected with siMAGE-A4 or non- targeting control (siCon) siRNAs. 48 hrs later cells were lysed and extracts were analyzed by SDS-PAGE and immunoblotting with the indicated antibodies.
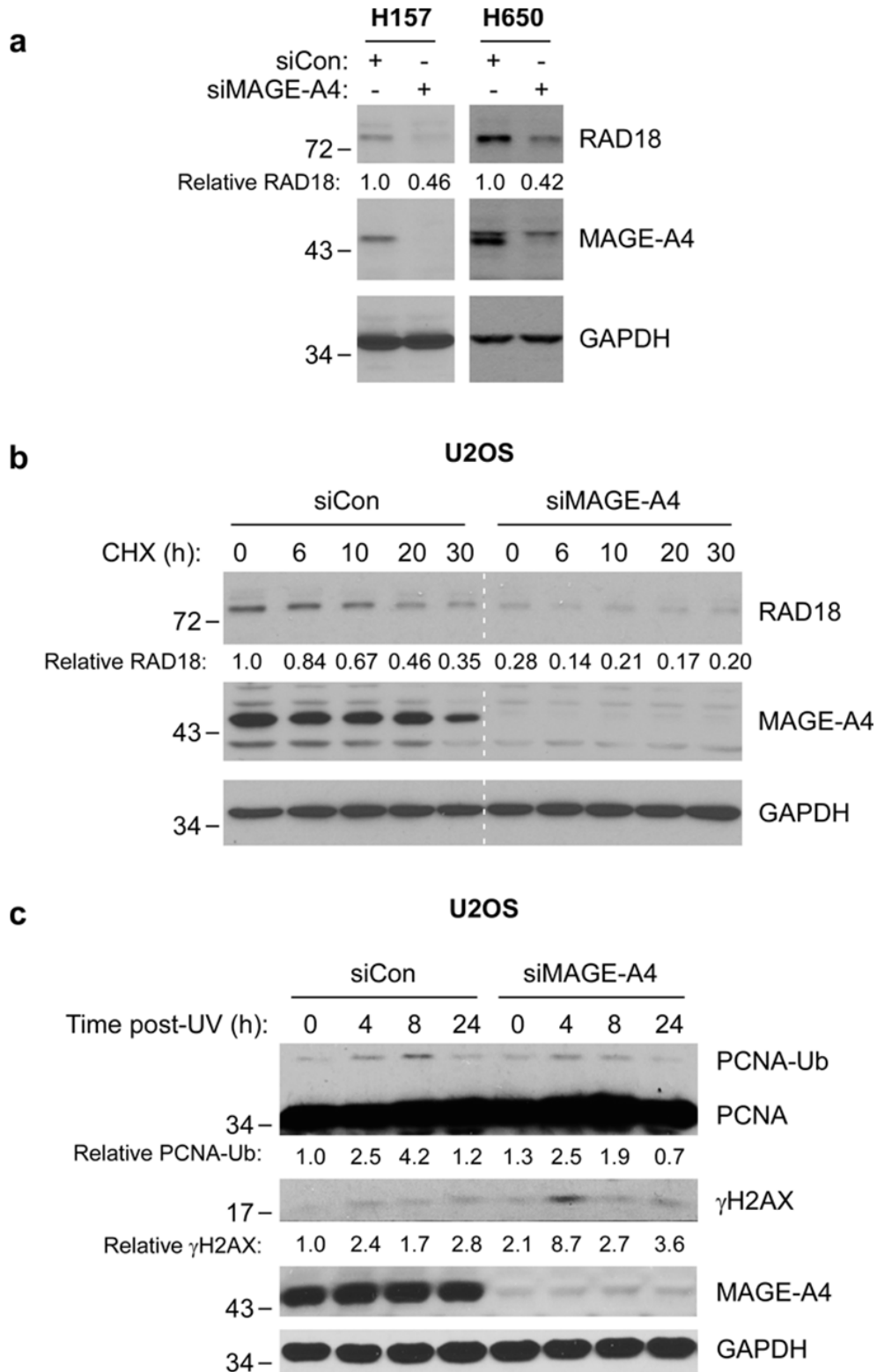**(B)-(C)** Replicate plates of exponentially-growing U2OS cells were transfected with siMAGE-A4 or non-targeting control (siCon) siRNAs. 48 hrs later, some cultures were treated with Cycloheximide (CHX, 100 g/ml) to block new protein synthesis. At indicated times after CHX treatment, control and MAGE-A4-depleted cells were analyzed by SDS-PAGE and immunoblotting with antibodies against RAD18 and MAGE-A4 **(B)**. Other replicate cultures were irradiated with UV-irradiated (5 J/m2), or sham-treated for controls. At different times after UV-treatment, cells were harvested and analyzed by SDS-PAGE and immunoblotting using antibodies against PCNA and γH2AX.
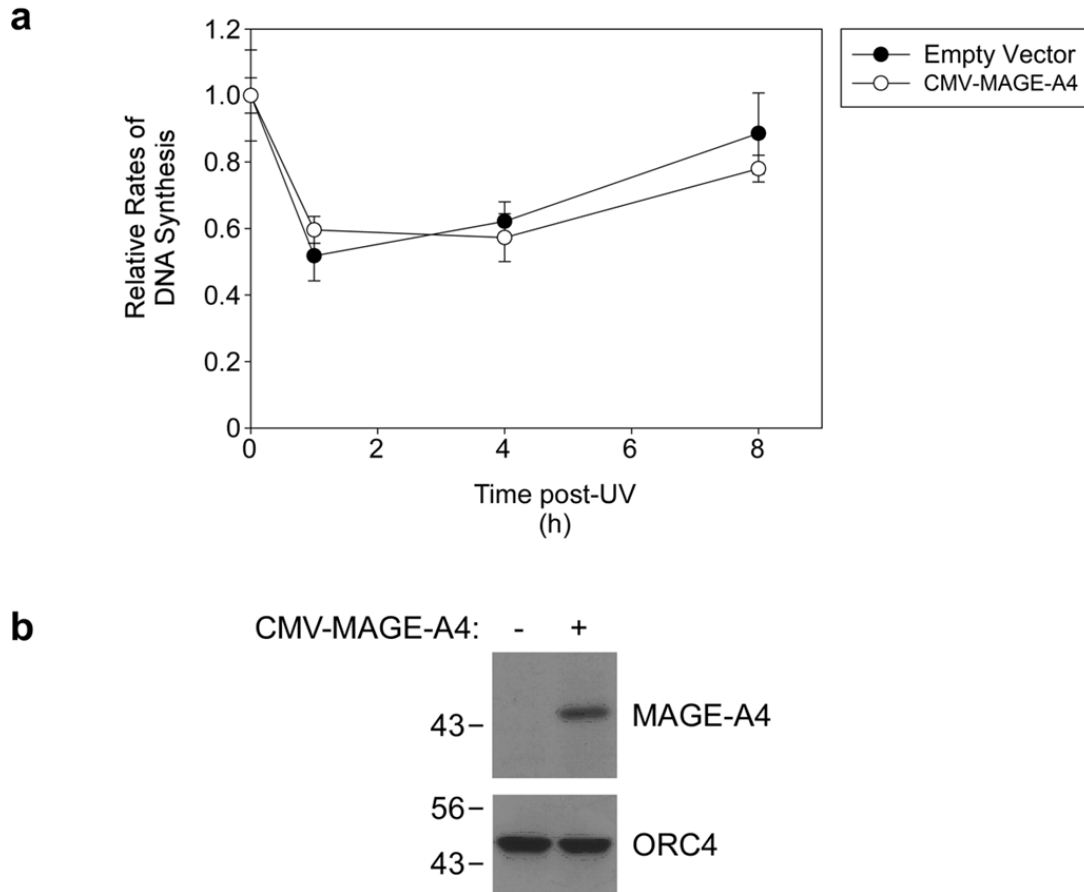
Figure 3.14 MAGE-A4 expression in 293T cells does not affect inhibition or recovery of DNA synthesis after UV-irradiation.

(A) Duplicate 10 cm plates of 293T cells were transfected with MAGE-A4 expression plasmid (CMV-MAGE-A4) or an empty vector for control. 24 hrs later the transfected cells were re-plated in 60 mm tissue culture dishes (for protein analysis) or 24-well plates (for DNA synthesis assays). The cells were UV-irradiated (5 J/m2) or sham-treated and rates of DNA synthesis at various times post-UV were determined by measurements of [3H]-thymidine incorporation. For each time point, rates of DNA synthesis were measured in triplicate and are normalized to DNA synthesis rates immediately prior to irradiation. Each data point represents the mean of the triplicate determinations and the error bars represent the range. **(B)** Coincident with UV-treatments, the 60 mm plates were used to prepare cell extracts for SDS-PAGE and immunoblotting to verify MAGE-A4 expression.

116

Figure 3.15 Heterogeneous expression of MAGE-A4 and TLS proteins in commonly-studied cell lines.

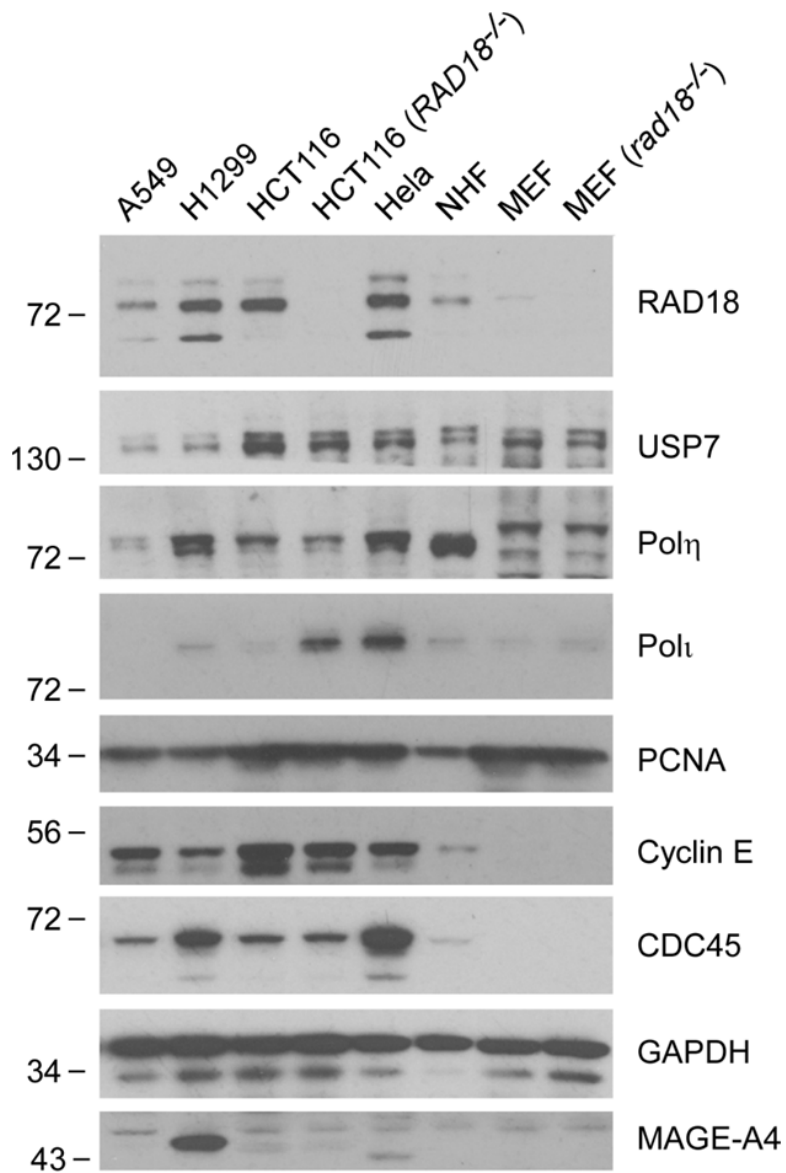Extracts from different cell lines were subject to immunoblot analysis using antibodies against TLS proteins and cell cycle regulators as indicated.

REFERENCES

1.   Hanahan, D. and R. A. Weinberg (2011). "Hallmarks of cancer: the next generation." Cell **144**(5): 646-674.

2.   Ciccia, A. and S. J. Elledge (2010). "The DNA damage response: making it safe to play with knives." Mol Cell **40**(2): 179-204.

3.   Prakash, S., et al. (2005). "Eukaryotic translesion synthesis DNA polymerases: specificity of structure and function." Annu Rev Biochem **74**: 317-353.

4.   Ohmori, H., et al. (2001). "The Y-family of DNA polymerases." Mol Cell **8**(1): 7-8.

5.   Bi, X., et al. (2006). "Rad18 regulates DNA polymerase kappa and is required for recovery from S-phase checkpoint-mediated arrest." Mol Cell Biol **26**(9): 3527-3540.

6.   Bi, X., et al. (2005). "DNA polymerase kappa is specifically required for recovery from the benzo[a]pyrene-dihydrodiol epoxide (BPDE)-induced S-phase checkpoint." J Biol Chem **280**(23): 22343-22355.

7.   Limoli, C. L., et al. (2000). "Polymerase eta deficiency in the xeroderma pigmentosum variant uncovers an overlap between the S phase checkpoint and double-strand break repair." Proc Natl Acad Sci U S A **97**(14): 7939-7946.

8.   Ziv, O., et al. (2009). "DNA polymerase zeta cooperates with polymerases kappa and iota in translesion DNA synthesis across pyrimidine photodimers in cells from XPV patients." Proc Natl Acad Sci U S A **106**(28): 11552-11557.

9.   Masutani, C., et al. (1999). "The XPV (xeroderma pigmentosum variant) gene encodes human DNA polymerase eta." Nature **399**(6737): 700-704.

10.   Kannouche, P. L. and A. R. Lehmann (2004). "Ubiquitination of PCNA and the polymerase switch in human cells." Cell Cycle **3**(8): 1011-1013.

11.   Stelter, P. and H. D. Ulrich (2003). "Control of spontaneous and damage-induced mutagenesis by SUMO and ubiquitin conjugation." Nature **425**(6954): 188-191.

12.   Davies, A. A., et al. (2008). "Activation of ubiquitin-dependent DNA damage bypass is mediated by replication protein a." Mol Cell **29**(5): 625-636.

13.   Tsuji, Y., et al. (2008). "Recognition of forked and single-stranded DNA structures by human RAD18 complexed with RAD6B protein triggers its recruitment to stalled replication forks." Genes Cells **13**(4): 343-354.

14. Bienko, M., et al. (2005). "Ubiquitin-binding domains in Y-family polymerases regulate translesion synthesis." Science **310**(5755): 1821-1824.

15. Hendel, A., et al. (2011). "PCNA ubiquitination is important, but not essential for translesion DNA synthesis in mammalian cells." PLoS Genet **7**(9): e1002262.

16. Kannouche, P. L., et al. (2004). "Interaction of human DNA polymerase eta with monoubiquitinated PCNA: a possible mechanism for the polymerase switch in response to DNA damage." Mol Cell **14**(4): 491-500.

17. Hashimoto, K., et al. (2012). "The vital role of polymerase zeta and REV1 in mutagenic, but not correct, DNA synthesis across benzo[a]pyrene-dG and recruitment of polymerase zeta by REV1 to replication-stalled site." J Biol Chem **287**(12): 9613-9622.

18. Watson, I. R., et al. (2013). "Emerging patterns of somatic mutations in cancer." Nat Rev Genet **14**(10): 703-718.

19. Loeb, L. A. (2001). "A mutator phenotype in cancer." Cancer Res **61**(8): 3230-3239.

20. Loeb, L. A. (2011). "Human cancers express mutator phenotypes: origin, consequences and targeting." Nat Rev Cancer **11**(6): 450-457.

21. Kawasumi, M., et al. (2011). "Protection from UV-induced skin carcinogenesis by genetic inhibition of the ataxia telangiectasia and Rad3-related (ATR) kinase." Proc Natl Acad Sci U S A **108**(33): 13716-13721.

22. Sekimoto, T., et al. (2015). "Both high-fidelity replicative and low-fidelity y-family polymerases are involved in DNA rereplication." Mol Cell Biol **35**(4): 699-715.

23. Simpson, A. J., et al. (2005). "Cancer/testis antigens, gametogenesis and cancer." Nat Rev Cancer **5**(8): 615-625.

24. Meek, D. W. and L. Marcar (2012). "MAGE-A antigens as targets in tumour therapy." Cancer Lett **324**(2): 126-132.

25. Doyle, J. M., et al. (2010). "MAGE-RING protein complexes comprise a family of E3 ubiquitin ligases." Mol Cell **39**(6): 963-974.

26. Day, T. A., et al. (2010). "Phosphorylated Rad18 directs DNA polymerase eta to sites of stalled replication." J Cell Biol **191**(5): 953-966.

27. Barkley, L. R., et al. (2012). "c-Jun N-terminal kinase-mediated Rad18 phosphorylation facilitates Poleta recruitment to stalled replication forks." Mol Biol Cell **23**(10): 1943-1954.

28. Watanabe, K., et al. (2004). "Rad18 guides poleta to replication stalling sites through physical interaction and PCNA monoubiquitination." EMBO J **23**(19): 3886-3896.

29. Durando, M., et al. (2013). "A non-catalytic role of DNA polymerase eta in recruiting Rad18 and promoting PCNA monoubiquitination at stalled replication forks." Nucleic Acids Res **41**(5): 3079-3093.

30. Liu, P., et al. (2006). "The Chk1-mediated S-phase checkpoint targets initiation factor Cdc45 via a Cdc25A/Cdk2-independent mechanism." J Biol Chem **281**(41): 30631-30644.

31. Hernandez-Pigeon, H., et al. (2005). "hMutS alpha is protected from ubiquitin-proteasome-dependent degradation by atypical protein kinase C zeta phosphorylation." J Mol Biol **348**(1): 63-74.

32. Song, I. Y., et al. (2010). "Rad18-mediated translesion synthesis of bulky DNA adducts is coupled to activation of the Fanconi anemia DNA repair pathway." J Biol Chem **285**(41): 31525-31536.

33. Parris, C. N. and M. M. Seidman (1992). "A signature element distinguishes sibling and independent mutations in a shuttle vector plasmid." Gene **117**(1): 1-5.

34. Raschle, M., et al. (2015). "DNA repair. Proteomics reveals dynamic assembly of repair complexes during bypass of DNA cross-links." Science **348**(6234): 1253671.

35. Zlatanou, A., et al. (2011). "The hMsh2-hMsh6 complex acts in concert with monoubiquitinated PCNA and Pol eta in response to oxidative DNA damage in human cells." Mol Cell **43**(4): 649-662.

36. Rual, J. F., et al. (2005). "Towards a proteome-scale map of the human protein-protein interaction network." Nature **437**(7062): 1173-1178.

37. Sinnott, R., et al. (2014). "Mechanisms promoting escape from mitotic stress-induced tumor cell death." Cancer Res **74**(14): 3857-3869.

38. Eglen, R. M., et al. (2008). "The use of AlphaScreen technology in HTS: current status." Curr Chem Genomics **1**: 2-10.

39. Yanagihara, H., et al. (2011). "NBS1 recruits RAD18 via a RAD6-like domain and regulates Pol eta-dependent translesion DNA synthesis." Mol Cell **43**(5): 788-797.

40. Zlatanou, A., et al. (2015). "USP7 is essential for maintaining Rad18 stability and DNA damage tolerance." Oncogene.

41.   Nagao, T., et al. (2003). "MAGE-A4 interacts with the liver oncoprotein gankyrin and suppresses its tumorigenic activity." J Biol Chem **278**(12): 10668-10674.

42.   Sakurai, T., et al. (2004). "A cleaved form of MAGE-A4 binds to Miz-1 and induces apoptosis in human cells." J Biol Chem **279**(15): 15505-15514.

43.   Zeman, M. K., et al. (2014). "DNA damage-specific deubiquitination regulates Rad18 functions to suppress mutagenesis." J Cell Biol **206**(2): 183-197.

44.   Sun, J., et al. (2009). "Rad18 is required for long-term maintenance of spermatogenesis in mouse testes." Mech Dev **126**(3-4): 173-183.

45.   Masuda, Y., et al. (2012). "En bloc transfer of polyubiquitin chains to PCNA in vitro is mediated by two different human E2-E3 pairs." Nucleic Acids Res **40**(20): 10394-10407.

46.   Kermi, C., et al. (2015). "RAD18 Is a Maternal Limiting Factor Silencing the UV-Dependent DNA Damage Checkpoint in Xenopus Embryos." Dev Cell **34**(3): 364-372.

47.   Tissier, A., et al. (2000). "poliota, a remarkably error-prone human DNA polymerase." Genes Dev **14**(13): 1642-1650.

48.   Ogi, T., et al. (1999). "Mutation enhancement by DINB1, a mammalian homologue of the Escherichia coli mutagenesis protein dinB." Genes Cells **4**(11): 607-618.

49.   Huang, J., et al. (2009). "RAD18 transmits DNA damage signalling to elicit homologous recombination repair." Nat Cell Biol **11**(5): 592-603.

50.   Halazonetis, T. D., et al. (2008). "An oncogene-induced DNA damage model for cancer development." Science **319**(5868): 1352-1355.

51.   Di Micco, R., et al. (2006). "Oncogene-induced senescence is a DNA damage response triggered by DNA hyper-replication." Nature **444**(7119): 638-642.

52.   Geng, L., et al. (2010). "RAD18-mediated ubiquitination of PCNA activates the Fanconi anemia DNA repair network." J Cell Biol **191**(2): 249-257.

53.   Palle, K. and C. Vaziri (2011). "Rad18 E3 ubiquitin ligase activity mediates Fanconi anemia pathway activation and cell survival following DNA Topoisomerase 1 inhibition." Cell Cycle **10**(10): 1625-1638.

CHAPTER 4: CANCER TESTIS ANTIGENS PROMOTE RESISTANCE TO CANCER THERAPIES THROUGH GENOME MAINTENANCE

4.1 Introduction

Lung cancer is the deadliest form of cancer worldwide. Non-small cell lung cancer (NSCLC) constitutes over 80% of lung cancer cases, for which most current treatments are ineffective[1]. Major limitations of existing pharmaceutical agents used in lung cancer treatment include the development of chemoresistance and unintentional toxicity in normal tissue[2]. Traditional treatment regimens for many lung cancer patients involve poly-therapies that utilize a combination of surgical intervention, ionizing radiation and chemotherapeutics, including platinum-based crosslinking agents (e.g. cisplatin) and DNA topoisomerase (topo) inhibitors (e.g. Camptothecin analogs, Etoposide and doxorubicin). Ionizing radiation and the aforementioned chemotherapeutics work by inducing DNA damage and limiting cell proliferation. These therapies are particularly toxic in cancer cells, where cell growth is aberrantly up-regulated (e.g. cancer cells)[3-5].

Cells undergoing carcinogenesis use DNA damage repair to not only survive intrinsic oncogenic stresses and environmental carcinogenic exposures, but also to evade damage induced by genotoxic pharmaceutical agents[6-8]. Thus, neoplastic cells may acquire chemoresistance through use of highly adapted DNA repair mechanisms that allow them to tolerate therapy-induced DNA damage (Fig. 4.1). However, the mechanisms determining how cancer cells use DNA damage repair pathways to adapt

and resist chemotherapies are not known. Elucidating mechanisms of DNA damage tolerance and repair will allow us to improve the efficacy of cancer treatment while limiting off target toxicities.

Ionizing radiation (IR) therapy as a cancer treatment is mediated through its ability to damage DNA, both directly and indirectly via the generation of free radicals. IR produces a wide variety of lesions types including damaged bases, crosslinks and the most severe type of lesion, a DNA double stranded break (DSB)[9]. Many chemotherapeutics also induce DSBs as their mechanism of action. The topoisomerase-I inhibiting Camptothecins prevent re-ligation of nicked DNA generated during coil relaxation via a covalently trapped DNA:topo adduct and induce DSBs during subsequent attempts to replicate through the damage[10, 11]. Similarly, Etoposide and doxorubicin prevent re-ligation of DNA strands by complexing with type II topoisomerases, leading to the formation of DSB. While the antitumor activity of cisplatin is generally attributed to the formation of DNA crosslinks, repair of cisplatin-induced lesions is thought to primarily be done through a combination of nucleotide excision repair and a DSB repair pathway known as homologous recombination[12-14]. Thus, competent DSB repair may contribute to the high rates of chemoresistance observed in lung cancer patients.

DSB repair is primarily mediated through error-free homologous recombination (HR) and error-prone nonhomologous end joining (NHEJ). Although high fidelity repair of DSB is preferred, the dependence of HR on the availability of a sister chromatid limits its activity to S and G2 phases of the cell cycle. NHEJ, however, is capable of acting throughout the cell cycle. A third pathway termed alternative end-joining (alt-EJ), is

thought to primarily act as a 'back-up' for HR and NHEJ, and is preferentially repairs DSB lesions through the use of microhomology found between the broken ends (Fig. 4.2).

Interestingly, several recent publications have implicated a group of proteins known as cancer/testis antigens (CTAs) in resistance to common chemotherapeutics including Cisplatin, Etoposide and Doxorubicin[15-17]. CTAs comprise a group of over 200 proteins that are ordinarily germline-restricted and absent from normal somatic cells but aberrantly overexpressed in many different cancers[18]<< citation from ch1>>. The first CTA, MAGEA1, was discovered in the 1990s when a patient with melanoma who was remarkably responsive to therapy was found to have cytotoxic T cells that recognized autologous cancer cells. MAGEA1 belongs to the Melanoma Antigen (MAGE) family of CTAs, a group of over 45 CTAs that share a high degree structure and sequence similarity, indicative of common biological functions[19, 20]. MAGE proteins have since been found to be aberrantly overexpressed in many other cancers, including NSCLC, and linked to the promotion of tumorigenesis and metastasis [21-25]. The biological function of MAGE proteins is largely unknown, however, recent studies have identified a link between CTAs and E3 ubiquitin ligases, suggesting CTAs may reprogram ubiquitin signaling networks in cancer cells[19, 26, 27]. Interestingly, E3 ubiquitin ligases mediate a wide array of DNA damage signaling pathways.

Based on our recent discovery that MAGEA4 promotes DNA damage tolerance via TLS, we postulated that other CTAs may also promote DNA damage tolerance in cancer cells[26]. We considered the CTA HORMAD1 as a candidate DNA repair mediator in cancer cells because in mouse germ cells mHormad1 is an ATM substrate, co-

localizes with gH2AX and facilitates DSB processing[28, 29]. We show here that depletion of HORMAD1 sensitizes NSCLC cells, but not triple negative breast cancer cells, to ionizing radiation. HORMAD1 forms irradiation-induced foci that co-localize with γH2AX, which we also identified as a novel binding partner. We also found that HORMAD1 loss reduces rates of recombination by DR-GFP while also diminishing recruitment of RAD51 to DSB.

4.2 Methods

Cell culture and transfection

Cancer cell lines H1299, U2OS, and H358 were purchased from the American Type Culture Collection (ATCC) and used for the described experiments without further authentication. H1299 RAD18-/- cells were generated by Dr. Yanzhe Gao[26]. MDAMB436 and MDAMB468 were provided by the lab of Dr. Carey Anders. All cell lines (except MDAMB468) were cultured in DMEM medium supplemented with 10% fetal bovine serum and penicillin–streptomycin (1%). MDAMB468 cells were cultured in RPMI1640 supplemented with 10% FBS and maintained in non-vented flasks without aeration. Plasmid DNA and siRNA oligonucleotides were transfected using Lipofectamine 2000 (Invitrogen) according to the manufacturer's instructions, except that concentrations of plasmid DNA and Lipofectamine 2000 used in each transfection reaction were decreased by 50% to reduce toxicity.

Expression plasmids and RNAi

HA-HORMAD1 was a gift from Dr. Angelique Whitehurst (UT Southwestern).

Sequences of siRNA oligonucleotides used here are as follows: control non-targeting siRNA, (5'-UAGCGACUAAACACAUCAA-3') (Thermo Fisher Scientific); siMAGEA4 (targeting the 3'-untranslated region); Smartpool siGENOME siHORMAD1 (Dharmacon CAT# M-018596-02); siMAGEA10 (GGUCAAAGCU GUGGGACAUU); Smartpool siGENOME siBRCA1 (Cat# M-003461-02); Smartpool siGENOME siBRCA2 (Cat# M-003462-01).

For transfection, two separate tubes were prepared, one containing siRNA and serum-free Optimem, and the other with Lipofectamine 2000 and serum-free Optimem. These separate mixtures were incubated for 5 min at room temperature in the dark before being combined and incubated for an additional 20min, according to Dharmacon and Lipofectamine manufacturer's protocols. For plasmid transfection, the transfection mixture was plated directly onto cells (in antibiotic-free). For siRNA transfection cells were trypsinized and resuspended in antibiotic-free medium and plated directly into the siRNA/Optimem/Lipofectamine solution at 50% confluence to incubate overnight. The following morning cells were then trypsinized and plated in 6-well plates (24 hrs prior to genotoxin treatment).

Fluorescence microscopy

In experiments with siRNA H1299 cells were treated with siControl or siHORMAD1. Twenty-four hrs post transfection/ (or plating in non-siRNA experiments) cells were irradiated (10 Gy) or sham treated and fixed 1 hr later for staining with indicated antibodies. Fixed-cell imaging was done on a Zeiss 710 confocal microscope, in the UNC Microscopy Services Laboratory core facility, as described previously[26].

Immunoprecipitation and immunoblotting

Lysates of cultured cells were washed three times in ice-cold PBS and lysed in 500 µl of ice-cold cytoskeleton buffer (CSK buffer; 10 mM Pipes pH 6.8, 100 mM NaCl, 300 mM sucrose, 3 mM MgCl2, 1 mM EGTA, 1 mM dithiothreitol, 0.1 mM ATP, 1 mM Na3VO4, 10 mM NaF and 0.1% Triton X-100) freshly supplemented with Protease Inhibitor Cocktail and Phostop (Roche). For subfractionation, lysates were centrifuged at 4,000 RPM for 4 min at 4°C. The supernatant containing a mixture of cytosolic plus nucleosolic proteins was aliquoted and detergent-insoluble nuclear fractions were washed once with 1 ml of CSK buffer. Insoluble (chromatin) fractions were then resuspended in a minimal volume of CSK and sonicated to release chromatin before analysis by SDS–PAGE and immunoblotting.

For all immunoprecipitation experiments, input samples were normalized for protein concentration. Magnetic beads containing covalently conjugated antibodies against epitope tags were added to the extracts and incubations were performed overnight at 4°C using rotating racks. Immune complexes were recovered using magnetic stands. The beads were washed five times with 1 ml CSK to remove nonspecifically bound proteins. The washed immune complexes were boiled in Laemmli buffer for 10 min, to release and denature for SDS–PAGE.

For immunoblotting, cell extracts or immunoprecipitates were separated by SDS-PAGE, transferred to nitrocellulose membranes, and incubated overnight with the following primary antibodies: GAPDH (sc-32233), HA.F7 (sc-7392) for IP, MAGEA4 (sc-292429), BRCA1 (sc-6954), RAD51 (sc-8349) from Santa Cruz Biotech; RAD18 (A301-340A) from Bethyl; H2A (05-678), γH2AX (05-636) from Millipore; ORC4 (H83120)

127

Transduction Labs; FlagM2 (F1804) from Sigma-Aldrich; HA.11 (ENZ-ABS118) for IB

Enzo Life Sciences; and FANCD2 Epitomics (2986). Antibody dilutions used for

immunoblotting were 1:1,000, with exceptions for the following antibodies: FANCD2

(1:3000), GAPDH (1:3,000) and γH2AX (1:5,000).

GFP Reporter and Survival Assays

H1299 cells stably integrated with DR-GFP (or EJ2-5) were treated with ISCE1 to

simulate DSB, and carried out as described by Pierce et al.[30]. DNA damage tolerance

was measured using survival assays, which have been used extensively to reveal the

phenotypes resulting from genotoxic insult[19, 31]. Replicate plates cells treated with the

indicated siRNAs were transfected as described above and plated at low density ~200-

1000 cells (depending on cell line). Cells were treated with genotoxic agent 24 hrs post-

plating and exposed to chemotherapeutics for 24 hrs; cisplatin (in H2O), Camptothecin

(in DMSO), Etoposide (in DMSO), Paclitaxel (Sigma T7402) (in DMSO), Doxorubicin

(Sigma D1515) (in H2O). Two weeks after genotoxin treatment plates were fixed and

stained with crystal violet. Plates were scanned and the Image J colony counter plugin

was used to quantify density[32, 33].

4.3 Results

MAGE-A members promote resistance to DSB-inducing therapeutics in NSCLC
cells

Analysis of The Cancer Genome Atlas (TCGA) data shows enhanced expression of

MAGEA4 in lung adenocarcinoma tumors as compared with non-malignant tissue (Fig.

4.3). Given our recent finding that MAGEA4 participates in DNA damage tolerance

through trans-lesion synthesis and the abundance of literature implicating a role for CTAs in chemoresistance we decided to investigate if there was a role for MAGEA4 in mediating tolerance to commonly used DNA-damaging chemotherapeutics. H1299 lung adenocarcinoma cells depleted of MAGEA4 exhibit increased sensitivity to ionizing radiation in addition to a variety of DNA-damaging chemotherapeutics (Fig. 4.4A-E). Treatment with ionizing radiation, Camptothecin, Etoposide, doxorubicin and cisplatin activates DSB repair pathways in cells. Thus, MAGEA4 may promote resistance to DNA damaging anti-cancer agents in NSCLC via promotion of DSB repair. Of note, survival following treatment with paclitaxel, a mitotic spindle poison that prevents normal progression of mitosis was unaffected by MAGEA4 status (Fig. 4.4F)[34]. Combined, these results indicate that MAGEA4 may specifically promote therapeutic resistance in NSCLC through activation of DSB repair pathways.

We recently identified MAGEA4 as a novel binding partner and stabilizer of RAD18[26]. RAD18 participates in many facets of DNA damage tolerance repair including trans-lesion synthesis, the Fanconi Anemia pathway and DSB repair[35-38]. H1299 RAD18-/- cells treated with Camptothecin and Cisplatin (agents that activate the Fanconi Anemia pathway) exhibit similar sensitivity, as do MAGEA4-depleted H1299 cells (Fig. 4.5A-B). In fact, H1299 cells with reduced MAGEA4 levels were defective in recruitment of a key regulator in Fanconi Anemia Pathway activation, FANCD2, following Camptothecin treatment (Fig. 4.5C). Thus, part of MAGEA4-dependent chemoresistance may be mediated through RAD18-dependent DNA damage tolerance mechanisms (Fig. 4.5D). However, not all MAGEA4-mediated resistance to DSB cancer therapeutics is through RAD18, as is exhibited by the compounded sensitivity in H1299

RAD18-/- cells depleted of MAGEA4 and exposed to ionizing radiation (Fig. 4.6).

Additionally the MAGE family CTA MAGEA10, which was absent from the RAD18

interaction network we previously published, was also capable of sensitizing lung

adenocarcinoma cells to topoisomerase II inhibitors and ionizing radiation[26] (Fig. 4.7A-

C). This suggests that while the RAD18-MAGEA4 complex may contribute to

chemoresistance, MAGEA members can more generally contribute to resistance of

DSB-inducing chemotherapeutics in a RAD18-independent manner.

To determine whether MAGEA-mediated NSCLC chemoresistance is indeed

mediated through enhanced DSB repair we measured rates of recombination via a

reporter assay that is indicative of HR activity. The DR-GFP HR reporter assay utilizes a

stably integrated DR-GFP vector to initiate recombination activity following ISceI-

induced DSBs[30, 39, 40]. BRCA1, an established HR protein, was used as a control.

Interestingly, both MAGEA4 and MAGEA10 depletion increased homologous

recombination activity, suggesting that these two proteins could be promoting DSB

repair through a pathway that is competitive with HR (e.g. NHEJ or alt-EJ) (Fig. 4.8).

HORMAD1 promotes homologous recombination and radioresistance

Analysis of TCGA gene expression data from over 450 NSCLC revealed that

HORMAD1 mRNA is highly expressed in lung cancer relative to non-malignant tissues

(Fig. 4.9A). Genes affiliated with HORMAD1 meiotic DSB processing (*HORMAD2*,

SPO11, *SYCE1*, *SYCP1-3*) were not overexpressed in NSLC (Fig. 4.9B), suggesting

that HORMAD1 activity in cancer cells may be distinct from its known role in meiosis.

A previous report from Watkins et al. suggested a role for HORMAD1 in suppressing

RAD51-dependent HR in triple negative breast cancer[41]. To investigate a potential role

130

for HORMAD1 in DSB repair in the lung cancer we depleted HORMAD1 in H1299 lung adenocarcinoma cells to look at clonogenic survival following treatment with ionizing radiation. Contrary to the previous report, we saw diminished survival after IR where in cells with reduced HORMAD1 protein levels, suggesting instead that HORMAD1 contributes to radioresistance (Fig. 4.9C). Similar results were seen in another NSCLC cell line, H358 (bronchoalveolar carcinoma) (Fig 4.9D). However, HORMAD1 depletion in triple negative breast cancer cell lines (MDAMB436 and 468) had no impact on radiosensitization (Fig. 4.9E-F). Interestingly, a comparison of mRNA levels across multiple data sets from the TCGA shows lower HORMAD1 mRNA levels in breast cancer as compared with the lung cancer studies (Fig. 4.9G).

To examine the contribution of HORMAD1 to DNA repair following DSB induction in H1299, we measured rates of recombination and endjoining, indicative of HR and NHEJ activity, respectively. HORMAD1-depletion led to a 60% decrease in homologous recombination activity as measured by DR-GFP, however did not influence end joining in an analogous NHEJ reporter assay EJ2-5 (Fig. 4.10A-B).

Under undamaged conditions, H1299 lung adenocarcinoma cells exhibit pan-nuclear staining of HORMAD1 that form foci upon exposure to ionizing radiation. HORMAD1 irradiation induced foci (IRIF) also co-localized with gH2AX. Additionally, abrogation of histone H2AX phosphorylation (γH2AX) through use of the ATM kinase inhibitor KU55933 prevented the IR-induced redistribution of HORMAD1 (Fig. 4.10C). Immunoprecipitation of HORMAD1 identified γH2AX as a novel binding partner (Fig. 4.10D). Taken together these results suggest that HORMAD1 is directed to chromatin following formation of DSB.

To determine whether HORMAD1 influences DNA repair proteins we examined the effect of HORMAD1 depletion on the recruitment of RAD51 (a key protein in HR) to IRIF. HORMAD1-depletion led to reduced numbers of RAD51-containing IRIF, indicating that HORMAD1 functions upstream of RAD51 in the HR pathway (Fig. 4.10E). In corresponding immunoblots we also found that HORMAD1-depletion diminished RAD51 chromatin-binding (Fig. 4.10F). Taken together these results suggest that HORMAD1 promotes recruitment of RAD51 to chromatin following the production of DSB.

As a positive control in these experiments we also depleted BRCA1, a known HR protein. BRCA1-depletion attenuated chromatin-binding of RAD51, as expected, but also diminished the levels of chromatin-bound HORMAD, suggesting a new relationship between HORMAD1 and BRCA1 (Fig. 4.10F). Taken together these results suggest a new role for HORMAD1 in homologous recombination repair following ionizing radiation (Fig. 4.11)

4.4 Discussion

MAGE-A members promote resistance to DSB-inducing therapeutics in NSCLC cells

Resistance to traditional cancer therapies contributes to the high mortality rate seen in lung cancer. Recent reports have discovered links between MAGE-family CTAs, highly expressed in NSCLC (Fig. 4.3), and E3 ubiquitin ligases, suggesting that MAGEs may aberrantly reprogram ubiquitin signaling events in cancer cells [19, 26, 42-46]. Ubiquitin signaling plays a key role in many DNA damage response pathways and thus MAGE

proteins may contribute to or enhance the repair of DNA damage induced by cancer therapies, ultimately stimulating chemoresistance. Indeed, H1299 lung adenocarcinoma cells depleted of MAGEA4 exhibit increased sensitivity to ionizing radiation and a variety of chemotherapeutics (Camptothecin, Etoposide, Doxorubicin and Cisplatin) (Fig. 4.4A-E). Notably, treatment with the pro-apoptotic mitotic spindle poison paclitaxel was unaffected by MAGEA4 status (Fig. 4.4F). Increased HR activity as measured by the DR-GFP assay in NSCLC cells depleted of MAGEA4 and MAGEA10 further support the notion of a role in DSB repair, potentially via pathways that antagonize HR (Fig. 4.8).

We recently identified MAGEA4 as a novel binding partner and stabilizer of RAD18[26]. RAD18 plays an important role in genome maintenance; in addition to activating the FA pathway and TLS, RAD18 is also thought to participate in DSB repair through homologous recombination (HR). We observed that H1299 RAD18-/- cells treated with agents that activate the Fanconi Anemia pathway (Camptothecin and Cisplatin) exhibit similar sensitivity to MAGEA4-depleted H1299 (Fig. 4.5A-B). MAGEA4 depletion was also found to ablate recruitment of FANCD2 (a key regulator of Fanconi Anemia Pathway) following Camptothecin treatment. Interestingly, FANCD2 is also thought to participate in HR, downstream of the FA pathway through promotion of BRCA2 chromatin loading and subsequent modulation of RAD51 activity[38, 47, 48]. Thus Camptothecin/Cisplatin sensitivities from MAGEA4/RAD18 depletion could be due to defective DSB repair via HR or alternative end joining (alt-EJ/ TMEJ)- pathways that handle replication fork collapse[49-51].

MAGEA proteins share considerable structural similarity, their expression is associated with poor patient outcomes, and family members can contribute to

resistance of DSB-inducing chemotherapeutics[19, 52]. MAGEA10 also sensitized lung

adenocarcinoma cells to topoisomerase II inhibitors and ionizing radiation (Fig. 4.7A-C),

but not Camptothecin or Cisplatin (data not shown). While the RAD18-MAGEA4

complex may contribute to chemoresistance in a RAD18-independent manner, not all

MAGEA4-mediated resistance to DSB cancer therapeutics is through RAD18, as

indicated by the additive radiosensitivity in H1299 RAD18-/- cells depleted of MAGEA4

(Fig. 4.6). Future studies should examine recruitment and survival epistasis with

canonical DSB repair proteins (e.g. BRCA1, Ku, POLQ) to identify the exact

mechanisms by with MAGE-A4 is contributing to DNA damage repair and therapeutic

resistance.

HORMAD1 promotes homologous recombination and radioresistance

TCGA gene expression data revealed that HORMAD1 mRNA is highly expressed in

lung tumors as compared to non-cancerous tissues, an observation not seen with genes

that facilitate HORMAD1-mediated meiotic DSB processing (e.g. HORMAD2, SPO11,

SYCE1, SYCP1-3) (Fig. 4.9A-B). This suggests that HORMAD1 activities in cancer

cells that are mechanistically distinct from its established role in meiosis.

A previous report from Watkins et al. suggests that HORMAD1 expression

suppresses RAD51-dependent HR and sensitizes triple negative breast cancer (TNBC)

cells to chemotherapeutic treatment[41]. However, after depleting HORMAD1 in TNBC

lines (MDAMB436 and 468) we saw no impact on radiosensitization (Fig. 4.9E-F).

Survival experiments described by Watkins et al., however, compared cancer cell lines

with contrasting 'high' or 'low' levels of HORMAD1[41]. Thus, the direct impact of

HORMAD1 in these experiments was not investigated and it is possible that other cellular differences contributed to this correlation.

HORMAD1 depletion sensitized H1299 and H38 NSCLC cells to radiotherapy and decreased homologous recombination by DR-GFP, the inverse of what was anticipated based on the findings in TNBC (Fig. 4.9C-D, 4.10A-B). Interestingly, a comparison of mRNA levels across multiple data sets from the TCGA shows lower HORMAD1 mRNA levels in breast cancer as compared with the lung cancer studies (Fig. 4.9G). It is possible that discrepancies in these observations could be the result of differential regulation of HORMAD1 in these cancers or cell lines.

When attempting to uncover the mechanism for HORMAD1 in HR we found that HORMAD1 formed IRIF that co-localized with γH2AX (Fig. 4.10C) and that was abrogated following treatment with ATM kinase inhibitor, suggesting that HORMAD1 is directed sites of DSB on chromatin. HORMAD1-depletion also decreased RAD51 IRIF and chromatin binding (by immunoblot) (Fig. 4.10E-F). These results indicate that HORMAD1 promotes recruitment of RAD51 to chromatin following the production of DSB. Follow up studies should include structure-function analyses utilizing HORMAD1 mutants to more precisely uncover the role of HORMAD1 in HR.

Association between HORMAD1 and the HR-protein BRCA1 was detected in a screen for BRCA1-interactors[53]. We found that BRCA1 depletion unexpectedly diminishes the levels of chromatin-bound HORMAD, suggesting a new relationship between HORMAD1 and BRCA1 (Fig. 4.10F). Further studies should be done to determine whether HORMAD1 and BRCA1 participate epistatically in the DSB repair

response. This could potentially validate HORMAD1 as a key mediator in chemoresistance and as a new target for treatment of NSCLC.
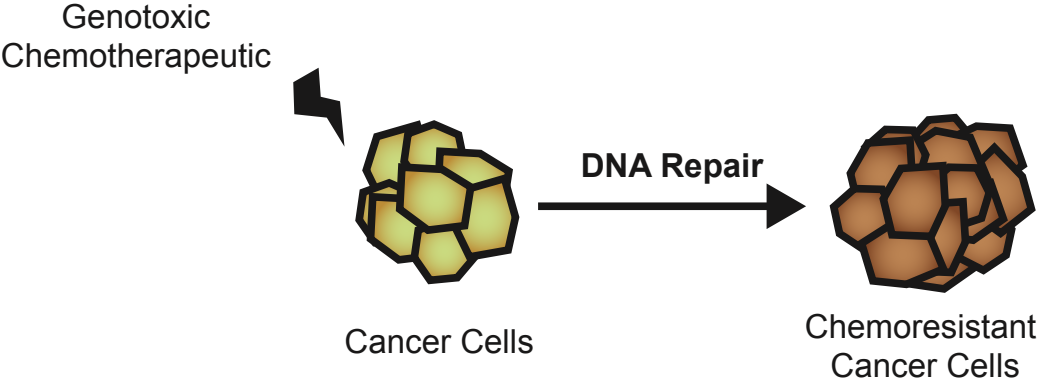

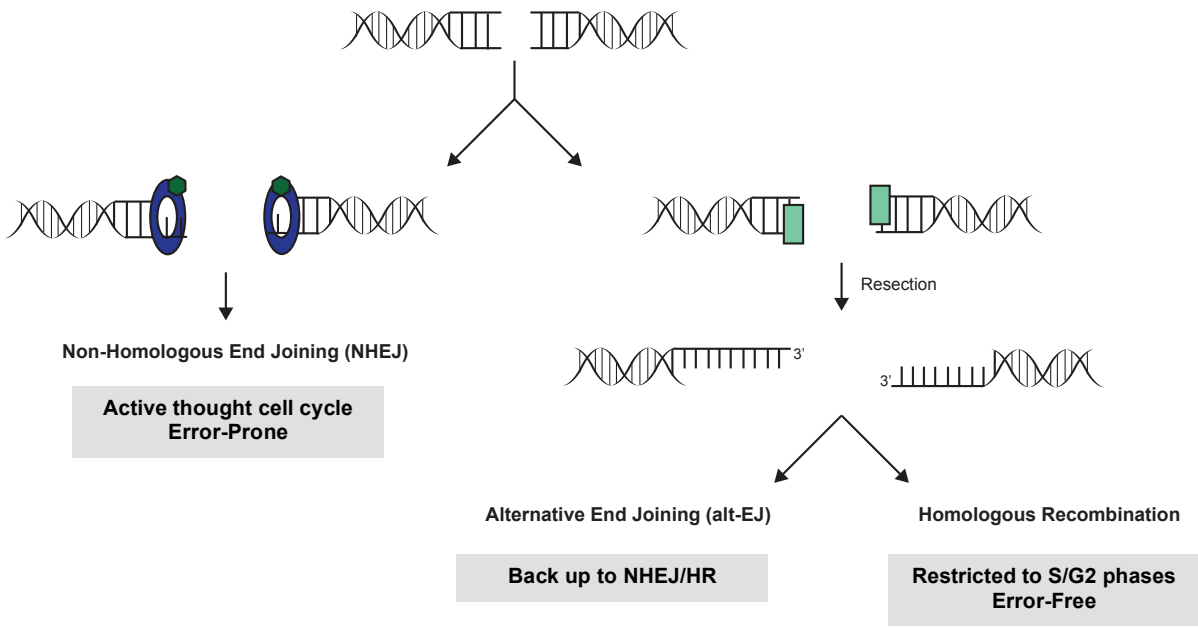**Figure 4.1 Role of DNA repair in chemoresistance**

Figure 4.2 Pathways of DNA double strand break repair

MAGE-A4 Expression by Tissue Type
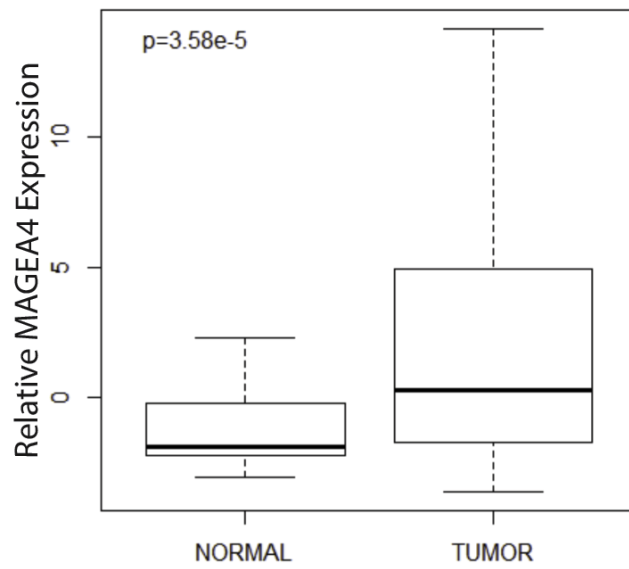
p=3.58e-5

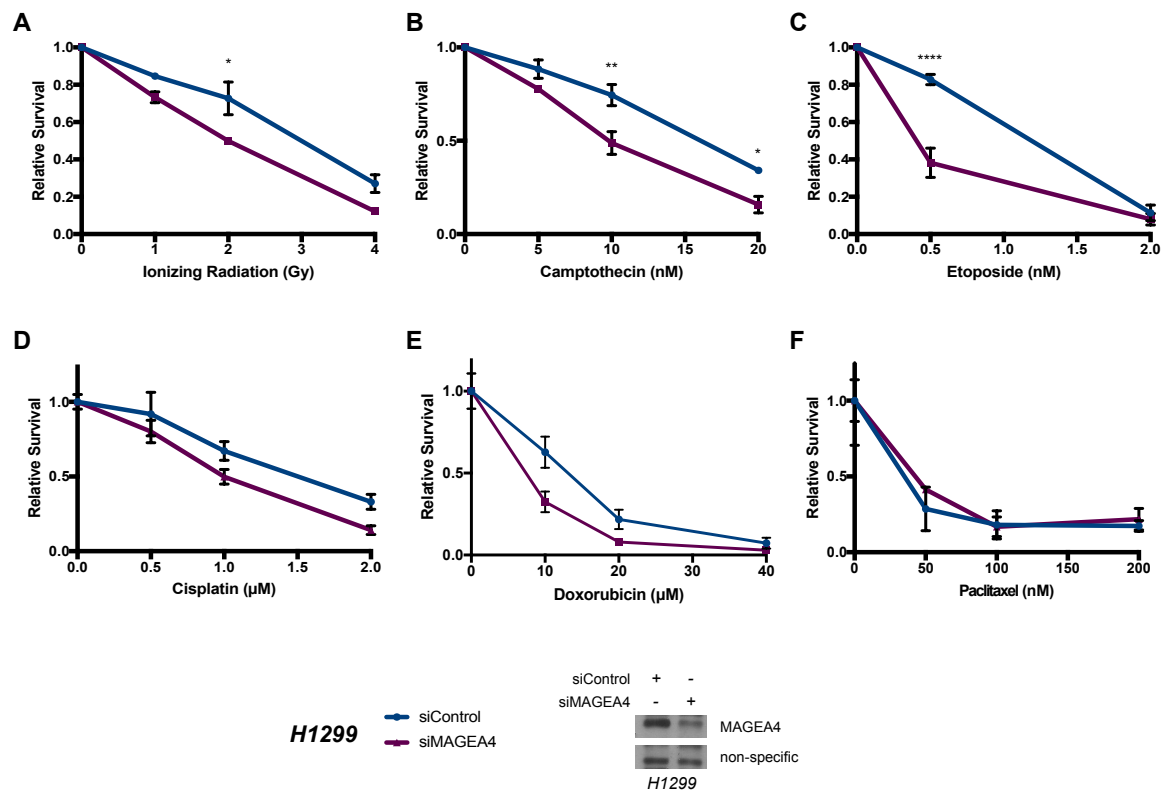**Figure 4.3 Increased expression of MAGEA4 in lung adenocarcinoma cells**

Figure 4.4 MAGEA4 depletion sensitizes H1299 cells to DNA damaging cancer therapies

(A) H1299 lung adenocarcinoma cells treated with control or MAGEA4 siRNA were subjected to mock or ionizing radiation. Survival data represent the mean +/- SEM (n=2). Relative survival of H1299 siControl was significantly higher than siMAGEA4 at the indicated dose (*p=0.0109). Significance was determined using ANOVA with Bonferroni's multiple comparisons test.

(B) H1299 lung adenocarcinoma cells treated with siRNA as in (A) were subjected to treatment with Camptothecin or vehicle. Survival data represent the mean +/- SEM (n=3). Relative survival of H1299 siControl was significantly higher than siMAGEA4 at the indicated doses (*p=0.0019, **p=0.0115). Significance was determined using ANOVA with Bonferroni's multiple comparisons test.

(C) H1299 lung adenocarcinoma cells treated with siRNA as in (A) were subjected to treatment with Etoposide or vehicle. Survival data represent the mean +/- SEM (n=3). Relative survival of H1299 siControl was significantly higher than siMAGEA4 at the indicated dose (****p<0.0001). Significance was determined using ANOVA with Bonferroni's multiple comparisons test.

(D) H1299 lung adenocarcinoma cells treated with siRNA as in (A) were subjected to treatment with cisplatin or vehicle. In this preliminary experiment, each survival data point represents the mean of triplicate determinations, and error bars represent the standard deviation.

Figure 4.4 MAGEA4 depletion sensitizes H1299 cells to DNA damaging cancer therapies

(E) H1299 lung adenocarcinoma cells treated with siRNA as in (A) were subjected to treatment with doxorubicin or vehicle. In this preliminary experiment, each survival data point represents the mean of triplicate determinations, and error bars represent the standard deviation.

(F) H1299 lung adenocarcinoma cells treated with siRNA as in (A) were subjected to treatment with Paclitaxel or vehicle. In this preliminary experiment, each survival data point represents the mean of triplicate determinations, and error bars represent the standard deviation.

Figure 4.5 MAGEA4/RAD18-dependent resistance to Fanconi Anemia pathway-activating chemotherapeutics

(A), (B) H1299 WT and RAD18 -/- lung adenocarcinoma cells were subjected to treatment with Camptothecin, cisplatin, or vehicle. In these preliminary experiments, each survival data point represents the mean of triplicate determinations, and error bars represent the standard deviation.
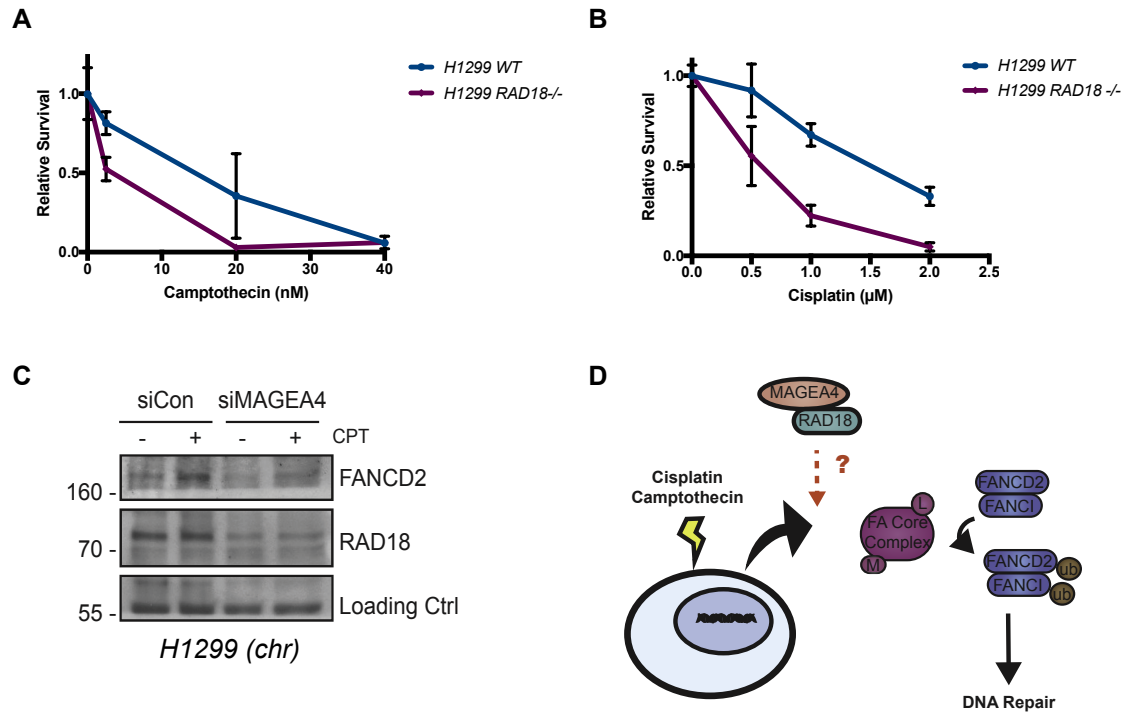
(C) H1299 lung adenocarcinoma cells treated with control or MAGEA4 siRNA were subjected to treatment with vehicle or 100 nM Camptothecin. After 24 hrs lysates were fractionated and processed for immunoblotting with the indicated antibodies.

(D) Schematic of potential MAGEA4/RAD18 role in repair of Cisplatin/ Camptothecin lesions.
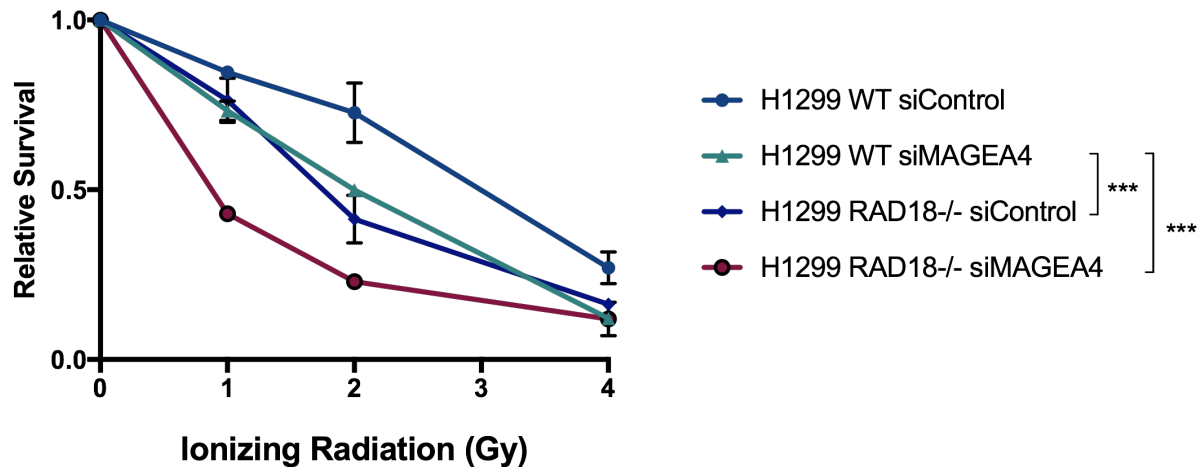
Figure 4.6 MAGEA4 promotes radioresistance independent of RAD18

H1299 WT and RAD18 -/- lung adenocarcinoma cells treated with control or MAGEA4 siRNA were subjected ionization radiation (or mock). Survival data represent the mean +/- SEM (n=2). At all doses the relative survival of H1299 WT siControl was significantly higher than H1299 WT siMAGEA4 (p=0.0021), H1299 RAD18 -/- siControl (p=0.0016) and H1299 RAD18 -/- siMAGEA4 (p<0.0001). H1299 RAD18 -/- siMAGEA4 had significantly diminished relative survival as compared with H1299 WT siMAGEA4 (p=0.0004) and H1299 RAD18-/- siControl (p=0.0006). In all cases significance was determined using ANOVA with Bonferroni's multiple comparisons test.
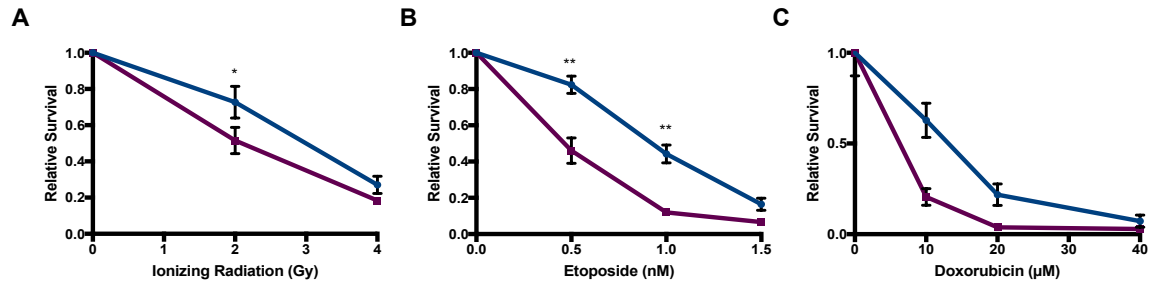
Figure 4.7 MAGEA10 promotes resistance to ionizing radiation and topoisomerase II inhibitors

(A) H1299 lung adenocarcinoma cells treated with control or MAGEA10 siRNA were subjected to mock or ionizing radiation. Survival data represent the mean +/- SEM (n=2). Relative survival of H1299 siControl was significantly higher than siMAGEA10 at the indicated dose (*p=0.0760). Significance was determined using ANOVA with Bonferroni's multiple comparisons test.

(B) H1299 lung adenocarcinoma cells treated with siRNA as in (A) were subjected to treatment with Etoposide or vehicle. Survival data represent the mean +/- SEM (n=3). Relative survival of H1299 siControl was significantly higher than siMAGEA10 at the indicated doses (**$p_{0.5nM}$=0.0020, **$p_{1.0nM}$=0.0032). Significance was determined using ANOVA with Bonferroni's multiple comparisons test.

(C) H1299 lung adenocarcinoma cells treated with siRNA as in (A) were subjected to treatment with Etoposide or vehicle. . In this preliminary experiment, each survival data point represents the mean of triplicate determinations, and error bars represent the standard deviation.
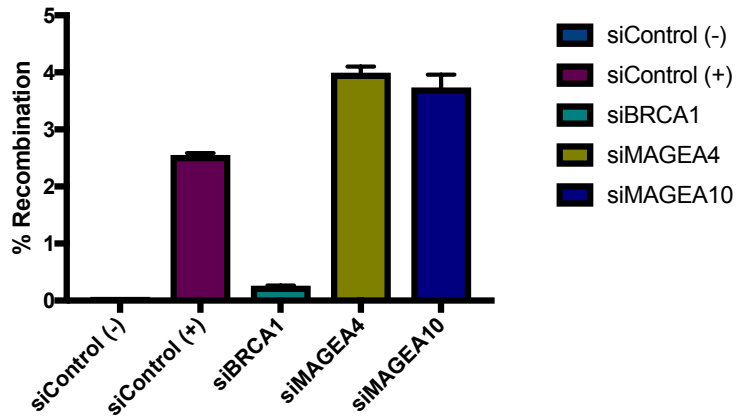
Figure 4.8 MAGEA4 and MAGEA10 depletion increase homologous recombination activity
H1299 lung adenocarcinoma cells with stably integrated DR-GFP were treated with ISCE1 virus (or mock) to induce DSB and measure rates of recombination. In this preliminary experiment, each data point represents the mean of triplicate determinations, and error bars represent the standard deviation.
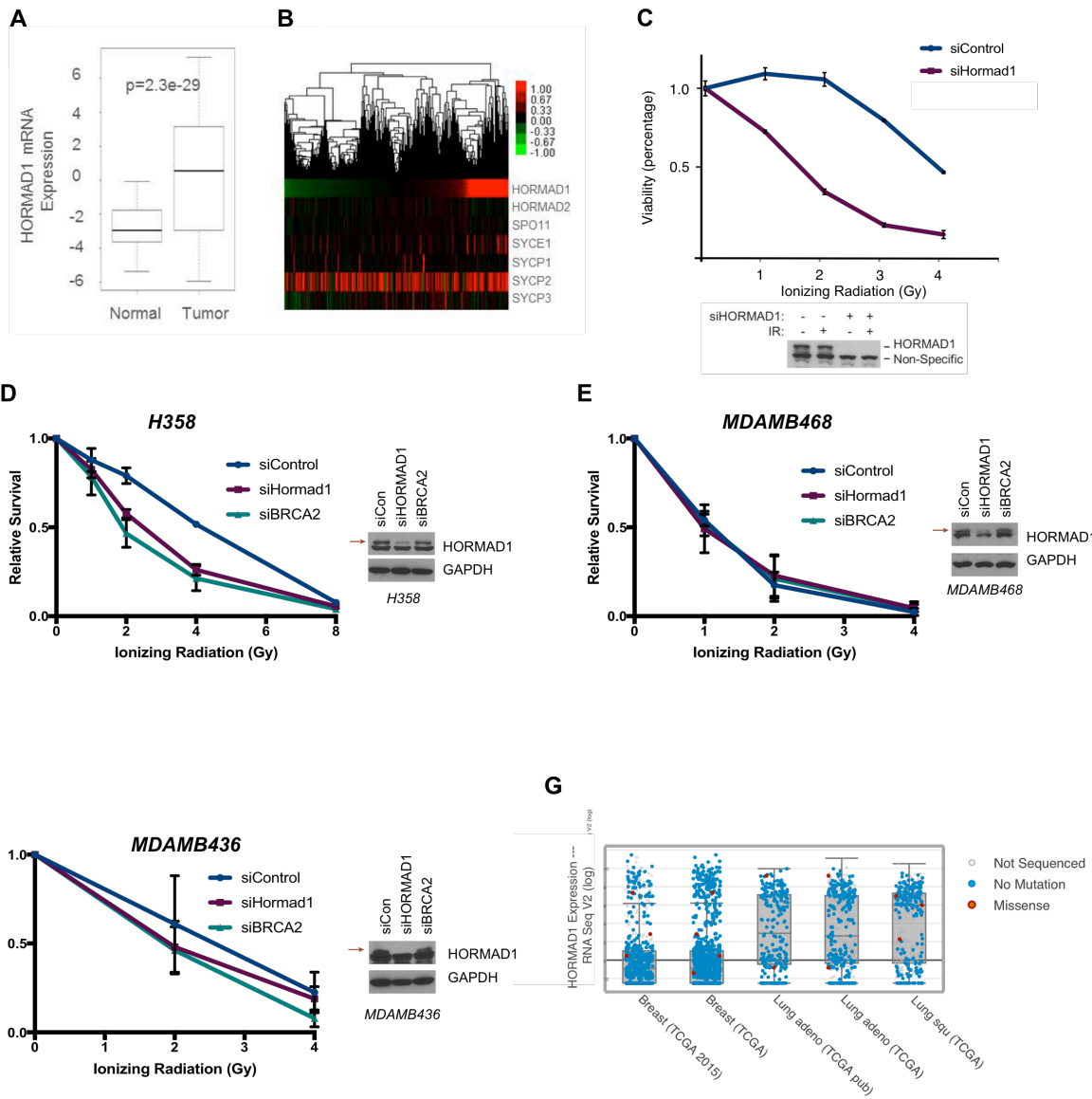
Figure 4.9 HORMAD1 promotes radioresistance in lung adenocarcinoma
(A) The Cancer Genome Atlas (TCGA) HORMAD1 expression data for normal and NSCLC tissue.
(B) Genes that cooperate with HORMAD1 in meiotic DSB processing (e.g. HORMAD2, SPO11, SYCE1, SYCP1-3) are not overexpressed in NSLC (TCGA).
(C) H1299 lung adenocarcinoma cells treated with control or HORMAD1 siRNA were subjected to mock or ionizing radiation. Each survival data point represents the mean of triplicate determinations, and error bars represent the standard deviation (n=1).
(D) H358 lung bronchoalveolar carcinoma cells treated with control or HORMAD1 siRNA were subjected to treatment with Camptothecin or vehicle. Survival data represent the mean +/- SEM (n=3). At all doses the relative survival of H358 cells modified with siControl was significantly higher than those with siHORMAD1 (**p=0.0023) and siBRCA2 (****p<0.0001). Significance was determined using ANOVA with Bonferroni's multiple comparisons test. Lysates (right) were validated for efficient knockdown and probed with the indicated antibodies. Red arrow indicates specific top band.
(E) MDAMB468 triple negative breast adenocarcinoma cells treated with control or HORMAD1 siRNA were subjected to mock or ionizing radiation. Survival data represent the mean +/- SEM (n=3). Lysates (right) were validated for efficient knockdown and probed with the indicated antibodies. Red arrow indicates specific top band.
(F) MDAMB436 triple negative breast adenocarcinoma cells treated with control or HORMAD1 siRNA were subjected to mock or ionizing radiation. Survival data represent the mean +/- SEM (n=2). Lysates (right) were validated for efficient knockdown and probed with the indicated antibodies. Red arrow indicates specific top band.
(G) TCGA data comparing expression of HORMAD1 in breast and lung cancer.

A

Homologous Recombination Efficiency (% of Ctrl)

siCtrl / siHormad1

B

Endjoining Efficiency (% of Ctrl)

si ctrl / si Hormad1

C

	DMSO	DMSO	ATM inhibitor
DAPI			
HORMAD1			
γH2AX			
	-IR	+IR	+IR

D

input   HA-IP

HA-Hormad1   − +   − +

HA-Hormad1

Y-H2AX

H2A

E

	siCon	siCon + IR	siHORMAD1 + IR
DAPI			
RAD51			
γH2AX			

F

siBRCA1:   −   −   +
siHORMAD1:   −   +   −
IR: +   +   +

BRCA1

RAD51

Relative RAD51:   1.0   0.6   0.4

HORMAD1
Non-specific

ORC4
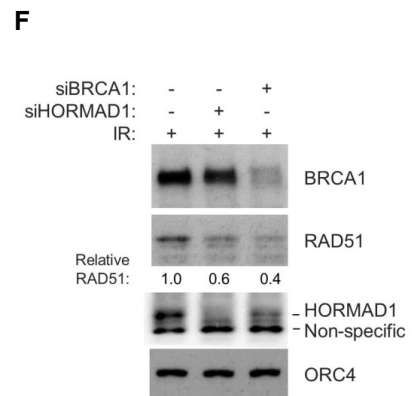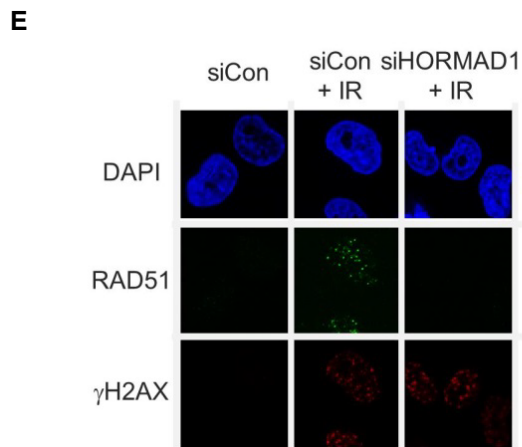
Figure 4.10 HORMAD1 promotes homologous recombination after ionizing radiation treatment

(A), (B) H1299 cells containing a stably-integrated DR-GFP or EJ2-5 vector, were treated with control or HORMAD1 siRNA and harvest to determine homologous recombination (DR-GFP) or endjoining activity (EJ2-5). Data represents the mean and +/- the SEM (n=3).
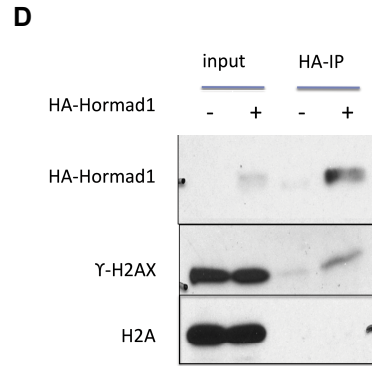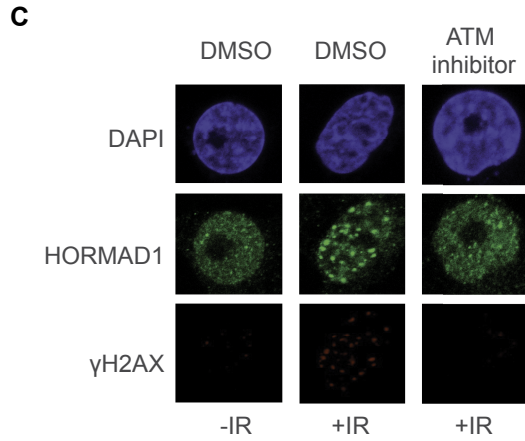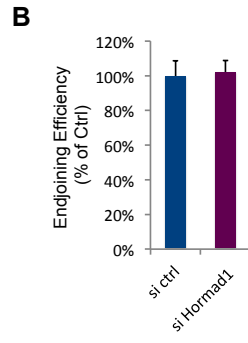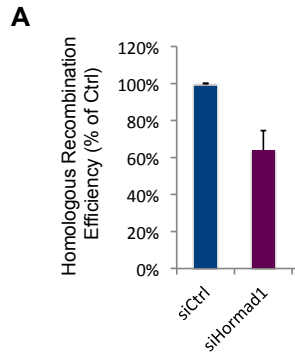
(C) H1299 cells were treated with mock or ionizing irradiation and DMSO or ATM (KU55933) inhibitor and immunostained with γH2AX and HORMAD1 antibodies. DNA was stained with DAPI.

(D) H1299 cells treated with vector or HA-HORMAD1 were subjected to HA-immunoprecipitation. Input lysates and immunoprecipitated HORMAD1 complexes were probed with the indicated antibodies.

(E) H1299 cells treated with control or HORMAD1-targetting siRNA were subjected to mock or ionizing radiation and immunostained with γH2AX and RAD51 antibodies. DNA was stained with DAPI.

(F) H1299 cells treated with control, BRCA1 or HORMAD1 siRNA were exposed to ionizing radiation and immunoblotted with the indicated antibodies.
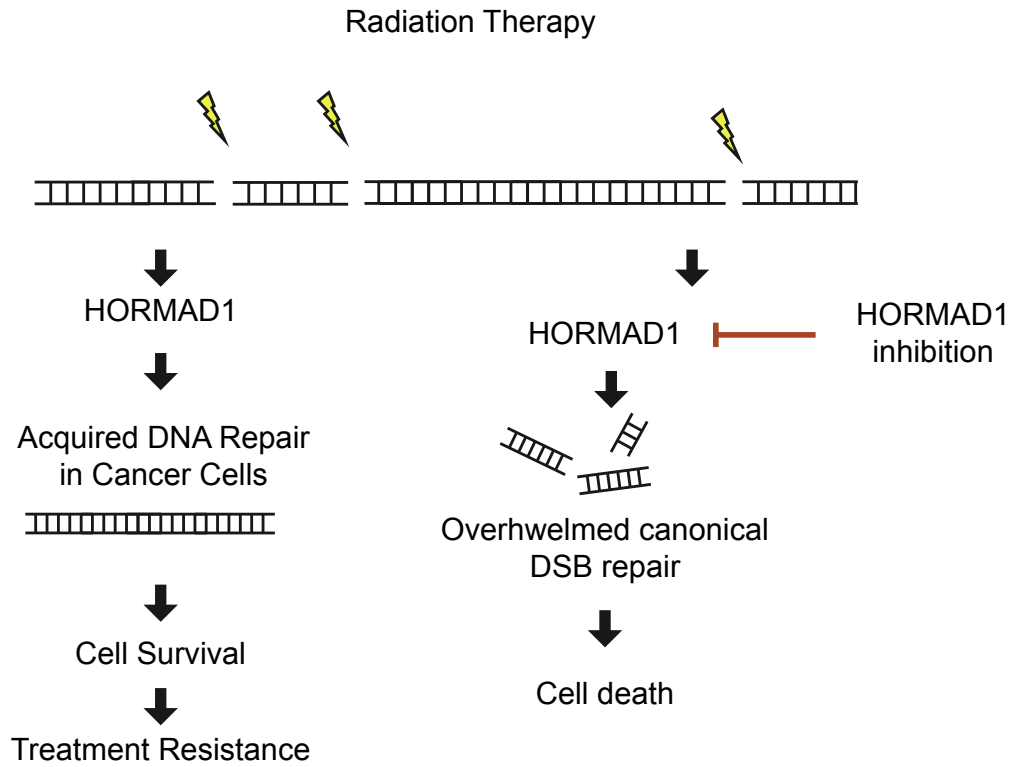
Figure 4.11 Model of potential role for HORMAD1 in DSB repair and radioresistance

REFERENCES

1.   Stewart, B. W., et al. <u>World cancer report 2014</u>.

2.   "Cancer multidrug resistance." <u>Nat Biotech</u>.

3.   Swift, L. H. and R. M. Golsteyn (2014). "Genotoxic anti-cancer agents and their relationship to DNA damage, mitosis, and checkpoint adaptation in proliferating cancer cells." <u>Int J Mol Sci</u> **15**(3): 3403-3431.

4.   Helleday, T., et al. (2008). "DNA repair pathways as targets for cancer therapy." <u>Nat Rev Cancer</u> **8**(3): 193-204.

5.   Cheung-Ong, K., et al. (2013). "DNA-damaging agents in cancer chemotherapy: serendipity and chemical biology." <u>Chem Biol</u> **20**(5): 648-659.

6.   Stansbury, K. H., et al. (2000). "Enzyme-mediated dialdehyde formation: an alternative pathway for benzo[a]pyrene 7,8-dihydrodiol bioactivation." <u>Chem Res Toxicol</u> **13**(11): 1174-1180.

7.   Halliwell, B. (1991). "Reactive oxygen species in living systems: source, biochemistry, and role in human disease." <u>Am J Med</u> **91**(3C): 14S-22S.

8.   Alt, A., et al. (2007). "Bypass of DNA lesions generated during anticancer treatment with cisplatin by DNA polymerase eta." <u>Science</u> **318**(5852): 967-970.

9.   Santivasi, W. L. and F. Xia (2014). "Ionizing radiation-induced DNA damage, response, and repair." <u>Antioxid Redox Signal</u> **21**(2): 251-259.

10.   Xu, Y. and C. Her (2015). "Inhibition of Topoisomerase (DNA) I (TOP1): DNA Damage Repair and Anticancer Therapy." <u>Biomolecules</u> **5**(3): 1652-1670.

11.   Fan, Y., et al. (1998). "Molecular modeling studies of the DNA-topoisomerase I ternary cleavable complex with camptothecin." <u>J Med Chem</u> **41**(13): 2216-2226.

12.   Raschle, M., et al. (2015). "DNA repair. Proteomics reveals dynamic assembly of repair complexes during bypass of DNA cross-links." <u>Science</u> **348**(6234): 1253671.

13.   O'Grady, S., et al. (2014). "The role of DNA repair pathways in cisplatin resistant lung cancer." <u>Cancer Treat Rev</u> **40**(10): 1161-1170.

14.   Fuertes, M. A., et al. (2003). "Biochemical modulation of Cisplatin mechanisms of action: enhancement of antitumor activity and circumvention of drug resistance." <u>Chem Rev</u> **103**(3): 645-662.

15.	Monte, M., et al. (2006). "MAGE-A tumor antigens target p53 transactivation function through histone deacetylase recruitment and confer resistance to chemotherapeutic agents." Proc Natl Acad Sci U S A **103**(30): 11160-11165.

16.	Hartmann, S., et al. (2017). "MAGE-A11 expression contributes to cisplatin resistance in head and neck cancer." Clin Oral Investig.

17.	Duan, Z., et al. (2003). "Overexpression of MAGE/GAGE genes in paclitaxel/doxorubicin-resistant human cancer cell lines." Clin Cancer Res **9**(7): 2778-2785.

18.	Simpson, A. J., et al. (2005). "Cancer/testis antigens, gametogenesis and cancer." Nat Rev Cancer **5**(8): 615-625.

19.	Doyle, J. M., et al. (2010). "MAGE-RING protein complexes comprise a family of E3 ubiquitin ligases." Mol Cell **39**(6): 963-974.

20.	Chomez, P., et al. (2001). "An overview of the MAGE gene family with the identification of all human members of the family." Cancer Res **61**(14): 5544-5551.

21.	Forghanifard, M. M., et al. (2011). "Cancer-testis gene expression profiling in esophageal squamous cell carcinoma: identification of specific tumor marker and potential targets for immunotherapy." Cancer Biol Ther **12**(3): 191-197.

22.	Daudi, S., et al. (2014). "Expression and immune responses to MAGE antigens predict survival in epithelial ovarian cancer." PLoS One **9**(8): e104099.

23.	Li, X., et al. (2015). "Evaluation of melanoma antigen (MAGE) gene expression in human cancers using The Cancer Genome Atlas." Cancer Genet **208**(1-2): 25-34.

24.	Xie, C., et al. (2016). "Melanoma associated antigen (MAGE)-A3 promotes cell proliferation and chemotherapeutic drug resistance in gastric cancer." Cell Oncol (Dordr).

25.	Zou, C., et al. (2012). "Cancer-testis antigens expressed in osteosarcoma identified by gene microarray correlate with a poor patient prognosis." Cancer **118**(7): 1845-1855.

26.	Gao, Y., et al. (2016). "A neomorphic cancer cell-specific role of MAGE-A4 in trans-lesion synthesis." Nat Commun **7**: 12105.

27.	Maxfield, K. E., et al. (2015). "Comprehensive functional characterization of cancer-testis antigens defines obligate participation in multiple hallmarks of cancer." Nat Commun **6**: 8840.

28. Fukuda, T., et al. (2012). "Phosphorylation of chromosome core components may serve as axis marks for the status of chromosomal events during mammalian meiosis." PLoS Genet **8**(2): e1002485.

29. Fukuda, T., et al. (2010). "A novel mammalian HORMA domain-containing protein, HORMAD1, preferentially associates with unsynapsed meiotic chromosomes." Exp Cell Res **316**(2): 158-171.

30. Pierce, A. J., et al. (1999). "XRCC3 promotes homology-directed repair of DNA damage in mammalian cells." Genes Dev **13**(20): 2633-2638.

31. Doil, C., et al. (2009). "RNF168 binds and amplifies ubiquitin conjugates on damaged chromosomes to allow accumulation of repair proteins." Cell **136**(3): 435-446.

32. Franken, N. A., et al. (2006). "Clonogenic assay of cells in vitro." Nat Protoc **1**(5): 2315-2319.

33. Guzman, C., et al. (2014). "ColonyArea: an ImageJ plugin to automatically quantify colony formation in clonogenic assays." PLoS One **9**(3): e92444.

34. Sinnott, R., et al. (2014). "Mechanisms promoting escape from mitotic stress-induced tumor cell death." Cancer Res **74**(14): 3857-3869.

35. Hu, Q., et al. (2017). "Mechanisms of Ubiquitin-Nucleosome Recognition and Regulation of 53BP1 Chromatin Recruitment by RNF168/169 and RAD18." Mol Cell **66**(4): 473-487 e479.

36. Notenboom, V., et al. (2007). "Functional characterization of Rad18 domains for Rad6, ubiquitin, DNA binding and PCNA modification." Nucleic Acids Res **35**(17): 5819-5830.

37. Saberi, A., et al. (2007). "RAD18 and poly(ADP-ribose) polymerase independently suppress the access of nonhomologous end joining to double-strand breaks and facilitate homologous recombination-mediated repair." Mol Cell Biol **27**(7): 2562-2571.

38. Palle, K. and C. Vaziri (2011). "Rad18 E3 ubiquitin ligase activity mediates Fanconi anemia pathway activation and cell survival following DNA Topoisomerase 1 inhibition." Cell Cycle **10**(10): 1625-1638.

39. Weinstock, D. M., et al. (2006). "Modeling oncogenic translocations: distinct roles for double-strand break repair pathways in translocation formation in mammalian cells." DNA Repair (Amst) **5**(9-10): 1065-1074.

40. Weinstock, D. M., et al. (2006). "Assaying double-strand break repair pathway choice in mammalian cells using a targeted endonuclease or the RAG recombinase." Methods Enzymol **409**: 524-540.

41. Watkins, J., et al. (2015). "Genomic Complexity Profiling Reveals That HORMAD1 Overexpression Contributes to Homologous Recombination Deficiency in Triple-Negative Breast Cancers." Cancer Discov **5**(5): 488-505.

42. Yang, B., et al. (2007). "MAGE-A, mMage-b, and MAGE-C proteins form complexes with KAP1 and suppress p53-dependent apoptosis in MAGE-positive cell lines." Cancer Res **67**(20): 9954-9962.

43. Yang, B., et al. (2007). "Select cancer testes antigens of the MAGE-A, -B, and -C families are expressed in mast cell lines and promote cell viability in vitro and in vivo." J Invest Dermatol **127**(2): 267-275.

44. Sasaki, A., et al. (2002). "A RING finger protein Praja1 regulates Dlx5-dependent transcription through its ubiquitin ligase activity for the Dlx/Msx-interacting MAGE/Necdin family protein, Dlxin-1." J Biol Chem **277**(25): 22541-22546.

45. Marcar, L., et al. (2015). "MAGE-A Cancer/Testis Antigens Inhibit MDM2 Ubiquitylation Function and Promote Increased Levels of MDM4." PLoS One **10**(5): e0127713.

46. Espantman, K. C. and C. C. O'Shea (2010). "aMAGEing new players enter the RING to promote ubiquitylation." Mol Cell **39**(6): 835-837.

47. Wang, X., et al. (2004). "Functional interaction of monoubiquitinated FANCD2 and BRCA2/FANCD1 in chromatin." Mol Cell Biol **24**(13): 5850-5862.

48. Song, I. Y., et al. (2010). "Rad18-mediated translesion synthesis of bulky DNA adducts is coupled to activation of the Fanconi anemia DNA repair pathway." J Biol Chem **285**(41): 31525-31536.

49. Yousefzadeh, M. J., et al. (2014). "Mechanism of suppression of chromosomal instability by DNA polymerase POLQ." PLoS Genet **10**(10): e1004654.

50. Wyatt, D. W., et al. (2016). "Essential Roles for Polymerase theta-Mediated End Joining in the Repair of Chromosome Breaks." Mol Cell **63**(4): 662-673.

51. Heyer, W. D., et al. (2010). "Regulation of homologous recombination in eukaryotes." Annu Rev Genet **44**: 113-139.

52. Weon, J. L. and P. R. Potts (2015). "The MAGE protein family and cancer." Curr Opin Cell Biol **37**: 1-8.

53. Hill, S. J., et al. (2014). "Systematic screening reveals a role for BRCA1 in the response to transcription-associated DNA damage." Genes Dev **28**(17): 1957-1975.

CHAPTER 5: DISCUSSION

Mutagenesis is a hallmark of cancer that not only incites carcinogenesis and promotes tumor progression, but can also lead to the development of chemotherapeutic resistance[1-3]. Mutations can occur when DNA damage (from endogenous, environmental or medicinal sources) interferes with DNA synthesis, causing replication errors. Cells undergoing multi-step tumorigenesis depend on DNA damage tolerance to survive intrinsic oncogenic stresses (e.g. reactive oxygen species) and environmental carcinogenic exposures (e.g. solar ultraviolet (UV) radiation)[4, 5]. Importantly, the DNA damage tolerance acquired during tumorigenesis also endows cancer cells with resistance to chemotherapeutic drugs (e.g. platinating agents)[6] (Fig. 5.1). Elucidating mechanisms of DNA damage tolerance and mutagenesis will allow us to better understand tumor progression and develop superior treatments for the disease.

We have identified several proteins that influence cancer cell survival through tolerance of genotoxic injury. Our first two discoveries uncover two novel regulators (MAGEA4 and RNF168) of RAD18, a prominent activator of DNA damage tolerance via error-prone Trans-lesion Synthesis (TLS) and error-free Template Switching (TS). MAGEA4 belongs to a group of genes termed Cancer/Testis Antigens (CTA), that are absent from normal somatic cells but are abnormally expressed in many neoplastic cells[7],while RNF168 is, canonically, a double strand break (DSB) repair signaling protein that is mutated in human RIDDLE syndrome, a genetic disease characterized by

severe immunodeficiency, developmental defects, radiosensitivity and a predisposition to cancer[8].

We show here that MAGEA4 is a stabilizing binding partner of RAD18 that is able to promote DNA damage tolerance through TLS[9] and further identify a novel, DSB repair-independent role for RNF168 in promoting replication-associated DNA damage tolerance through RAD18 in a manner that is consistent with TS. Interestingly, RNF168 is also overexpressed in many cancers, emphasizing the importance of tightly controlled regulation of DNA damage tolerance pathways where both aberrant activation and deficiency contribute to mutagenesis. Together, these results provide a greater insight as to how aberrant RAD18 activation through MAGEA4 and RNF168 contribute to pathological DNA damage tolerance in cancer.

CTAs were first discovered nearly three decades ago and immediately identified as a promising candidate for cancer cell-specific therapy[10-12]. Since their discovery, expression of CTAs has been correlated with increased tumor incidence and size, metastasis, and poor prognostic outcomes[13-16]. More recently, several publications have suggested that CTAs may promote resistance to DNA-damaging therapeutics, however information regarding the mechanistic contributions of CTAs to chemoresistance is severely lacking[17-19].

The third major contribution to carcinogenesis that we describe is that several additional CTAs (MAGEA4 as well as MAGEA10 and HORMAD1) directly promote resistance to DNA-damaging chemotherapeutics. This work may lead to novel treatments that specifically target damage tolerance mediators in cancer cells, thereby enhancing the efficacy and reducing the liabilities of current chemotherapeutics.

5.1 RNF168 promotes replication-associated DNA damage tolerance via RAD18

Defects in proteins utilized for DNA repair and genome maintenance are associated with severe genetic diseases and cancer. Chromatin modification can significantly alter access of DNA damage response machinery to lesion sites and thus, defects in chromatin modifiers have been linked with a predisposition to cancer[20]. We have identified the RIDDLE syndrome and histone-modifier protein RNF168 as a novel mediator of DNA damage tolerance in response to replication-associated stress. Lesions encountered during DNA replication can be particularly problematic as they stall the replication fork and can lead to the development of unstable, mutagenesis-prone structures, or cell death. We discovered that RNF168 localizes to replication factories following treatment with fork-stalling agents. RNF168 was also revealed as a unique component of the RAD18:RAD6 complex. RAD18 is a key mediator of several DNA damage tolerance pathways (e.g. TLS and TS) and was found to redistribute to replication forks following RNF168-dependent substrate ubiquitination. RNF168 was also found to promote poly-ubiquitination of the DNA polymerase processivity factor, PCNA, in an intrinsic ligase activity-independent manner when RAD18 is present. While RAD18 has been shown to promote HLTF/SHPRH-mediated poly ubiquitination to initiate template switching, RAD18 itself does not poly-ubiquitinate PCNA[21]. Depletion of RNF168 also reduced levels of HLTF on the chromatin and reduced the amount of RAD18-bound HLTF, suggesting a potential novel role for RNF168 in TS that should be further investigated in future studies.

RNF168-depletion was also found to reduce recruitment of TLS polymerase η to UV-induced lesions - a high-fidelity substrate of Pol η and loss of RNF168 in UV-irradiated cells lead to prolonged replication fork stalling and the generation of vulnerable, single-stranded DNA. Consistently, in a reciprocal experiment, RNF168 overexpression diminished UV-induced mutagenesis. These results support a potential role for RNF168 in altering RAD18-mediated DNA damage tolerance via TS. Future work should explore whether blocking RNF168-mediated K63 linked poly-ubiquitin chain formation is able to increase UV-induced mutagenesis to determine if RNF168-mediated poly-ubiquitination of H2A/H2AX or a new substrate is contributing to UV tolerance[22].

It is now clear that initiation of template switching requires both PCNA poly-ubiquitination and SUMOylation[23, 24]. Important next steps should include examining how other post-translational modifications (as well as negative regulators of post-translational modifications) cooperate in regulating DNA damage tolerance mechanisms[25-27].

5.2 Novel role for MAGEA4 in trans-lesion DNA synthesis

Trans-lesion synthesis is a low-fidelity DNA damage tolerance process that allows replication of damaged DNA (e.g. from environmental agents like solar radiation or chemotherapeutics such as Cisplatin) at the expense of increased mutagenesis. While TLS is postulated to mediate mutagenesis in neoplastic cells, the full contribution of TLS to carcinogenesis remains largely unexplored. We have identified a novel mechanism by which cancer cells utilize a germ cell protein to reprogram and enhance DNA damage tolerance and mutagenesis pathways. Several cancer cell lines rely on

MAGEA4 to stabilize the E3 ubiquitin ligase and DNA damage tolerance mediator, RAD18. By sustaining RAD18 levels, MAGEA4 promotes recruitment of Pol η to chromatin to resume DNA synthesis following UV irradiation, thus preventing the accumulation of DNA double stranded breaks. Further, MAGE-A4-depleted cells recapitulate many hallmarks observed in TLS-deficient cells (e.g. delayed recovery from replication fork-stalling lesions), suggesting that MAGE-A4-RAD18 interactions promote trans-lesion synthesis in neoplastic cells.

TLS polymerases are highly error prone and must be used sparingly to prevent mutagenesis. Previous results from our lab and others have identified lesion-specific roles of distinct TLS polymerases in conferring tolerance to different genotoxins[28-30]. In fact, the TLS polymerases also have distinct dependencies on ub-PCNA; e.g. Polη is less dependent than Polκ)[31, 32]. Thus, recruitment of certain TLS polymerases may be more affected by MAGEA4-induced ub-PCNA. Because excess TLS activity can produce mutations, any imbalance stemming from MAGEA4 expression will have profound implications for mechanisms of mutagenesis in response to different exposures. Future studies should determine the extent to which MAGEA4-RAD18 drives inappropriate recruitment of TLS polymerases during a normal cell cycle cells and under conditions with extensive replication fork-stalling. The identification of specific damaging agents or inter-individual polymorphisms in MAGEA4, RAD18, or other DNA damage tolerance genes that influence propensity for mutagenesis will also greatly enhance our understanding of how to leverage these pathways for therapeutic benefit.

Several studies have demonstrated a role for TLS in conferring chemoresistance in tumors. In defining MAGEA4-RAD18 as a mediator of DNA damage tolerance and

mutagenesis we also identify a new therapeutic target that is present only in cancer cells and thus its inhibition would be innocuous to normal tissue.

5.3 The Cancer/Testis Antigens MAGEA4, MAGEA10, and HORMAD1 promote chemoresistance in cancer cells

Owing to their tumor-specific expression, CTA proteins have received attention primarily because they represent potential targets for more specific cancer therapies. We have identified novel roles for CTAs in the promotion of resistance to traditional therapies used in the treatment of Non Small Cell Lung Cancer (NSCLC).

We show here that MAGEA4 loss sensitized H1299 lung adenocarcinoma cells to treatment with agents used in the treatment of NSCLC (ionizing radiation (IR), Camptothecin, Cisplatin, Doxorubicin and Etoposide). All of these agents induce DNA lesions that are normally handled by homologous recombination (HR). Interestingly, MAGEA4 depletion did not sensitize H1299 cells to paclitaxel, a mitotic spindle poison that blocks normal progression through mitosis. MAGEA4 promotes both RAD18-dependent and independent mechanisms of chemoresistance. Both MAGEA4 and RAD18 loss sensitize NSCLC cells to Cisplatin and Etoposide, pathways that employ the use of the Fanconi Anemia pathway. Indeed, MAGEA4 loss reduces recruitment of FANCD2 (a mediator of the Fanconi Anemia pathway). Following IR treatment, individual MAGEA4 and RAD18 depletion, sensitized H1299 levels to a similar extent, however, co-depletion exacerbated this effect, suggesting that the two proteins are not acting in the same pathway to mediate radioresistance. MAGEA10 loss sensitized NSCLC cells to DSB induced by ionizing radiation and topoisomerase II inhibitors, but

not to Cisplatin or Camptothecin (data not shown). Finally, both MAGEA4 and MAGEA10 loss increased rates of recombination seen by DR-GFP, suggesting that MAGEA4/10-mediated resistance to cancer therapies may be mediated through a DNA repair mechanism.

The MAGE proteins lack any known enzymatic activity and are therefore presumed to function as adaptors or mediators. Thus, an important next step should employ affinity purification and mass spectrometry to define MAGE-dependent interaction networks both basally and following treatment with a DNA-damaging chemotherapeutic. An interesting control in these studies would be to include the MAGE-homology domain (MHD), ~170 amino acid region that is highly conserved amongst MAGE family members[7]. DNA damage tolerance mediators that are able to bind multiple full-length MAGE proteins (and isolated MHD) may substantiate utilizing the MHD in a small molecule inhibitor screen to more broadly target MAGEs in cancer. Future studies should also include the direct determination of the contribution of CTAs to repair of therapy-induced DNA lesions (e.g. via Comet Assay).

Hyperactive DNA repair is one of the mechanisms for acquired chemoresistance. A 2013 study by the Jacks group found that chronic cisplatin treatment enhances DNA repair and tumor progression in a mouse model of lung cancer[33]. MAGE expression has been linked to poor outcomes in patients with NSCLC, thus an important next step is to examine the contribution of CTAs to chemoresistance in vivo[34]. Although some studies have suggested a link between CTA expression and chemoresistance, the direct effect of MAGEs on chemoresistance has not been investigated *in vivo*, nor have any CTA transgenic mice been reported to date. Our lab has developed the first known

transgenic MAGEA4 mouse that conditionally expresses MAGEA4 at the Rosa26 locus. We will use this mouse in a preclinical model to look at the contribution of MAGEA4 to chemoresistance in lung cancer. In a pilot experiment with a small cohort of mice we have confirmed MAGEA4 expression in tumors from *Rosa26*[+/MAGEA4] *LSL-Kris*[+/G12D] mice[35, 36] (Fig. 5.2). Using this model, we will be able to determine the impact of Cree-induced MAGEA4 expression on resistance to chemotherapeutics used in the treatment of NSCLC *in vivo*.

Our studies have also identified a role for the CTA HORMAD1 in promoting HR and radioresistance in NSCLC. Depletion of HORMAD1 sensitizes NSCLC cells, but not triple negative breast cancer cells, to ionizing radiation. However, relative expression levels may indicate reliance on HORMAD1 for radioresistance. HORMAD1 forms irradiation-induced foci that co-localize with γH2AX, which was also identified as a novel binding partner. HORMAD1 loss reduced rates of recombination by DR-GFP and abrogated recruitment of RAD51 to DSB. These findings are the first report of a cancer cell-specific mechanism for therapy resistance by HORMAD1 that might be exploitable for therapy. Future studies should further delineate the mechanistic roles between HORMAD1 and its known HR-affiliated binding partners (BRCA1) to generate an interaction network with and without IR treatment[37].

Arguably, the most important contribution of this research is the potential for development of new, cancer-cell specific therapies. To drive the discovery of small molecules that may interrupt CTA function, we have developed an AlphaScreen (Amplified Luminescent Proximity Homogeneous Assay Screen) for the MAGE:RAD18 interaction (Fig. 5.3). The AlphaScreen is a high-throughput proximity assay that uses

anti-affinity tag beads to measure the binding interaction of tagged proteins and can be used as a platform for screening small molecules inhibitors of the MAGEA4:RAD18 interaction. Importantly, this platform can be adapted to accommodate future CTA:DNA-repair-factor protein:protein interactions. Due to the inherent cancer cell-specific expression of CTAs, these interactions represent untapped therapeutic targets whose inhibition would selectively sensitize cancer cells to therapy-induced DNA damage. Therefore, our work could eventually validate multiple CTA:DNA-repair-factor interactions as new therapeutic targets and facilitate the development of small molecule inhibitors to be used in a personalized medicine based treatment regimen that is informed by the CTA expression profile of the patient.

5.4 Concluding remarks

DNA damage tolerance is critical for multi-step carcinogenesis, allowing cancer cells to proliferate, adapt, invade and resist treatment. Determining how cancer cells adapt to tolerate environmental, endogenous, and therapy-induced DNA damage will expose molecular vulnerabilities that can be used to improve cancer prevention and treatment. We have identified several mediators of DNA damage tolerance (RNF168, MAGEA4, and HORMAD1) that will help us better understand how dysregulation of DNA repair in cancer cells can drive carcinogenesis, allowing cancer cells to proliferate, adapt, invade and resist chemotherapy. We have also identified multiple cancer cell-specific proteins that promote resistance to commonly used cancer therapies (MAGEA4, MAGEA10, and HORMAD1) offering exciting potential candidates for targeted therapies that may ultimately improve patient outcomes.
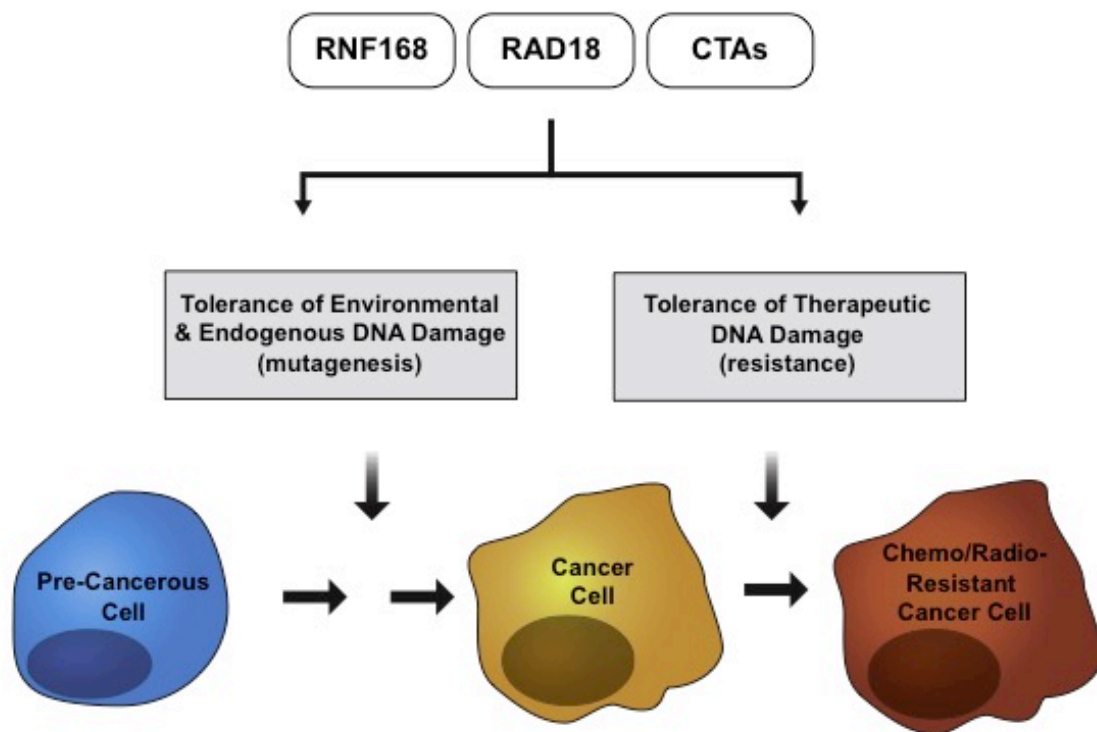
Figure 5.1 Potential roles of RNF168, RAD18, MAGEA4, MAGEA10 and HORMAD1 in carcinogenesis
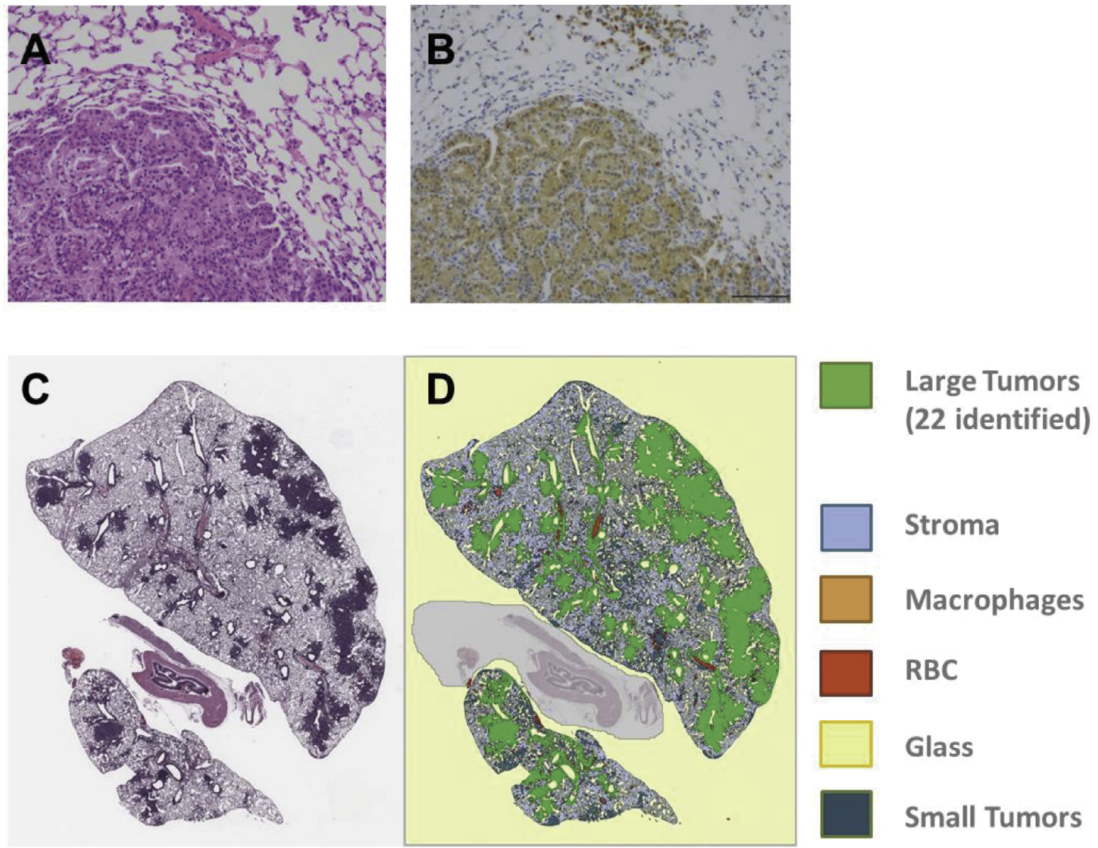
Figure 5.2 MAGEA4 as a mediator of chemoresistance in a pre-clinical mouse model of lung cancer

H&E-staining (A) and MAGEA4 staining (brown) (B) in a representative lung tumor from a *LSL-KrasG12D/+ Rosa26+/MAGEA4* mouse. (C) and (D) show automated analyses of Kras-induced lung tumors.
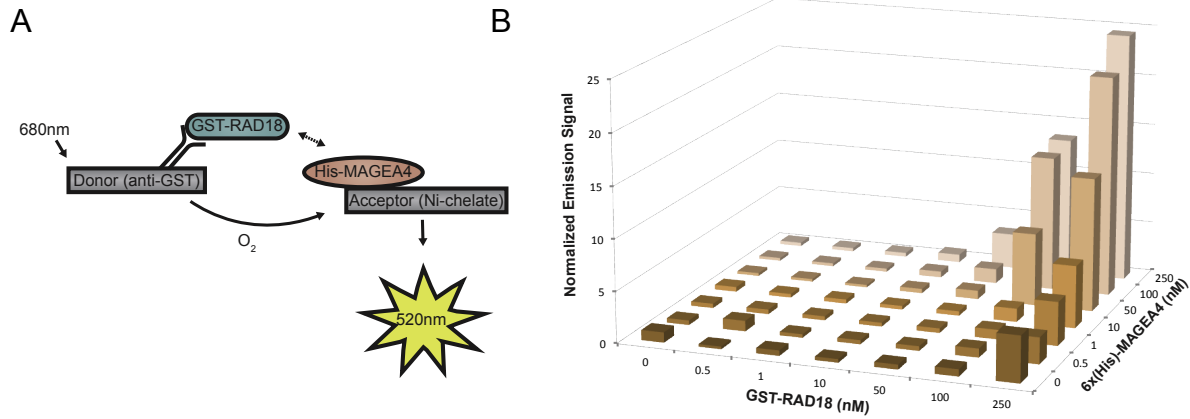
Figure 5.3 AlphaScreen platform to screen for small molecule inhibitors of CTA:DNA repair factor interactions

(A) Schematic of AlphaScreen assay
(B) Concentration-dependent association of GST-RAD18 and His-MAGEA4

REFERENCES

1.	Watson, I. R., et al. (2013). "Emerging patterns of somatic mutations in cancer." Nat Rev Genet **14**(10): 703-718.

2.	Roach, J. C., et al. (2010). "Analysis of genetic inheritance in a family quartet by whole-genome sequencing." Science **328**(5978): 636-639.

3.	Loeb, L. A. (2011). "Human cancers express mutator phenotypes: origin, consequences and targeting." Nat Rev Cancer **11**(6): 450-457.

4.	Valko, M., et al. (2004). "Role of oxygen radicals in DNA damage and cancer incidence." Mol Cell Biochem **266**(1-2): 37-56.

5.	Hendel, A., et al. (2008). "Reduced efficiency and increased mutagenicity of translesion DNA synthesis across a TT cyclobutane pyrimidine dimer, but not a TT 6-4 photoproduct, in human cells lacking DNA polymerase eta." DNA Repair (Amst) **7**(10): 1636-1646.

6.	Alt, A., et al. (2007). "Bypass of DNA lesions generated during anticancer treatment with cisplatin by DNA polymerase eta." Science **318**(5852): 967-970.

7.	Doyle, J. M., et al. (2010). "MAGE-RING protein complexes comprise a family of E3 ubiquitin ligases." Mol Cell **39**(6): 963-974.

8.	Stewart, G. S., et al. (2009). "The RIDDLE syndrome protein mediates a ubiquitin-dependent signaling cascade at sites of DNA damage." Cell **136**(3): 420-434.

9.	Gao, Y., et al. (2016). "A neomorphic cancer cell-specific role of MAGE-A4 in trans-lesion synthesis." Nat Commun **7**: 12105.

10.	van der Bruggen, P., et al. (1991). "A gene encoding an antigen recognized by cytolytic T lymphocytes on a human melanoma." Science **254**(5038): 1643-1647.

11.	Traversari, C., et al. (1992). "Transfection and expression of a gene coding for a human melanoma antigen recognized by autologous cytolytic T lymphocytes." Immunogenetics **35**(3): 145-152.

12.	Knuth, A., et al. (1989). "Cytolytic T-cell clones against an autologous human melanoma: specificity study and definition of three antigens by immunoselection." Proc Natl Acad Sci U S A **86**(8): 2804-2808.

13.	Zou, C., et al. (2012). "Cancer-testis antigens expressed in osteosarcoma identified by gene microarray correlate with a poor patient prognosis." Cancer **118**(7): 1845-1855.

14. Li, X., et al. (2015). "Evaluation of melanoma antigen (MAGE) gene expression in human cancers using The Cancer Genome Atlas." Cancer Genet **208**(1-2): 25-34.

15. Forghanifard, M. M., et al. (2011). "Cancer-testis gene expression profiling in esophageal squamous cell carcinoma: identification of specific tumor marker and potential targets for immunotherapy." Cancer Biol Ther **12**(3): 191-197.

16. Daudi, S., et al. (2014). "Expression and immune responses to MAGE antigens predict survival in epithelial ovarian cancer." PLoS One **9**(8): e104099.

17. Monte, M., et al. (2006). "MAGE-A tumor antigens target p53 transactivation function through histone deacetylase recruitment and confer resistance to chemotherapeutic agents." Proc Natl Acad Sci U S A **103**(30): 11160-11165.

18. Hartmann, S., et al. (2017). "MAGE-A11 expression contributes to cisplatin resistance in head and neck cancer." Clin Oral Investig.

19. Xie, C., et al. (2016). "Melanoma associated antigen (MAGE)-A3 promotes cell proliferation and chemotherapeutic drug resistance in gastric cancer." Cell Oncol (Dordr).

20. Raschle, M., et al. (2015). "DNA repair. Proteomics reveals dynamic assembly of repair complexes during bypass of DNA cross-links." Science **348**(6234): 1253671.

21. Hibbert, R. G., et al. (2011). "E3 ligase Rad18 promotes monoubiquitination rather than ubiquitin chain formation by E2 enzyme Rad6." Proc Natl Acad Sci U S A **108**(14): 5590-5595.

22. Chiu, R. K., et al. (2006). "Lysine 63-polyubiquitination guards against translesion synthesis-induced mutations." PLoS Genet **2**(7): e116.

23. Stelter, P. and H. D. Ulrich (2003). "Control of spontaneous and damage-induced mutagenesis by SUMO and ubiquitin conjugation." Nature **425**(6954): 188-191.

24. Hoege, C., et al. (2002). "RAD6-dependent DNA repair is linked to modification of PCNA by ubiquitin and SUMO." Nature **419**(6903): 135-141.

25. Kashiwaba, S., et al. (2015). "USP7 Is a Suppressor of PCNA Ubiquitination and Oxidative-Stress-Induced Mutagenesis in Human Cells." Cell Rep **13**(10): 2072-2080.

26. Huang, T. T., et al. (2006). "Regulation of monoubiquitinated PCNA by DUB autocleavage." Nat Cell Biol **8**(4): 339-347.

27. Gallego-Sanchez, A., et al. (2012). "Reversal of PCNA ubiquitylation by Ubp10 in Saccharomyces cerevisiae." PLoS Genet **8**(7): e1002826.

28. Avkin, S., et al. (2004). "Quantitative analysis of translesion DNA synthesis across a benzo[a]pyrene-guanine adduct in mammalian cells: the role of DNA polymerase kappa." J Biol Chem **279**(51): 53298-53305.

29. Shachar, S., et al. (2009). "Two-polymerase mechanisms dictate error-free and error-prone translesion DNA synthesis in mammals." EMBO J **28**(4): 383-393.

30. Ziv, O., et al. (2009). "DNA polymerase zeta cooperates with polymerases kappa and iota in translesion DNA synthesis across pyrimidine photodimers in cells from XPV patients." Proc Natl Acad Sci U S A **106**(28): 11552-11557.

31. Bi, X., et al. (2005). "DNA polymerase kappa is specifically required for recovery from the benzo[a]pyrene-dihydrodiol epoxide (BPDE)-induced S-phase checkpoint." J Biol Chem **280**(23): 22343-22355.

32. Acharya, N., et al. (2008). "Roles of PCNA-binding and ubiquitin-binding domains in human DNA polymerase eta in translesion DNA synthesis." Proc Natl Acad Sci U S A **105**(46): 17724-17729.

33. Oliver, T. G., et al. (2010). "Chronic cisplatin treatment promotes enhanced damage repair and tumor progression in a mouse model of lung cancer." Genes Dev **24**(8): 837-852.

34. Gure, A. O., et al. (2005). "Cancer-testis genes are coordinately expressed and are markers of poor outcome in non-small cell lung cancer." Clin Cancer Res **11**(22): 8055-8062.

35. Singh, M., et al. (2010). "Assessing therapeutic responses in Kras mutant cancers using genetically engineered mouse models." Nat Biotechnol **28**(6): 585-593.

36. Jackson, E. L., et al. (2001). "Analysis of lung tumor initiation and progression using conditional expression of oncogenic K-ras." Genes Dev **15**(24): 3243-3248.

37. Hill, S. J., et al. (2014). "Systematic screening reveals a role for BRCA1 in the response to transcription-associated DNA damage." Genes Dev **28**(17): 1957-1975.